



Dear Search Committee,

I am writing to express my enthusiastic interest in the research faculty position at the University of Michigan Transportation Research Institute (UMTRI). I am currently completing my Ph.D. in Berkeley Artificial Intelligence Research(CEE and EECS) at UC Berkeley, advised by Prof. Maria Laura Delle Monache and Prof. Alexandre Bayen. My research focuses on the control of connected autonomous vehicles (CAV) in mixed traffic flow.

Specifically, I am interested in the opportunity to work in the Michigan Traffic Lab and MCity under Professor Henry Liu's leadership. The lab's innovative work in traffic flow optimization, CAV systems, and smart transportation solutions aligns closely with my research trajectory and vision in the CAV field.

Alignment with Research Interests The Michigan Traffic Lab's innovative work at MCity in advancing CAV systems, coupled with its interdisciplinary approach to testing and deploying advanced mobility solutions, directly aligns with my research background and goals. My doctoral studies at UC Berkeley focused on using multi-agent systems and vehicular automation to optimize traffic flow and enhance transportation safety. As a leading researcher in the [CIRCLES project](#), I led the development of a centralized speed planner for the world's largest open-road AV experiment on Tennessee's [I-24 MOTION](#) open highway testbed. By integrating reinforcement learning and hybrid PDE-ODE models, I achieved an 8% improvement in overall traffic efficiency, with a significant 52% reduction in congestion during bottleneck formation phases.

In addition, my work on [Probabilistic Occupancy Risk Assessment \(PORA\)](#) addresses critical safety challenges by generating probabilistic risk metrics for AVs, thereby enhancing real-time decision-making capabilities in dynamic environments. This aligns with MCity's mission of ensuring the seamless and safe integration of automated vehicles into urban settings. My research methodology—combining stochastic modeling, machine learning, and real-world validation—aligns with MCity's commitment to collaborative, data-driven innovation in advancing mobility systems.

Contributions to Publications Across my projects, I have actively led and contributed to high-impact publications that showcase my expertise in traffic control systems and large-scale generative modeling. The MegaController paper, which I co-authored as part of the CIRCLES consortium and was published in IEEE Control Systems Magazine, highlights my leadership in developing a hierarchical control framework for managing large-scale traffic flow using connected and automated vehicles. This work exemplifies how centralized speed planning and decentralized vehicle control can mitigate congestion and enhance traffic efficiency in mixed autonomy settings. The following research will be presented on [AAAI 2025](#) at the Multi-Agent Reinforcement Learning for Transportation Autonomy ([MALTA](#)) workshop.

My paper on [PDE/ODE modeling](#) forms the mathematical foundation of the CIRCLES project, integrating partial differential equations and ordinary differential equations to capture the dynamics of traffic flow. This theoretical framework underpins the reinforcement learning-based control strategies deployed in real-world tests, demonstrating their scalability and effectiveness in improving traffic conditions.

In addition, our paper, recognized as [Best Paper at ACM UIST 2024](#) and in which I was listed as the second author, demonstrates my contributions to large-scale generative modeling. The work introduces an LLM-based runtime behavior generation system for Unity-based environments, enabling dynamic creation and integration of behaviors in response to user input. This project underscores my effort to extend generative AI techniques to complex, interdisciplinary systems, bridging advancements in traffic simulation and interactive environments.

Experience in Proposal Development My reliable ties with General Motors (GM), Toyota, Nissan, and Allstate have resulted in successfully completed and ongoing funded projects, with proposals for Allstate-funded initiatives independently developed by me. These experiences highlight my ability to conceptualize and secure funding from industry partnerships. Looking ahead, I aim to expand funding sources to include agencies such as the National Science Foundation (NSF), U.S. Department of Energy (DOE), and ARPA-E.

Teamwork and Leadership My experience spans both independent research and collaborative team environments. As a leading researcher in the CIRCLES project, I coordinated the efforts of 63 scholars, ensuring seamless integration of AV controllers and traffic simulation systems. I have co-led interdisciplinary collaborations and large-scale experiments involving engineers, behavioral scientists, and industry partners. As a principal investigator, I guided graduate and undergraduate students in designing traffic state estimation models and implementing real-time traffic simulation frameworks. Additionally, my leadership involved hosting daily stand-ups and troubleshooting sessions to address challenges and foster teamwork.

Commitment to Mentorship and Diversity I have consistently prioritized creating inclusive and empowering learning environments. In collaboration with UC Berkeley's Safe Transportation Research and Education Center (SafeTREC) and the nonprofit Self-eSTEM, I adapted a [Virtual Reality \(VR\) Bicycle Simulator](#) to engage BIPOC girls in STEM fields. This initiative encouraged participants to explore engineering and technology careers while emphasizing transportation safety and urban planning. Additionally, my research on assistive technologies, such as an [augmented reality \(AR\) driving assistance system for visually impaired individuals](#), highlights my commitment to equity-centered design.

At UC Berkeley, I have mentored six graduate and undergraduate students from diverse backgrounds, supporting their growth as researchers in transportation engineering and autonomous systems. My mentorship emphasized developing technical skills, overcoming challenges, and aligning research projects with their individual goals.

In conclusion, I am eager to bring my expertise in CAV, traffic flow modeling, and multi-agent systems to UMTRI and the Michigan Traffic Lab. I am confident that my skill set and research background at the intersection of AI and CAV will contribute to advancing MCity's mission of redefining mobility systems for a safer, more equitable future.

Thank you for considering my application. I would be delighted to discuss how my skills and experiences align with the goals of UMTRI and the Michigan Traffic Lab. I look forward to the possibility of contributing to your innovative team.

Sincerely,

Han Wang, Ph.D. Candidate
University of California, Berkeley
Email: hanw@berkeley.edu | Website: hanwcal.github.io

Han Wang

■ +1 510-409-2998

✉ hanw@berkeley.edu

Ω hanwcal.github.io

in/in/hanwcal

Profile and Objective

Ph.D. candidate at the Berkeley Artificial Intelligence Research(BAIR) and Berkeley Deep Drive(BDD), focusing on Self-Driving, Computer Vision, and Multi-agent Reinforcement Learning. Looking for research positions starting in 2025, fall.

Education

University of California, Berkeley	GPA 3.93/4.0	CA, United States
Ph.D. in Transportation Engineering	Advisor: Maria Laura Delle Monache	08/2021 – 05/2025(Exp.)
M.S. in Electrical Engineering and Computer Science	Advisor: Alexandre Bayen	08/2023 – 05/2025(Exp.)
M.Eng. in Transportation Engineering	Advisor: Alexander Skabardonis	08/2020 – 05/2021
Relevant Courses: Deep Reinforcement Learning / Responsible GenAI and Decentralized Intelligence / Advanced Control System / Reproducible and Collaborative Statistical Data Science / Computer Vision / Immersive Computing and Virtual Reality / Foundations of Computer Graphics / Intelligent Transportation Systems / Data Driven Control Methods for Civil Systems / Highway Traffic Operations / Operation of Transportation Facilities / Systems Analysis in Transportation / Public Transportation Systems / Traffic Safety and Injury Control		
Southeast University	GPA 85.75/100	Nanjing, China
M.Eng. in Transportation Engineering	Advisor: Jian Zhang, Bin Ran	09/2017 – 05/2020
Southwest Jiaotong University	GPA 80.27/100	Chengdu, China
B.S. in Transportation Engineering		09/2013 – 06/2017

Research Experience

Congestion Impacts Reduction via CAV-in-the-loop Lagrangian Energy Smoothing (CIRCLES)	03/2022-12/2024
<i>World's largest open-track fieldtest, sending 100 auto-vehicle(AVs) to I-24 during the morning peak to improve traffic. Funded by Toyota, Nissan, and General Motors. Supported by Tennessee Department of Transportation</i>	
• <u>Role:</u> Led the centralized speed planner to publish the optimized speed for all 100 AVs in real-time during the experiment.	
• <u>Tools:</u> RL Speed Planner: PyTorch, Ray, Gym Backend: MySQL, Python API: PHP	
• <u>Outcome:</u> From the field test data, we observed an 8% improvement overall, with 7% and 10% improvements upstream and downstream, respectively, and a 52% improvement during congestion formation at the bottleneck.	
Collision Indeterminacy Prediction via Stochastic Trajectory Generation	06/2023-06/2024
<i>Predicting the motion of AV with the pre-trained image generative model. Funded by Berkeley Deep Drive and Allstate</i>	
• <u>Role:</u> Lead the occupancy image dataset collecting, generative decoder pre-training, end-to-end training with perception encoder, the building of the simulation platform, and the design & training of the AV controller in the simulator.	
• <u>Tools:</u> ML Model Design & Training: PyTorch, Ray Simulation: SUMO Dataset: Argoverse	
• <u>Outcome:</u> Developed a probabilistic occupancy risk assessment (PORA) metric, validated through a scenario-generation-based microsimulation platform, demonstrated to be effective in predicting 87% of the conflicts that could not be predicted by TTC-2.	
Understanding Resilience and Equity of Transportation System During Hazardous Events	07/2021-12/2024
<i>An equity-focused resilience framework for urban transportation. Funded by California Department of Transportation</i>	
• <u>Role:</u> Designed a social-physical integrated evaluation index to quantify resilience and equity, integrating social equity considerations with system resilience to ensure equitable recovery for underserved communities. Formulated recovery strategies as a Markov Decision Process (MDP) and implemented reinforcement learning (RL) algorithms using Actor-Critic methods. Conducted large-scale simulations of the San Francisco Bay Area transportation network, leveraging GMNS and OpenStreetMap data to validate the framework's scalability and effectiveness.	
• <u>Tools:</u> Network Modeling: GMNS, OpenStreetMap Simulation: Python, TensorFlow RL Algorithm: Actor-Critic	
• <u>Outcome:</u> Achieved a significant reduction in inequity penalties, enhancing recovery performance by 13.8% over capacity-based strategies and 26.3% over population-based strategies. Results demonstrated effective prioritization and equitable recovery under various hazard scenarios.	

Creating an Inclusive Bicycle Level of Service: Virtual Bicycle Simulator study

01/2021-08/2023

Gather user feedback on biking environments with VR simulator survey. Funded by California Department of Transportation

- Role: Built the VR biking simulator, including hardware & software integration. Rebuilt the California streets in 3D scenarios.
- Tools: Simulator Development: Unity, C#, SteamVR | Modeling: Blender
- Outcome: The feedback from the survey proved the VR simulator provided a more realistic and engaging experience for participants, which enhanced their ability to make informed decisions about their route preferences.

Opportunities and Challenges for Runtime Behavior Generation in Games and Simulations

09/2023-06/2024

Runtime behavior generation using large language models in game/simulation development.

Personal Project

- Role: Developed the runtime code compile module. Implemented the semantic search and prompt engineering of the agent. Develop the element tree system of test scenarios. Conducted generalization tests in various scenarios.
- Tools: System Development: Unity, C# | LLM: OpenAI API
- Outcome: The pressure test demonstrated the system in various game scenarios, achieving an 85% success rate. Thematic analysis of developer feedback indicates the improved dynamic game experience by integrating real-time behavior generation.

V2X-based Driving Perception Assistance System

09/2023-12/2024

Integration of foundation models and AR to enhance driving assistance systems via real-time visual aids

Personal Project

- Role: Designed and implemented a system integrating multimodal data (Lidar, cameras, maps, traffic updates) for real-time driving assistance. Developed AR visual aids for 3D object tracking and scene reconstruction. Utilized specialized LLMs for script generation and natural language interaction.
- Tools: System Development: Unity, C#, OpenCV | LLM: Ollama, LiteLLM
- Outcome: Achieved accurate 3D object tracking and reconstruction, enhancing driver situational awareness and safety through real-time AR visualizations. Refined functionality through human-in-loop interactions and driver feedback. Integrated foundation models for natural language command interpretation and script generation, improving adaptability and usability.

Vision-based Browser Automation using GenAI

01/2024-12/2024

Automating browser workflows using multimodal LLM agents.

Personal Project

- Role: Finetuned open-source LLMs with RAG for browser operation subtasks. Developed vision + HTML webpage scraper. Defined and implemented multi-agent workflow. Develop the browser operation API kit for LLM. Developed the Chrome extension for human-in-loop expert data collecting. Created the open dataset on HuggingFace.
- Tools: Finetune: Unsloth | Agent: Ollama, LangChain, LiteLLM
- Outcome: Enhanced automation stability and adaptability to website layout changes, enabling complex workflow automation across multiple sites. Integrated real-time debugging and visualization of automation steps, facilitating efficient troubleshooting.

Crowdsourcing Perceived Hazardous Pedestrian Locations

09/2020-05/2021

SafeTport: An IOS App allowing users to report and view traffic hazards and crashes.

Funded by SafeTREC

- Role: Developed the front-end and back-end of the system independently.
- Tools: IOS APP: Swift, Google Map Platform | Backend: MySQL, AWS, Restful API
- Outcome: Created a functional application, identified marketing strategy in user engagement and data collection.

Research on Multi-junction Energy-saving Access Control of Intelligent Electric Vehicles

07/2017-12/2020

Developed control models and simulations for energy-saving access control in intelligent electric vehicles.

Funded by SEU

- Role: Established a multi-agent control model using improved MADDPG algorithm for multi-intersections urban arterial in a connected environment. Designed traffic and communication network simulations using SUMO, OMNET++.
- Tools: Controller: TensorFlow | Simulation: SUMO, OMNET++

Resilience Research for Extremely Surging Traffic of Huning (Shanghai-Nanjing) Highway

03/2017-12/2019

Analyze and improve the resilience of the Huning Highway system under extremely large traffic flow

Funded by Joint Research Institute on Internet of Mobility: Southeast University and University of Wisconsin

- Role: Led the establishment of the SUMO micro-simulation scenario for the entire Huning Highway. Designed the ramp control algorithm based on deep reinforcement learning.
- Tools: Simulation: SUMO | Ramp Controller: keras

Course Design of the Traffic Analysis I Driven by Big Data

01/2019-12/2019

Enhanced traditional traffic analysis course content with data mining skills.

Funded by Didi Chuxing Technology Co.

- Role: Added data mining related skills to the traditional traffic analysis course content. Designed course paper requirements integrating data of the GAIA Initiative from Didi.

Publications

Peer-reviewed Journal Articles

- Lee, J. W., **Wang, H.**(co-first), Jang, K., Hayat, A., Bunting, M., Alanqary, A., ... (64 authors) & Bayen, A. M. (2025). Traffic control via connected and automated vehicles: An open-road field experiment with 100 cavs. *IEEE Control Systems*, 45(1), 28-60.
- **Wang, H.**, Fu, Z., Lee, J., Matin, H. N. Z., Alanqary, A., Urieli, D., ... (17 authors) & Monache, M. L. D. (2025). Hierarchical speed planner for automated vehicles: A framework for lagrangian variable speed limit in mixed autonomy traffic. *IEEE Control Systems*, 45(1), 111-138.
- Ameli, M., McQuade, S., Lee, J. W., Bunting, M., Nice, M., **Wang, H.**, ... & Bayen, A. M. (2025). Designing, simulating, and performing the 100-av field test for the circles consortium: Methodology and implementation of the largest mobile traffic control experiment to date. *IEEE Control Systems*, 45(1), 139-155.
- Zhang, J., Dong, S., Li, Z., Ran, B., Li, R., & **Wang, H.** (2019). An eco-driving signal control model for divisible electric platoons in cooperative vehicle-infrastructure systems. *IEEE Access*, 7, 83277-83285.

Conference Papers

- (Best Paper Award) Jennings, N., **Wang, H.**, Li, I., Smith, J., & Hartmann, B. (2024, October). What's the Game, then? Opportunities and Challenges for Runtime Behavior Generation. In Proceedings of the 37th Annual ACM Symposium on User Interface Software and Technology (pp. 1-13).
- Veksler, Y., Hornstein, S., **Wang, H.**, Monache, M. L. D., & Urieli, D. (2024). Cooperative Cruising: Reinforcement Learning based Time-Headway Control for Increased Traffic Efficiency. Accepted by AAAI2025, arXiv preprint arXiv:2412.02520.
- **Wang, H.**, Nick Zinat Matin, H.,& Delle Monache, M. L. (2024, June). Reinforcement learning-based adaptive speed controllers in mixed autonomy condition. In 2024 European Control Conference (ECC) (pp. 01-06). IEEE.
- Fu, Z., Kreidieh, A. R., **Wang, H.**, Lee, J. W., Delle Monache, M. L., & Bayen, A. M. (2023, June). Cooperative driving for speed harmonization in mixed-traffic environments. In 2023 IEEE Intelligent Vehicles Symposium (IV) (pp. 1-8). IEEE.
- **Wang, H.**, Wu, H., Lu, J., Tang, F., & Delle Monache, M. L. (2023, September). Communication Optimization for Multi-agent Reinforcement Learning-based Traffic Control System with Explainable Protocol. In 2023 IEEE 26th International Conference on Intelligent Transportation Systems (ITSC) (pp. 6068-6073). IEEE.
- **Wang, H.**, & Delle Monache, M. L. (2022, July). Urban network resilience analysis and equity emphasized recovery based on reinforcement learning. In 2022 European Control Conference (ECC) (pp. 01-06). IEEE.
- Tang, F., Cheng, L., **Wang, H.**, Mao, P., & Jiang, J. (2019). Research on the Impact of Car-Hailing on Travel Mode Choice: Evidence from Chengdu, China. In CICTP 2019 (pp. 6134-6145).
- Dong, S. Y., Zhang, J., **Wang, H.**, Ran, B., & Tan, H. C. (2018, July). A speed guidance-based signal control method for divisible platoon in CVIS. In 2018 IEEE 8th Annual International Conference on CYBER Technology in Automation, Control, and Intelligent Systems (CYBER) (pp. 1403-1408). IEEE.
- Dong, S. Y., Zhang, J., Chen, T. Y., **Wang, H.**, & Ran, B. (2018, July). CVIS-Based Intersection Signal Control Model for Indivisible Platoons. In 18th COTA International Conference of Transportation Professionals (pp. 359-368). Reston, VA: American Society of Civil Engineers.

Pre-prints

- **Wang, H.**, Yeo, Y., Paiva, A. R., Utke, J., Monache, M. L. D. (2025). Modular framework for uncertainty prediction in autonomous vehicle motion prediction within complex traffic scenarios. Submitted to IEEE Transactions on Intelligent Transportation Systems. arXiv preprint arXiv:2501.16480.
- Tang, F., **Wang, H.**, & Monache, M. L. D. (2024). Strategizing Equitable Transit Evacuations: A Data-Driven Reinforcement Learning Approach. Submitted to Transportation Research Part C: Emerging Technologies. arXiv preprint arXiv:2412.05777.
- Chekroun, R., **Wang, H.**, Lee, J., Toromanoff, M., Hornauer, S., Moutarde, F., & Monache, M. L. D. (2024). Mesoscale Traffic Forecasting for Real-Time Bottleneck and Shockwave Prediction. Submitted to Transportation Research Part C: Emerging Technologies. arXiv preprint arXiv:2402.05663.

Thesis

Thesis Title: Scalable Distributed Control for Large-Scale Multi-Agent Systems

Degree: Ph.D. in Transportation Engineering

December 2024

University of California, Berkeley, CA

Objective: To develop and validate a scalable distributed control framework that employs hierarchical and distributed control to optimize operation efficiency in large-scale multi-agent systems. The application goal is to integrate real-time data and machine learning algorithms to control the speed limits system, enhancing traffic efficiency and reducing fuel consumption.

Thesis Title: Multi-Agent Reinforcement Learning Method for Arterial Traffic Signal Control

May 2020

Degree: M.Eng. in Transportation Engineering

Southeast University, Nanjing, China

Objective: To address the complexity of coordinating multi-intersection arterial traffic signal control systems by implementing a reinforcement learning approach that effectively manages the delayed reward dynamics inherent in such environments.

Skills

Programming Languages:

Python, C#

Backends:

MySQL, AWS

Frameworks and Libraries:

PyTorch, Ray, OpenCV, Ollama, Unislot, LangChain

Simulation and Modeling:

Unity, SteamVR, Blender, SUMO

Honors

- Best Paper Award: 37th Annual ACM Symposium on User Interface Software and Technology (ACM UIST 2024)
- IEEE ITSC 2024 Institutional Lead Award - CIRCLES Consortium
- 2nd Prize Scholarship of Southeast University - 3 times (2017-2019)
- 3rd Prize of the National Cup Graduate Mathematical Contest in Modeling (2017)
- 3rd Prize of the Undergraduate Transportation Science and Technology Competition, SWJTU (2016)
- 1st Prize of the National Higher Education Association Cup Mathematical Contest in Modeling, Sichuan Province (2015)
- 3rd Prize Scholarship of Southwest Jiaotong University (2014)

Professional Service & Teaching

• Member and Reviewer of:

- IEEE Membership
 - Intelligent Transportation Systems Society
 - Control Systems Society
 - Robotics and Automation Society

- Reviewer for
 - Transportation Research Series
 - Transactions on Intelligent Transportation Systems
 - European Control Conference

• Teaching Assistant of:

- | | | |
|---|--|---|
| - CE265 Traffic Safety at UCB | - Advanced Mathematics I&II at SEU | - Traffic Analysis I at SEU |
| - Assisted in designing course material | - Conducted weekly recitation sessions | - Assisted in preparing lecture |
| - Led lab sessions and discussions about VR and crowdsourcing | - Provided one-on-one tutoring | - Facilitated student group projects |
| - Graded assignments and exams | - Developed supplementary learning materials | - Evaluated student performance through quizzes and exams |

Research Statement of Han Wang

Feb, 10, 2025

The evolution of mobility systems is rapidly transforming the landscape of urban transportation, driven by advancements in artificial intelligence, vehicular automation, and networked communication. My research focuses on leveraging multi-agent reinforcement learning (MARL) and vehicular automation technologies to address critical challenges in traffic management, congestion reduction, and urban network resilience. These efforts aim to advance the field of new mobility systems by optimizing traffic flow, improving safety, and promoting equity and trustworthiness in transportation technologies.

Human-Vehicle Interaction and Large-Scale Traffic Flow Optimization [1, 2, 3, 4, 5, 6, 7]

A central theme in my research is the development of intelligent control strategies for connected and automated vehicles (CAVs) that can effectively operate in mixed traffic conditions with a low penetration rate of automation. In particular, the *Congestion Impacts Reduction via CAV-in-the-loop Lagrangian Energy Smoothing (CIRCLES)* project demonstrates the ability of AVs to stabilize traffic flow and reduce congestion, even when accounting for human drivers' diverse behaviors. The project's emphasis on controlling traffic with only a 4% penetration rate of automated vehicles highlights the importance of understanding human-vehicle interactions and developing adaptive control mechanisms that integrate with existing traffic patterns.

Interpretable and Safe Multi-Agent Communication for Vehicle-to-Everything (V2X) Systems [8, 9]

A crucial focus of my research is the development of human-centered machine intelligence that enhances communication in vehicle-to-everything (V2X) systems and vehicle-highway automation. This line of work emphasizes the need for interpretable multi-agent communication protocols that facilitate safe and effective interactions between autonomous vehicles (AVs), human drivers, and pedestrians. By optimizing communication strategies within multi-agent systems, the research aims to enable clearer decision-making processes in traffic control scenarios. The *Predictive Occupancy Risk Assessment (PORa)* project further explores communication dynamics by investigating safety metrics for AVs. This project analyzes how communication impacts the interactions between AV controllers and surrounding traffic participants, thereby improving the reliability and interpretability of V2X systems.

Equity and Resilience in Urban Mobility Systems [10, 11]

Equity and resilience are critical considerations in designing sustainable urban mobility systems. My research addresses these issues by developing reinforcement learning-based strategies to enhance the resilience of urban transportation networks while ensuring equitable access to mobility. This work is divided into two phases: (1) *Network Resilience and Equity-Emphasized Recovery*, which focuses on optimizing control policies for equitable recovery in urban traffic networks during disruptions, and (2) *Equitable Evacuation Planning*, which extends the resilience analysis to large-scale evacuation scenarios, emphasizing fair and efficient allocation of post-hazard evacuation mobility resources across different communities. Together, these efforts aim to advance equitable and trustworthy technologies in urban mobility.

For future plan, my research goal at UMTRI is to develop a comprehensive framework for human-centered mobility systems that integrates AVs, human drivers, and infrastructure in a connected environment. This work aligns with the strategic priorities of new mobility research by advancing *human-vehicle-infrastructure connectivity*, addressing *equity in urban systems*, and contributing to the development of *resilient, sustainable, and scalable transportation solutions*.

References

- [1] **Han Wang**, Zhe Fu, Jonathan Lee, Arwa Alanqary, Hossein Nick Zinat Matin, Daniel Urieli, Sharon Hornstein, Abdul Rahman Kreidieh, Raphael Chekroun, William A. Richardson, Dan Work, Benedetto Piccoli, Benjamin Seibold, Jonathan Sprinkle, Alexandre M. Bayen, and Maria Laura Delle Monache. Hierarchical speed planner for automated vehicles: A framework for lagrangian variable speed limit in mixed autonomy traffic. *IEEE Control Systems*, 45(1):111–138, 2025.
- [2] Jonathan W. Lee, **Han Wang**(Co-first), Kathy Jang, Amaury Hayat, Matthew Bunting, Arwa Alanqary, William Barbour, Zhe Fu, Xiaoqian Gong, George Gunter, Sharon Hornstein, Abdul Rahman Kreidieh, Nathan Lictlé, Matthew Nice, William A. Richardson, Adit Shah, Eugene Vinitsky, Fangyu Wu, Xiang Shengquan, Sulaiman Almatrudi, Fahd Althukair, Rahul Bhadani, Joy Carpio, Rapha el Chekroun, Eric Cheng, Maria Teresa Chiri, Fang-Chieh Chou, Ryan DeLorenzo, Marsalis Gibson, Derek Gloudemans, Anish Gollakota, Junyi Ji, Alexander Keimer, Nour Khoudari, Malaika Mahmood, Mikail Mahmood, Hossein N. Z. Matin, Sean McQuade, Rabie Ramadan, Daniel Urieli, Yanbing Wang, Rita Xu, Mengsha Yao, Yiling You, Gergely Zachar, Yibo Zhao, Mirza Najamuddin Baig, Sarah Bhaskaran, Kenneth Butts, Manasi Gowda, John Lee, Liam Pedersen, Zimo Zhang, Chang Zhou, Daniel B. Work, Benjamin Seibold, Jonathan Sprinkle, Benedetto Piccoli, Maria Laura Delle Monache, and Alexandre M. Bayen. Traffic control via connected and automated vehicles (cavs): An open-road field experiment with 100 cavs. *IEEE Control Systems*, 45(1):28–60, 2025.
- [3] **Han Wang**, H Nick Zinat Matin, and Maria Laura Delle Monache. Reinforcement learning-based adaptive speed controllers in mixed autonomy condition. In *2024 European Control Conference (ECC)*, pages 1869–1874. IEEE, 2024.
- [4] Mostafa Ameli, Sean McQuade, Jonathan W Lee, Matthew Bunting, Matthew Nice, **Han Wang**, William Barbour, Ryan Weightman, Chris Denaro, Ryan Delorenzo, et al. Designing, simulating, and performing the 100-av field test for the circles consortium: Methodology and implementation of the largest mobile traffic control experiment to date. *IEEE Control Systems*, 45(1):139–155, 2025.
- [5] Raphael Chekroun, **Han Wang**, Jonathan Lee, Marin Toromanoff, Sascha Hornauer, Fabien Moutarde, and Maria Laura Delle Monache. Mesoscale traffic forecasting for real-time bottleneck and shockwave prediction. *arXiv preprint arXiv:2402.05663 (Transportation Research Part C: Emerging Technologies Under Review)*, 2024.
- [6] Yaron Veksler, Sharon Hornstein, **Han Wang**, Maria Laura Delle Monache, and Daniel Urieli. Cooperative cruising: Reinforcement learning based time-headway control for increased traffic efficiency. In *Multi-Agent reinforcement Learning for Transportation Autonomy*, 2025.
- [7] Zhe Fu, Abdul Rahman Kreidieh, **Han Wang**, Jonathan W Lee, Maria Laura Delle Monache, and Alexandre M Bayen. Cooperative driving for speed harmonization in mixed-traffic environments. In *2023 IEEE Intelligent Vehicles Symposium (IV)*, pages 1–8. IEEE, 2023.
- [8] **Han Wang**, Haochen Wu, Juanwu Lu, Fang Tang, and Maria Laura Delle Monache. Communication optimization for multi-agent reinforcement learning-based traffic control system with explainable protocol. In *2023 IEEE 26th International Conference on Intelligent Transportation Systems (ITSC)*, pages 6068–6073. IEEE, 2023.
- [9] **Han Wang**, Yuneil Yeo, Antonio Paiva, and Jean Utke. Generating future occupancy heatmaps for probabilistic collision risk assessment in autonomous driving. <https://arxiv.org/abs/2501.16480>, 2024.
- [10] **Han Wang** and Maria Laura Delle Monache. Urban network resilience analysis and equity emphasized recovery based on reinforcement learning. In *2022 European Control Conference (ECC)*, pages 01–06. IEEE, 2022.
- [11] Fang Tang, **Han Wang**, and Maria Laura Delle Monache. Strategizing equitable transit evacuations: A data-driven reinforcement learning approach. *arXiv preprint arXiv:2412.05777*, 2024.

Reference Contacts and Affiliations

- **Alexandre M. Bayen**

Title: Liao-Cho Innovation Endowed Chair Professor

Affiliation: UC Berkeley

Email: bayen@berkeley.edu

Website: <https://ce.berkeley.edu/people/faculty/bayen>

- **Maria Laura Delle Monache**

Title: Assistant Professor

Affiliation: UC Berkeley

Email: mldellemonache@berkeley.edu

Website: <https://ce.berkeley.edu/people/faculty/delle-monache>

- **Jonathan Sprinkle**

Title: Professor

Affiliation: Vanderbilt University

Email: jonathan.sprinkle@vanderbilt.edu

Website: <https://www.isis.vanderbilt.edu/jonathan-sprinkle>

Hierarchical Speed Planner for Automated Vehicles



©SHUTTERSTOCK.COM/ART STOCK CREATIVE

A FRAMEWORK FOR LAGRANGIAN VARIABLE SPEED LIMIT IN MIXED-AUTONOMY TRAFFIC

HAN WANG^{ID}, ZHE FU^{ID}, JONATHAN W. LEE^{ID}, HOSSEIN NICK ZINAT MATIN^{ID}, ARWA ALANQARY,
DANIEL URIELI^{ID}, SHARON HORNSTEIN, ABDUL RAHMAN KREIDIEH, RAPHAEL CHEKROUN,
WILLIAM BARBOUR, WILLIAM A. RICHARDSON, DAN WORK, BENEDETTO PICCOLI, BENJAMIN SEIBOLD,
JONATHAN SPRINKLE^{ID}, ALEXANDRE M. BAYEN, and MARIA LAURA DELLE MONACHE

The advent of *automated vehicles* (AVs) has the potential to revolutionize the field of transportation in the next decades, optimizing traffic flow, reducing congestion, and improving the overall efficiency of the transportation system. The focus of this article is to introduce a novel control framework specifically designed for managing variable speed limits (VSLs) in a hybrid traffic flow environment, combining both AVs and non-AVs. This framework hinges on the interplay between two key elements: server-side algorithms functioning as a centralized planner tasked with handling heavy computational loads and vehicle-side algorithms operating as the executing agents, adhering to the targets set by the central planner. This article focuses specifically on the development of the macroscopic centralized planner for managing VSLs in a hybrid traffic flow environment. Our novel approach aims to enhance *traffic state estimation* (TSE), optimize the design of target speed profiles for large-scale AV platoons, reduce

energy consumption, and boost the throughput of the overall traffic system.

This article details the design of the speed planner, a high-level algorithm that designs target speed profiles for vehicles in moving traffic, with the goal of smoothing traffic waves. The system was validated on a fleet of 100 connected AVs in the *MegaVanderTest* (MVT), which was the largest coordinated open-road test designed to smooth traffic flow. Overall, the speed planner tested in the MVT showcases capabilities in optimizing traffic flow. The full potential can be better realized with a holistic approach that considers both technological advancements and human-centric factors, such as driver acceptance rate and social acceptance.

INTRODUCTION

The burgeoning integration of AVs into existing traffic systems presents both opportunities and challenges for traffic management, particularly in mixed-autonomy environments. Efficient management of such environments is crucial for optimizing traffic flow and mitigating congestion.

Digital Object Identifier 10.1109/MCS.2024.3499212

Date of current version: 14 January 2025

Siri et al. [3] survey a range of freeway traffic control methods, discussing traditional and modern techniques, and highlight the integration of advanced technologies for improved traffic management. LeCun et al. [4] explore theoretical models and practical implementations for freeway traffic control, covering various strategies and real-world applications to showcase their effectiveness. Advances in technology play a pivotal role in addressing these challenges, offering new tools to enhance the dynamism and responsiveness of traffic control measures [5].

VSLs are recognized as a vital tool in the arsenal of traffic management strategies. They are designed to adjust speed limits dynamically based on real-time traffic conditions, aiming to improve traffic flow and reduce congestion. However, existing centralized VSL systems often fall short in real-time adaptability and fail to integrate with AV

Summary

This article introduces a novel control framework for Lagrangian VSLs in hybrid traffic flow environments utilizing AVs. The framework was validated using a fleet of 100 connected AVs as part of the largest coordinated open-road test designed to smooth traffic flow. The framework includes two main components: a high-level controller deployed on the server side, named the speed planner, and low-level controllers called vehicle controllers deployed on the vehicle side. The speed planner designs and updates target speeds for the vehicle controllers based on real-time TSE [S1]. The speed planner comprises two modules: a TSE enhancement module and a target speed design module. The TSE enhancement module is designed to minimize the effects of inherent latency in the received traffic information and to improve the spatial and temporal resolution of the input traffic data. The target speed design module generates target speed profiles with the goal of improving traffic flow. The vehicle controllers are designed to track the target speed while responding to the surrounding situation. Numerical simulations indicate the performance of the proposed method: the bottleneck throughput increases by 5.01%, and the speed standard deviation is reduced by a significant 34.36%. We further showcase an operational study with a description of how the controller was implemented on a field test with 100 AVs and its comprehensive effects on the traffic flow. The results show an overall 8% traffic density decrease, with a specific decrease of 7% upstream, 10% downstream, and a 52% decrease during the congestion formation phase at bottlenecks.

REFERENCE

- [S1] T. Seo, A. M. Bayen, T. Kusakabe, and Y. Asakura, "Traffic state estimation on highway: A comprehensive survey," *Annu. Rev. Control*, vol. 43, pp. 128–151, Apr. 2017, doi: [10.1016/j.arcontrol.2017.03.005](https://doi.org/10.1016/j.arcontrol.2017.03.005).

technologies. These systems typically rely on predefined algorithms that do not account for the unpredictable variations in mixed traffic environments, thereby limiting their effectiveness in real-time traffic optimization [6]. Moreover, while the integration of AVs in these systems improves the local controllability of the systems [7], [8], [9], [10], [11], [12], [13], [14], a precise and effective speed adjustment in large-scale networks requires and efficient communication and coordination mechanism.

To overcome the coordination and scalability challenges of centralized algorithms in large-scale traffic networks, the spirit of distributed control is adopted in the system design. A distributed VSL system leverages the computing power of many AVs to make local decisions, which may be partially coordinated using data communication, thus avoiding the dependence on a single central agent. This approach can alleviate the computational bottleneck and communication congestion associated with centralized VSL systems, making it easier to scale to larger and more complex road networks. In a distributed VSL system, each AV can collect and analyze data from its local observation. Based on these data, each AV can adjust its speed and communicate with nearby AVs and infrastructure to coordinate their target speed tracking and avoid collisions. By working together, the AVs can optimize traffic flow and reduce congestion on the road network, resulting in a safer and more efficient driving experience for all vehicles. In fact, prior works have proven that using each single vehicle as a traffic controller brings advantages from a traffic standpoint. This has been analyzed in field tests [15], [16] and in simulations [17]. Subsequently, this has advanced from the theoretical standpoint [18], [19], [20], [21] and in a control framework with a portion of the literature focusing on understanding the effects of AVs with intelligent speed controllers immersed in traffic [22], [23], [24], [25], [26].

The proposed speed planner introduces a novel approach to VSL control by incorporating a hierarchical control architecture that leverages both server-side algorithms and vehicle-side execution. This dual-layer strategy facilitates robust and responsive control mechanisms, essential for managing the complex dynamics of mixed-autonomy traffic [27].

The speed planner is designed to overcome significant challenges in traffic management systems as follows:

- » *Real-time TSE:* Traditional VSL systems often struggle with latency and inaccuracies in traffic data. The speed planner enhances TSE by integrating data from multiple sources, including AVs, to provide accurate, up-to-the-minute traffic assessments [28].
- » *Dynamic adjustment of speed limits:* It employs advanced algorithms that adjust speed limits dynamically, based not just on current traffic conditions but also on predictive models that anticipate future traffic patterns [29].
- » *Integration of server-side planning with vehicle-side execution:* The system ensures seamless communication

To overcome the coordination and scalability challenges of centralized algorithms in large-scale traffic networks, the spirit of distributed control is adopted in the system design.

between the server-side planning modules and vehicle-side controllers, enabling precise execution of speed adjustments that are critical in mixed traffic environments [30].

Contribution and Novelty

The speed planner's primary contribution lies in its ability to bridge the gap between theoretical traffic management models and practical, scalable applications. This is achieved through the innovative use of real-time data integration and predictive modeling, ensuring that the system remains adaptive and efficient under varying traffic conditions [31].

Despite considerable advancements in traffic management systems, existing solutions often do not fully exploit the potential of real-time data analytics and AV integration. The speed planner addresses these deficiencies by providing a scalable solution that enhances traffic flow dynamics through proactive speed regulation [32]. This article specifically focuses on the design, implementation, and validation of the speed planner within mixed-autonomy traffic environments.

Problem Statement

In this work, the main goal is to design a reinforcement learning (RL)-based control (speed planner) that improves the traffic status (density/flow) at the location of the

bottleneck. Broadly speaking, in doing so, the real-time traffic data (here INRIX) are collected. The TSE of the collected data is further improved, a so-called TSE enhancement, to compensate for the latency. Fusing the observed information from vehicles into the collected data improves the accuracy of the traffic statistics. Using smoothing techniques, a more stable speed limit is created, which alleviates the propagation of shockwaves. In designing a proper buffer zone, an RL-based control is trained through interaction with a micro-macro mathematical model, with the goal of improving the average density at the location of the bottleneck.

An Outline of the Structure of the Article

The structure of this article is organized as follows (the readers are encouraged to consult Figure 1 for the overview of the sections):

- 1) the “*Methodology*” section: describes the architecture and algorithms used in the speed planner
- 2) the “*Numerical Experiments*” section: discusses the simulation setup and the experiments conducted to validate the effectiveness of the speed planner
- 3) the “*Results*” section: presents the outcomes of the simulations and analyzes the performance of the system under different scenarios
- 4) the “*Conclusion*” section: summarizes the findings and discusses potential future work.

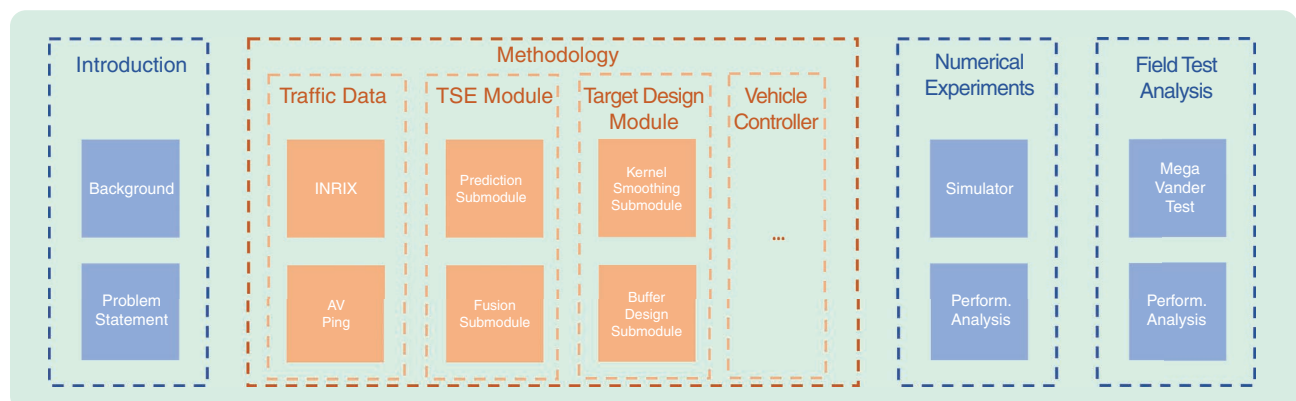


FIGURE 1 An overview of the article structure: The “Introduction” section outlines the background and the problem statement of traffic management in mixed-autonomy environments. The “Methodology” section describes the technical components including the traffic data collection (INRIX [2] and AV pings), the TSE module with prediction and fusion submodules, the target design involving kernel smoothing and buffer design, and the vehicle controller implementations. The “Numerical Experiments” section elaborates on the simulation framework used to test the theoretical models. The “Field Test Analysis” section discusses the application and results of the MVT, evaluating the performance and efficacy of the proposed traffic management strategies.

METHODOLOGY

The proposed speed planner introduces a hierarchical framework for VSLs, specifically designed to feed in-vehicle controllers in mixed traffic flow.

This section introduces a hierarchical framework for designing the RL-based VSL control that is specifically designed for mixed-autonomy traffic flow; [Figure 2](#) illustrates the modules that are defined for this purpose.

Hierarchical Framework

The hierarchical framework, as illustrated in [Figure 2](#), forms the foundation of the advanced traffic management system proposed in this work. Designed to amalgamate both macroscopic and microscopic TSE, the proposed framework generates an optimal target speed profile for the controlled vehicles. The primary objective of this framework is to harmonize traffic flow, alleviate congestion, and bolster road safety by harnessing real-time data and efficient algorithms. More accurately, the proposed control architecture (see [Figure 2](#)) leverages traffic data and the prediction module to find the optimal speed profile under different traffic conditions. It should be noted that while various hierarchical control structures have been proposed and analyzed in the literature (see, for example, [33] and the references therein), the proposed control framework in this article includes unique features from the data collection and prediction module to the developed mathematical model that makes our approach novel in both architectural design and the experiments.

The rest of the article is devoted to the detailed description of each element of [Figure 2](#).

Traffic Data

Central to our system is a comprehensive database deployed on the server side. This database is instrumental in accumulating and processing traffic data from two main sources.

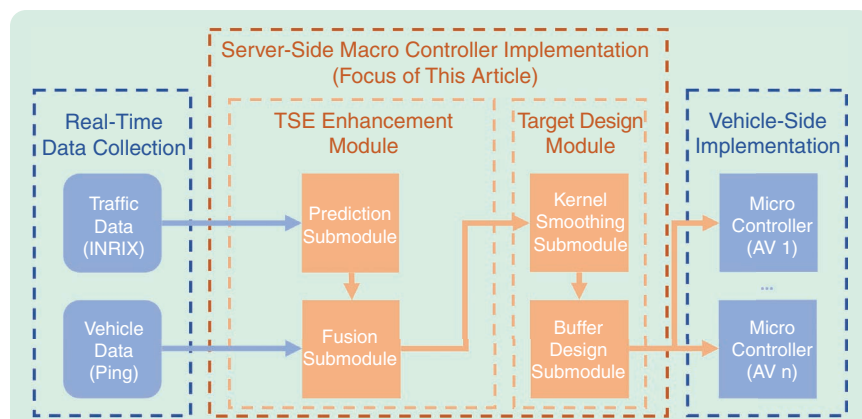


FIGURE 2 The hierarchical framework of the proposed VSL system: The Speed Planner module fetches inputs from the database to generate a real-time target speed profile. The target speed is assigned to vehicle controllers via an application programming interface together with local observations collected by an onboard unit (as the input) to decide the instant vehicle control command.

Macroscopic Traffic State From INRIX

INRIX [2] feeds our system with macroscopic data, presenting average speed metrics for predefined road segments, updated every minute. More details on INRIX data are available in “External Data Source: Average Segment Speed From INRIX.”

Microscopic Observations From Controlled Vehicles

Offering a more detailed view, controlled vehicles provide a microscopic snapshot of the traffic conditions. These vehicles, equipped with onboard detectors, capture data at 0.1-s intervals and relay this information to the central server every second. Each data transmission includes the status of the transmitting vehicle and its perception of its immediate surroundings. Data from GPS, as well as the vehicle state, are gathered directly from vehicle sensors through Libpanda [34], which uses the stream package [35] to decode vehicle data from proprietary formats at runtime. Using custom software bridges [36], a web service that runs as part of vehicle middleware [37] publishes data to the central server on which the speed planner is hosted at approximately 1 Hz.

TSE Module

The TSE serves as the real-time data that represent the traffic status and is employed as the input data for the proposed system. In other words, to refine the accuracy and reliability of the traffic data, we propose a TSE enhancement algorithm that estimates the traffic states based on traffic data (INRIX) infused with vehicle data.

The TSE enhancement module consists of a *prediction* and a *fusion* submodule; [Figure 3](#) shows the detailed relation of these submodules. The prediction submodule mitigates the effects of the latency of INRIX real-time data. The fusion submodule further improves the TSE by introducing real-time data from controlled vehicles’ observations of our system to obtain lane-level TSE with higher time-space resolution.

Prediction Submodule

The prediction module aims to alleviate the effects of the 3-min latency in INRIX data by forecasting the traffic conditions 3 min ahead. The prediction is achieved through a two-phase procedure: *frontier prediction* and *speed value filling*, which are discussed below.

Frontier Prediction

Frontier identification serves as the initial phase within the prediction module, where the historical TSE data are subjected to a systematic analysis

to pinpoint congestion frontiers. The frontiers, visualized in Figure 4(a) and (b), play the role of anchor points for speed slots in between in the prediction.

They manifest as either stationary bottlenecks or dynamic shockwaves that necessitate immediate attention for traffic management. Mathematically, a congestion

External Data Source: Average Segment Speed From INRIX

The application programming interface (API) provided by INRIX delivers a real-time assessment of aggregated velocity for distinct sections of the highway infrastructure. These data undergo regular updating as new information surfaces, thereby facilitating an instantaneous representation of prevailing traffic conditions. As illustrated in Figure S1, a heat map shows the average velocity of vehicles along Interstate 24 (I-24) where the experiment was conducted, updated at an interval of one minute.

Geographical segmentation underpins the operational modules of INRIX data. This implies that highways are separated into various segments, and the average speed is calculated separately for each segment. The segment size can vary, chosen to yield an appropriate level of detail. As an example, a segment could be the section of a highway between two interchanges. In correspondence with each highway segment, INRIX gathers data from vehicles located in the segment, and using these, INRIX computes the average speed. In this article, we adopt the following notation to represent the discrete data we fetched from the INRIX API. At any time t ,

$$\{\bar{v}(t, x_j) : j \in \mathcal{J}\} \quad (\text{S1})$$

where \mathcal{J} represents the collection of INRIX road segments; for any $j \in \mathcal{J}$, x_j is the milepost representing the center of the specific road segment j ; and $\bar{v}(t, x_j)$ is the average speed in the corresponding road segment at time t .

While INRIX's data are invaluable for many applications, especially in traffic analysis, there is an inherent latency in the data when considering real-time control tasks. Given the vast

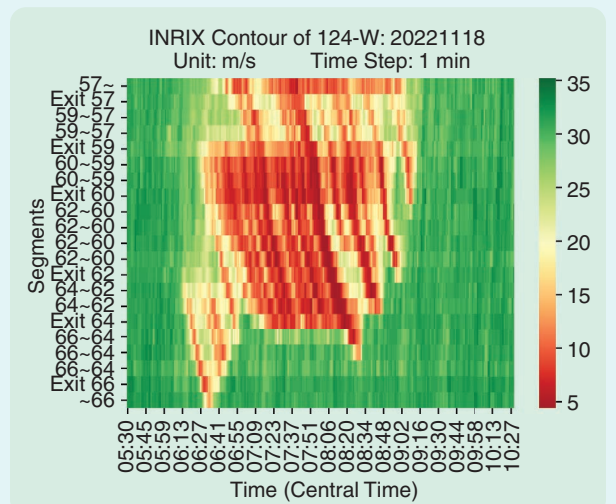


FIGURE S1 A speed heat map of I-24 westbound on 18 November 2022. The color of each cell indicates the average speed of vehicles in the corresponding time-space window. The traffic flow moves from the bottom toward the top. A standing bottleneck can be observed at exit 59.

coverage and the depth of analysis they provide, a latency of 3 min is commendably low. However, for our specific control task, even such a minor delay can be significant. This sensitivity to latency underscores the need for predictive models, like the TSE enhancement module implemented in this study, to anticipate and adjust for these delays, ensuring more accurate real-time TSE.

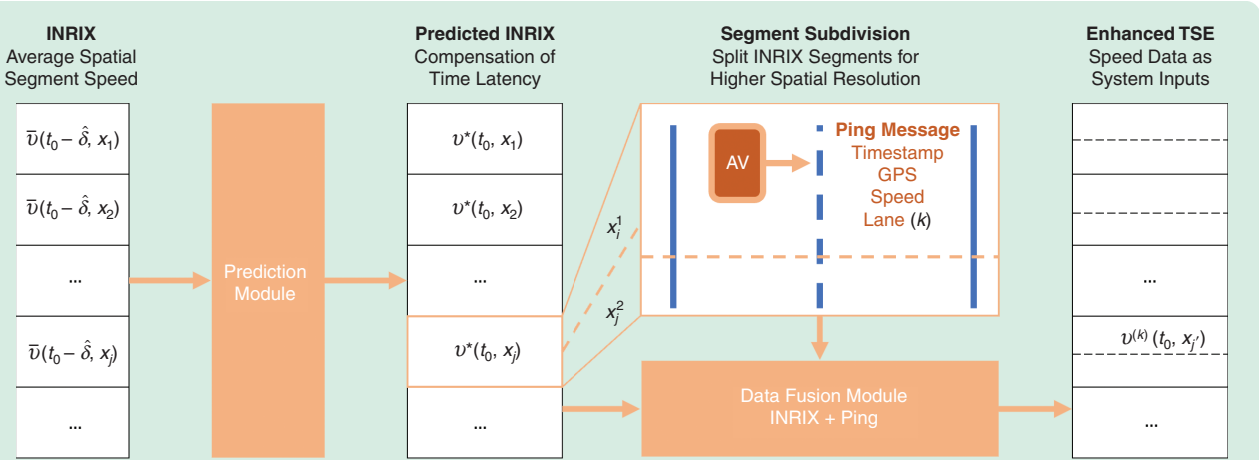


FIGURE 3 The TSE enhancement module: The prediction module utilizes INRIX data to forecast traffic conditions, mitigating latency and enhancing real-time accuracy. The fusion module integrates these predictions with real-time vehicle telemetry to refine the TSE at a higher spatial resolution. The index k indicates the lane number, and j is the index for the subdivision segments in fusion.

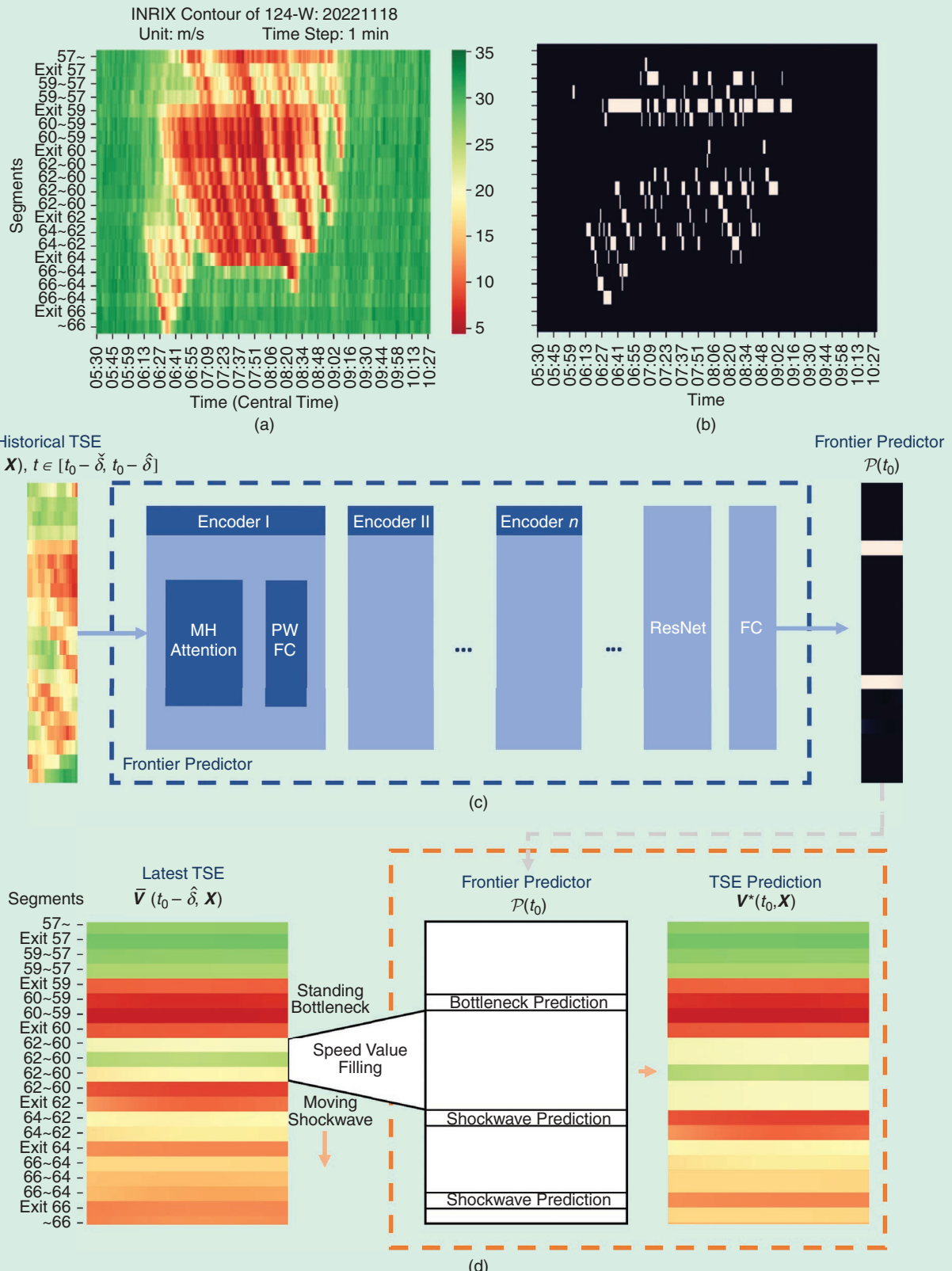


FIGURE 4 The prediction module for TSE enhancement: (a) The INRIX heat map on 18 November 2022 and (b) the congestion frontier identification result. (c) The network architecture of the frontier predictor. (d) Speed filling to obtain the TSE prediction.

frontier is characterized by an abrupt decline in the spatial derivative of velocity with respect to the spatial progression of traffic, exceeding a threshold V_{diff} . For two adjacent segments i, j , the identification criterion for a frontier at segment i is defined by [38] as follows:

$$\begin{cases} x_j - x_i < X_{\text{win}} \\ \bar{v}_k - \bar{v}_i > 0 \\ x_i \leq x_k < x_j \\ \bar{v}_j - \bar{v}_i > V_{\text{diff}} \\ \bar{v}_i < V_{\text{congest}} \end{cases} \quad (1)$$

where x_i values are the i th position, X_{win} represents the maximum spatial window within which traffic conditions are compared, V_{diff} is the minimum defined threshold relative speed required to identify a speed release downstream of wave frontier, and V_{congest} is the upper limit of speed defining congested conditions.

Each inequality in (1) serves a specific purpose in identifying the congestion frontier:

- 1) $x_j - x_i < X_{\text{win}}$: This inequality ensures that the spatial separation between the segments i and j is within a predefined window X_{win} . This window limits the scope of comparison to a local neighborhood, ensuring that only nearby segments are considered when identifying congestion frontiers.
- 2) $\bar{v}_k - \bar{v}_i > 0, \forall k, x_i \leq x_k < x_j$: This condition requires that the average speed \bar{v}_k in any segment k between i and j is higher than the average speed \bar{v}_i in segment i . It ensures that there is an increasing trend in speed from segment i toward segment j , indicating a release in traffic congestion downstream.
- 3) $\bar{v}_j - \bar{v}_i > V_{\text{diff}}$: This inequality establishes that the difference in average speeds between segments i and j exceeds a certain threshold V_{diff} . This threshold is manually chosen and serves to confirm a significant change in speed, which is indicative of a congestion frontier.
- 4) $\bar{v}_i < V_{\text{congest}}$: This condition ensures that the average speed in segment j is below a certain value V_{congest} , which defines congested traffic conditions. This guarantees that segment j is indeed within a congested state.

Based on the identification and tracking of the congestion frontiers, a learning-based predictor is developed to predict the movement of the frontier in the time interval of INRIX latency. The functional mapping \mathcal{P} of the frontier predictor is described as follows. Let $\delta, \hat{\delta} > 0$ be scalars. In addition, let us fix t_o to be the time for which the frontier prediction is desired. Such prediction employs the information on the position and velocity of the road segments in the time interval $[t_o - \delta, t_o - \hat{\delta}]$. More precisely, the predictor defined by the parameter set θ of the

neural network is formalized as a binary-valued function \mathcal{P} in the form of

$$(t, \bar{\mathbf{V}}(t, \mathbf{X})) \mapsto \mathcal{P}(t_o) \stackrel{\text{def}}{=} \mathcal{P}(t, \bar{\mathbf{V}}(t, \mathbf{X}); \theta) \in \{0, 1\}^{|\mathcal{J}|} \quad (2)$$

for $t \in [t_o - \delta, t_o - \hat{\delta}]$ and where

$$\bar{\mathbf{V}}(t, \mathbf{X}) \stackrel{\text{def}}{=} \begin{pmatrix} \bar{v}(t_o - \delta, x_1) & \dots & \bar{v}(t_o - \delta, x_{|\mathcal{J}|}) \\ \vdots & \dots & \vdots \\ \bar{v}(t_o - \hat{\delta}, x_1) & \dots & \bar{v}(t_o - \hat{\delta}, x_{|\mathcal{J}|}) \end{pmatrix} \quad (3)$$

where $|\mathcal{J}|$ is cardinality of set \mathcal{J} , $\bar{v}(t, x_j)$ are defined as in (S1) (in “External Data Source: Average Segment Speed From INRIX”), and \mathbf{X} is the set of spatial segments. The network parameters θ encapsulate the weight matrices, bias vectors, and the parameters of the self-attention and feed-forward layers, optimized during the training phase.

Neural network architecture: The neural network’s architecture comprises multiple encoding layers, each designed to discern complex traffic patterns. The structure, as shown in Figure 4(c), includes a sequence of encoders with multihead (MH) self-attention mechanisms and positionwise fully connected (PW-FC) networks. This can be formalized as

$$\mathbf{H}^{(l+1)} = \text{PW} - \text{FC}(\text{MH attention}(\mathbf{H}^{(l)})) \quad (4)$$

where $\mathbf{H}^{(l)}$ is the hidden state matrix of the l th layer, and $\mathbf{H}^{(0)}$ is the historical TSE $\bar{\mathbf{V}}(t, \mathbf{X})$, with $t \in [t_o - \delta, t_o - \hat{\delta}]$ as the model input. Residual connections (ResNet) and FC layers are used in the decoder to translate features in the hidden state into frontier predictions. The decoder can be formalized as

$$\mathcal{P}(t_o) = \text{FC}(\text{ResNet}(\mathbf{H}^{(\text{encoder})})). \quad (5)$$

Training and validation: The network is calibrated on the INRIX dataset collected from 1 January 2021 to 28 October 2022, with frontiers labeled via the approach in (1). The objective function is configured as a binary cross-entropy loss, defined by

$$\mathcal{L}(\theta) = - \sum_i [y_i \log(\hat{y}_i) + (1 - y_i) \log(1 - \hat{y}_i)] \quad (6)$$

where y_i is the ground truth label of frontier presence, and \hat{y}_i is the i th element of $\mathcal{P}(t_o)$, that is, the prediction of the i th data point being a congestion frontier.

Speed Filling Between Frontiers

To accurately fill the speed values between predicted congestion frontiers, we utilize historical data stored on the server to identify and classify these frontiers. A location continuously recognized as a congestion frontier is marked as a standing bottleneck. Conversely, if a frontier consistently moves upstream at a relatively uniform speed,

it is identified as a shockwave. Recognizing these types of congestion frontiers is essential for accurately filling speed values between them and tailoring countermeasures in the target speed profile.

The process of speed filling involves using the predicted positions of the frontiers as anchor points and interpolating the speed values between these points. The lengths between two frontiers in the INRIX data and the predicted frontiers may differ. To manage such discrepancy, we map the speed values from the INRIX data to the corresponding relative positions in the gap between the predicted frontiers. Mathematically, if the distance between two frontiers in the INRIX data is denoted by x_I and the distance between the corresponding predicted frontiers is x_P , then the mapping of the speed values is given by

$$v_P(x) = v_I \left(\frac{\Delta x_I}{\Delta x_P} x \right), x \in [0, x_P].$$

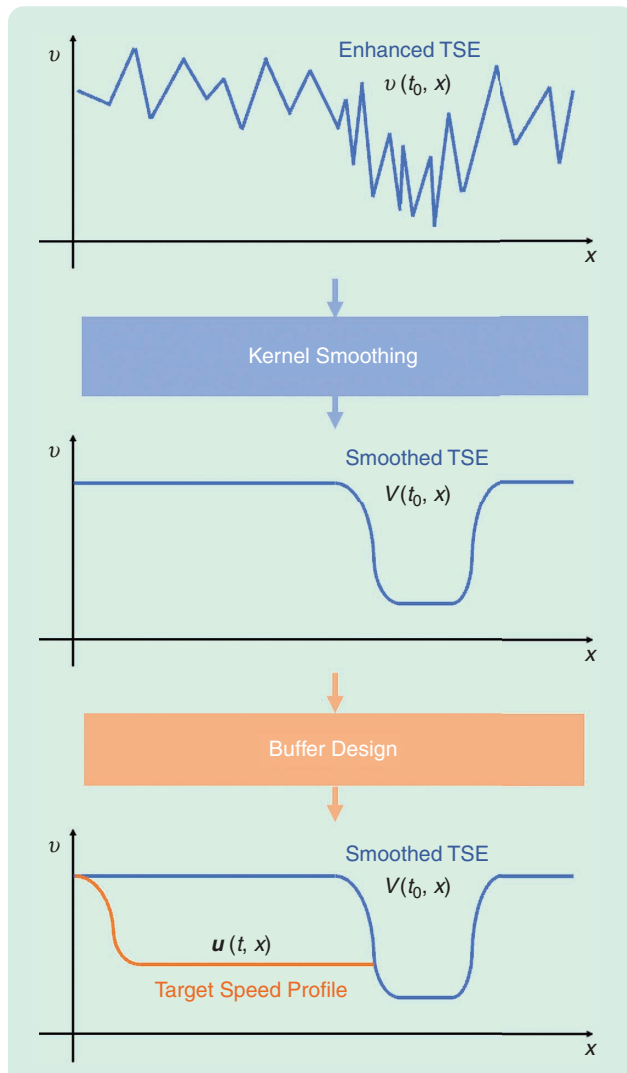


FIGURE 5 A schematic of the target design module. The target speed $\mathbf{u}(t, x)$ is defined in the “[Buffer Design Submodule](#)” section.

Here $v_P(x)$ is the predicted speed value at position x based on the INRIX speed value v_I between two frontiers adjusted for the relative distance. This mapping ensures that each speed value in the latest TSE is correctly aligned with the corresponding position in the TSE prediction.

[Figure 4\(d\)](#) illustrates this process, where the speed values in the slots of the latest TSE are mapped proportionally to the corresponding entries in the TSE prediction. This ensures that the filled speed values reflect the predicted traffic conditions, enabling the speed planner to generate a more reliable target speed profile for controlling vehicle speeds.

Fusion Submodule

To achieve a higher spatial resolution for lane-level TSE, we further segment the INRIX data into smaller subsegments; see [Figure 3](#) for the connection between prediction and the fusion submodules. Mathematically, we define a set \mathcal{J}' , the collection of discretized positions of the road, such that if $j, j+1 \in \mathcal{J}'$ and $j, j+1 \in \mathcal{J}$, then

$$|x_{j'+1} - x_j| < |x_{j+1} - x_j| \quad (7)$$

and \mathcal{J} are defined in [\(S1\)](#). In other words, the segments $[x_j, x_{j+1}]$ are further divided into smaller subsegments $[x_j, x_{j'+1}]$. Once the INRIX prediction is obtained, it is merged with real-time observations from controlled vehicles. In each target speed profile updating cycle, we obtain 30 ping records from each vehicle. These records compute each vehicle’s average speed over the past update interval, subsequently overwriting the TSE of the corresponding subsegment. Given that vehicle lane data are included in the pings, a distinct TSE is created for each lane by augmenting the corresponding vehicle’s observations with the overarching INRIX prediction. The INRIX data are incorporated by the controlled vehicle’s data for transparency and controllability of the system.

The output of the TSE enhancement at any fixed time t will be a collection of discrete data denoted by $\{v^{(k)}(t, x_j) : j \in \mathcal{J}', k = 1, 2, 3\}$, where \mathcal{J}' is defined in [\(7\)](#), and index k refers to the lane number [cf. [\(S1\)](#)].

Hierarchical coordinated speed planning for connected autonomous vehicles can be performed even in the absence of vehicle to vehicle coordination using commercial traffic data.

Target Design Module

The enhanced TSE is used in the design of a module to generate the target speed profile for the controlled vehicles. This section introduces the major function submodules, including kernel-based smoothing, learning-based buffer design, and the optimization-based planner. In particular, the irregularity of the traffic flow can be attributed to two traffic scenarios, 1) shockwaves and 2) standing bottlenecks. For each case, we introduce a specific speed profile strategy. [Figure 5](#) illustrates the target design module overview.

The *kernel smoothing submodule* processes the enhanced TSE at each time step using a chosen kernel to alleviate the oscillation caused by shockwaves in congested traffic status. In particular, the kernel smoothing submodule is specifically designed to improve such oscillations to prevent the inefficiencies caused by the propagation of the underlying shockwaves.

The *buffer design submodule*, on the other hand, utilizes RL to form a buffer area upstream of the standing bottleneck with the goal of improving *density* and *flow* at the bottleneck location. This design is an important part of managing traffic congestion at bottlenecks, where traffic tends to accumulate and slow down. Acting as the simulated environment dynamic for the RL training, the mathematical model of traffic is represented by a strongly coupled *partial and ordinary differential equation (PDE-ODE)*.

We now look into each of these modules in more detail.

Kernel Smoothing Submodule

The purpose of kernel smoothing is to create a speed profile that reduces the adverse effects of shockwaves and fuel inefficiency. The approach being proposed builds upon and enhances previous heuristic methods related to traffic flow harmonization [15], [39], [40], [41]. These methods suggest that traffic can be made more uniform at its desired driving speed by controlling a select group of vehicles to operate close to the accurate predictions of said speed.

To cover the lack of communication capability among all vehicles in mixed-autonomy conditions, we rely on enhanced TSE data to synchronize the driving speeds of AVs. In particular, vehicles are assigned target speed profiles contingent on traffic state information, which is shared and common among all AVs.

At any fixed time step t , a speed profile $\mathbf{v} : \mathbb{R}_+ \times \mathbb{R} \rightarrow \mathbb{R}_+$ is calculated from the enhanced TSE speed profile, $v^{(k)}(t, x_j)$ for $j \in \mathcal{J}'$, $k = 1, 2, 3$, and by employing kernel smoothing methods.

Remark 1

We note that the operations described in the following sections are the same for each lane and that the spatial segment division \mathcal{J}' [defined as in (7)] will not change. For simplicity of the notation, we drop the superscript (k) and denote the enhanced TSE speed data by $v(t, x_j)$.

First, we preprocess the sparse TSE data by interpolating the discrete spatial data $v(t, x_j)$ for $j \in \mathcal{J}$ to a continuous *so-called TSE speed profile* $(t, x) \in \mathbb{R}_+ \times \mathbb{R} \mapsto v(t, x)$, as an approximation of the average speed of higher-granularity traffic at a position x and at time t . Then, for any fixed time $t = t_o$, by applying a kernel function $K(\cdot)$ at a position $x = x_\alpha$, we obtain a speed profile of the form

$$\mathbf{v}(t_o, x_\alpha) = \frac{\int_{x=x_\alpha}^{x_\alpha+\mu} K(x_\alpha, x) v(t_o, x) dx}{\int_{x=x_\alpha}^{x_\alpha+\mu} K(x_\alpha, x) dx} \quad (8)$$

where μ is the width of the estimation window. Many different kernel functions, such as Gaussian kernel, triangular kernel, quadratic kernel, uniform kernel, etc., can be chosen. For the purposes of this article, we consider a uniform kernel, the simplest and most practical of such mapping. The *kernel smoothing speed profile at a position x_α* is accordingly defined as

$$\mathbf{v}(t_o, x_\alpha) = \frac{\int_{x=x_\alpha}^{x_\alpha+\mu} v(t_o, x) dx}{\mu}. \quad (9)$$

As demonstrated in Figure 5, kernel smoothing significantly dampens speed oscillations, effectively reducing both the frequency and the magnitude of accelerations and decelerations. This reduction in velocity fluctuations contributes directly to lower energy consumption by promoting a more constant speed, thereby enhancing fuel efficiency [42].

Buffer Design Submodule

When the frontier identification determines a standing bottleneck, the broad idea is to design a buffer area to minimize congestion (density) at the location of the bottleneck.

From the perspective of speed planning, the problem caused by congestion can be interpreted as a reduction in system efficiency due to the uneven distribution of traffic density in the time-space domain: the bottleneck causes a throughput reduction due to the high density of the queue area, and shockwaves cause the waste of energy due to the propagation of high-density waves. The speed planner achieves traffic flow efficiency by recommending target speeds to the controlled vehicles to regulate the traffic flow and improve the distribution of the density around the bottleneck location.

In this section, we detail the buffer area design process from a theoretical standpoint. We consider the interval $\mathcal{I} \subset \mathbb{R}$ as the region of interest. In addition, we consider a subregion $\mathcal{I}_c \subset \mathcal{I}$ as a congested area (see Figure 6). The idea is to determine the controlled vehicle target speed at a time step t_o , denoted by $\mathbf{u}(t_o, x)$, such that the density $\rho(t, x)$ for $x \in \mathcal{I}_c$ and $t \geq t_o$ is less concentrated at the location of the bottleneck and distributed in a more uniform way through the region \mathcal{I} . The main components of this submodule are summarized below.

- 1) *Designing the speed profile:* A target speed profile $\mathbf{u}(t_o, x)$ is developed for controlled vehicles, using inputs from the kernel smoothing speed profile $\mathbf{v}(t_o, x)$ to manage congestion by preventing the high concentration of the density around the bottleneck location.
- 2) *Mathematical model:* Using the designed speed profile $(t, x) \mapsto \mathbf{u}(t, x)$, a PDE-ODE model is developed to simulate traffic dynamics and calculates the density $\rho(t, x)$ and flow $f(\gamma, \rho)$. In particular, by predicting the behavior of traffic statistics, this mathematical model is used to train the RL for designing efficient control strategies.

- 3) *Training*: An actor–critic (AC) algorithm is employed to train the RL policy for optimizing the buffer design. The actor proposes actions based on the target density ρ_b , while the critic evaluates these actions to maximize the bottleneck throughput. The policy is iteratively improved based on the results predicted by the mathematical model.

Figure 7 indicates the data pipeline of the buffer design module in the training loop and the MVT implementation

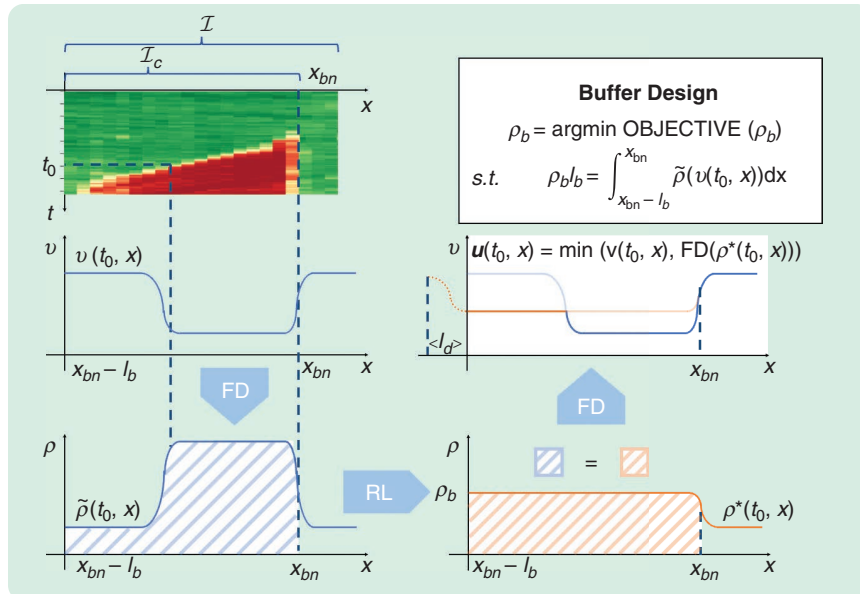


FIGURE 6 Obtaining the target speed profile: Once a standing bottleneck is identified, the speed profile $v(t, x)$ is converted to the density profile $\tilde{\rho}(t, x)$ by using a calibrated fundamental diagram (FD). RL policy selects the desirable density for the buffer area ρ_b based on $\tilde{\rho}(t, x)$, which is the critical parameter to determine a desirable density profile $\rho^*(t, x)$. The target speed profile is obtained by converting $\rho^*(t, x)$ to the speed profile and taking the minimum value at each position. The objective function adopted in this study is the average density at the target bottleneck.

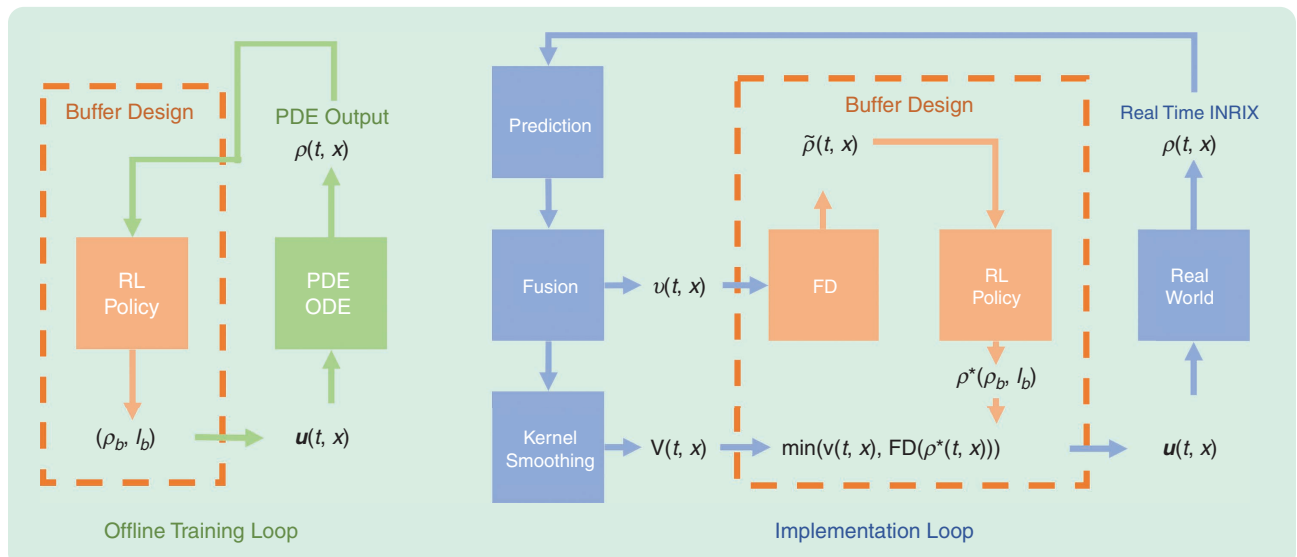


FIGURE 7 The training and field-testing pipeline of the buffer design module.

loop separately, which will be detailed in the “Designing the Speed Profile” section. A noteworthy difference is the TSE representation: in the training loop, the environment mechanism modeled by PDE-ODE takes the target speed profile as input and identifies the density profile $\rho(t, x)$ as the next step input. In the field test implementation, given that the available TSE only provides the estimation of the average speed in road segments, a mapping from speed to density, that is, a *fundamental diagram* (FD) in traffic flow theory [43], [44], is modeled to estimate the traffic density at different locations of the road. The FD model converts the estimation of the speed profile into the density profile of each road segment, that is, $v(t, x) \xrightarrow{\text{FD}} \tilde{\rho}(t, x)$ (see Figure 7). The Greenshields FD [45] was adopted and calibrated using the roadside speed radar data collected from 29 June 2021 to 29 November 2021 provided by the Tennessee Department of Transportation [46].

Designing the Speed Profile

Following the TSE enhancement and kernel smoothing, we find the congestion frontiers. If a standing bottleneck is identified, the lane-level TSE will be considered as an input for the buffer design module to generate a target speed profile. The spirit of buffer design is to inform the vehicles to start decelerating in advance when driving into congestion.

The buffer area is determined by two critical parameters: the desired

density ρ_b and the buffer length l_b . From the density profile, the continuous upstream sections of the bottleneck whose density exceeds a preset threshold are identified as a queue area, as shown in [Figure 6](#). To distribute the density evenly in the queue area upstream, ρ_b and l_b should be designed to satisfy the following equality:

$$l_b(t_o) = \frac{1}{\rho_b(t_o)} \int_{x_{bn}-l_b}^{x_{bn}} \rho(t_o, x) dx \quad (10)$$

where x_{bn} denotes the location of the standing bottleneck, and the desired density ρ_b is the control variable for the designed optimizer. If ρ_b is controlled, then the length of the buffer area l_b could be obtained by recursively solving (10). In the implementation phase, the integrand will be replaced by $\bar{\rho}(t_o, x)$, the observed density (see [Figure 7](#)).

A deceleration area connects the buffer area with the noncongested areas upstream to ensure that traffic decelerates smoothly while driving into the buffer area and prevents secondary shockwaves from being generated in this process. The deceleration area is designed in the time-speed domain and determined by two elements: the desired constant decelerate rate a_d and the deceleration area length l_d , which can be calculated by solving

$$l_d(t_o) = \frac{1}{2a_d} \{(\mathbf{v}(t_o, x_{bn} - l_b - l_d))^2 - (\mathbf{v}(t_o, x_{bn} - l_b))^2\}.$$

In MVT, we designed the controller utilizing the RL algorithm with a PDE-ODE based environment mechanism to dynamically update the parameters of target speed profiles according to real-time traffic conditions.

To apply the RL algorithm, we model the problem into a *Markov decision process (MDP)* problem [\[47\]](#). A finite MDP problem can be represented by a tuple $\mathcal{P}(\mathcal{S}, \mathcal{A}, P, R)$. For agents in MDP at any time step t_o , applying an action $a(t_o) \in \mathcal{A}$ to the observed state $s(t_o) \in \mathcal{S}$ results in a new state $s(t_o + 1)$ with probability $P(s(t_o + 1) | (s(t_o), a(t_o)))$ and a reward function $r(t_o) = R(s(t_o), a(t_o), s(t_o + 1))$. After updating the current state to $s(t_o + 1)$, the process will be repeated until the end criteria of the episode are met. In our problem setting, the state space \mathcal{S} is the enhanced and smoothed TSE defined as the speed profile $\mathbf{v}(t_o, x)$; the action space \mathcal{A} is the domain of the definition of the desired density ρ_b , which corresponds to the target speed $\mathbf{u}(t_o, x)$ as shown in [Figure 6](#). The policy then selects one value from the action space \mathcal{A} that will be used to design the buffer area in the target speed profile; the reward function is the throughput at the bottleneck. The transfer of state $\mathcal{P}(\mathcal{S}, \mathcal{A}, P, R)$ is obtained by solving the underlying mathematical model of traffic [see (11)]. The policy $\pi: s \in \mathcal{S} \rightarrow \mathcal{A}$ is a mapping from the state space \mathcal{S} to the action space \mathcal{A} . The objective of the MDP problem is to find the optimized policy π^* to maximize the total reward (expectation) and

calculate the target speed $\mathbf{u}(t_o, x)$ based on the observed state in a fixed time step t_o .

The Mathematical Model of Traffic Flow and Density

The behavior of the traffic flow in the presence of controlled vehicles will be modeled using a mathematical (dynamical) model comprising a PDE-ODE. Such problems are studied both in engineering communities [\[48\], \[49\], \[50\]](#) and from a mathematical point of view [\[18\], \[51\], \[52\], \[53\], \[54\]](#). In particular, for $(t, x) \in \mathbb{R}_+ \times \mathbb{R}$ and $i \in \{1, \dots, N\}$, we consider the traffic dynamics of the form

$$\begin{cases} \rho_t + [f(\gamma, \rho)]_x = 0 \\ \rho(0, x) = \rho_o(x) \\ \dot{y}_i(t) = w(y_i(t), \rho(t, y_i(t) +)) \\ y_i(0) = y_{o,i} \\ f(\rho(t, y_i(t))) - \dot{y}_i(t) \rho(t, y_i(t)) \leq F_\alpha(y_i, \dot{y}_i). \end{cases} \quad (11)$$

The PDE in (11) is the classical LWR model [\[55\], \[56\]](#) augmented with a discontinuous flux. We divide the highway \mathcal{I} into $M + 1$ subregions I_m , for $m \in \{0, \dots, M\}$. The function $\gamma(x)$ represents the maximal speed $V_{\max}^{(m)}$ in each region I_m , $m \in \{0, \dots, M\}$ of the road, and it is considered to be piecewise constant; that is, $\gamma(x) = V_{\max}^{(m)} = \gamma_m$ for each m .

Remark 2

Note that during MVT the speed limit remains constant; that is, $\gamma(x) = V_{\max}$ for all $x \in \mathcal{I}$. However, in this description, we adopt a more general analytical approach.

Function $(t, x) \in \mathbb{R}_+ \times \mathbb{R} \mapsto \rho(t, x) \in [0, \rho_{\max}]$ denotes the density function. The flux function $f: \{\gamma_0, \dots, \gamma_M\} \times [0, \rho_{\max}] \rightarrow \mathbb{R}_+$ is defined by

$$f(\gamma, \rho) \stackrel{\text{def}}{=} \gamma \rho \left(1 - \frac{\rho}{\rho_{\max}}\right) = \rho v(\gamma, \rho). \quad (12)$$

The mean traffic speed $v: \{\gamma_0, \dots, \gamma_M\} \times [0, \rho_{\max}] \rightarrow \mathbb{R}_+$ is defined by

$$v(\gamma, \rho) \stackrel{\text{def}}{=} \gamma \left(1 - \frac{\rho}{\rho_{\max}}\right). \quad (13)$$

It should be noted that in (13), $v(\gamma, \rho_{\max}) = 0$ and $v(\gamma, 0) = \gamma$, the maximum permitted speed.

The ODEs describe the trajectories of the N controlled vehicles. In particular, the function $t \mapsto y_i(t)$ denotes the trajectory of the i th AV at time t . Then, for $i = 1, \dots, N$ we define the velocity of the controlled vehicle by

$$w(y_i, \rho) \stackrel{\text{def}}{=} \min\{V(y_i), v(\gamma(y_i), \rho)\} \quad (14)$$

where $v(\gamma, \rho)$ is defined as in (13), and $V(\cdot)$ is the speed of the controlled vehicle such that $V^{(m)} = V(x) \stackrel{\text{def}}{=} \mathbf{u}(t_o, x)$ for $x \in I_m$, where the target speed $\mathbf{u}(t_o, x)$ (RL suggested speed) at the time step t_o is the maximal speed of the controlled vehicle at any $x \in \mathcal{I}$ region and at the current time step.

The inequality in (11) represents the reduction of the flow caused by the controlled vehicles. In particular, for any $i = 1, \dots, N$,

$$\begin{aligned} F_\alpha(y_i, \dot{y}_i) &\stackrel{\text{def}}{=} \operatorname{argmax}_\rho \{ f_\alpha(\gamma(y_i(t)), \rho) - \dot{y}_i(t)\rho \} \\ &= \frac{\alpha\rho_{\max}}{4\gamma(y_i(t))} (\gamma(y_i(t)) - \dot{y}_i(t))^2 \end{aligned} \quad (15)$$

where

$$f_\alpha(\gamma, \rho) \stackrel{\text{def}}{=} \gamma\rho \left(1 - \frac{\rho}{\alpha\rho_{\max}}\right), \quad \alpha \in (0, 1). \quad (16)$$

Here α represents the reduction rate of the capacity caused by the controlled vehicles.

Theorem 1 (Existence of Solution)

Let the initial condition $\rho_0 \in BV(\mathbb{R}; [0, \rho_{\max}]) \cap L^1(\mathbb{R})$. Then, there exists an n -tuple $(\rho, y_i) \in C(\mathbb{R}_+, L^1_{\text{loc}}(\mathbb{R}; [0, 1])) \times W^{1,1}_{\text{loc}}(\mathbb{R}_+, \mathbb{R})$ for $i = 1, \dots, N$ that weakly solves the Cauchy problem (11) in the sense that it satisfies the following:

- 1) Function $(t, x) \mapsto \rho(t, x)$ satisfies

$$\int_{\mathbb{R}_+} \int_{\mathbb{R}} (\rho \partial_t \varphi + f(\gamma, \rho) \partial_x \varphi) dx dt + \int_{\mathbb{R}} \rho_0(x) \varphi(0, x) dx = 0$$

for all $\varphi \in C_c^\infty(\mathbb{R}_+ \times \mathbb{R})$.

- 2) The function y_i for $i = 1, \dots, N$ is a Carathéodory solution, that is, for a.e. $t \in \mathbb{R}_+$, in (11),

$$y_i(t) = y_{0,i} + \int_0^t \omega(y_i(s), \rho(s, y_i(s))) ds.$$

In other words, $y_i \in \mathcal{A}_c([0, T]; \mathbb{R})$ for any $T > 0$, where \mathcal{A}_c is the class of absolutely continuous functions.

Algorithm 1: RL Policy Training Procedure

- 1: Initialize Actor parameters θ and Critic parameter w
- 2: Initialize a speed profile $v(t_0, x)$ at a fixed time step t_0 .
- 3: **while** not terminated **do**
- 4: Choose desire density ρ_b using policy π_θ
- 5: Obtain target speed profile and implement to controlled vehicles.
- 6: Obtain the bottleneck throughput as r and the TSE of next step $v(t_0 + 1, x)$ by solving (11)
- 7: Compute the Critic's TD error:
$$\delta = r + \gamma A_w(v(t_0 + 1, x)) - A_w(v(t_0, x))$$
- 8: Update the Actor's parameters:
$$\theta \leftarrow \theta + \alpha \delta \nabla_\theta \log \pi_\theta(\rho_b | v(t_0, x))$$
- 9: Update the Critic's parameters:
$$w \leftarrow w + \beta \delta \nabla_w A_w(v(t_0, x))$$
- 10: $v(t_0, x) \leftarrow v(t_0 + 1, x)$
- 11: **end while**

- 3) The bottleneck constraint is satisfied in the sense that for a.e. $t \in \mathbb{R}_+$,

$$\lim_{x \rightarrow y_i(t)^\pm} f(\gamma(x), \rho(t, x)) - \rho(t, x) \dot{y}_i(t) \leq F_\alpha(y_i(t), \dot{y}_i(t)).$$

The complete proof of Theorem 1 can be found in [21].

Training the Performance of the Speed Profile

In the training step, two updates are considered. First, the density function $\rho(t, x)$ is used in calculating $v(t_0 + 1, x)$. Second, as defined in MDP, the performance of the policy, that is, the reward function $r(t_0) = R(s(t_0), a(t_0), s(t_0 + 1))$, is evaluated by the density/flow at the bottleneck. The AC algorithm was adopted in *evaluating and updating* the policy for target speed profile generation. In this section, we discuss the structure of the applied AC algorithm and detail the mechanism for updating policy parameters.

The AC algorithm comprises two primary components: the actor and the critic. The actor is responsible for determining the actions based on the current policy, whereas the critic evaluates these actions by computing the value function.

- 1) **Actor:** Given a TSE $v(t_0, x)$, the actor outputs a distribution over possible desired density according to a policy denoted by $\pi_\theta(\rho_b | v(t_0, x))$, where θ is the policy parameter.
- 2) **Critic:** The critic estimates a value function denoted by $A_w(v(t_0, x))$ of the current state, where w is the value function parameter. This function represents the expected cumulative bottleneck throughput from state $v(t_0, x)$ onward.

The actor is updated by performing gradient ascent on the expected cumulative reward. The parameter update procedure is shown in Algorithm 1.

Microcontroller Design

Another important component of the proposed hierarchical VSL framework is the microscopic traffic control algorithms deployed in individual vehicles. In the most general sense, these controllers receive the target speed information, as well as locally sensed input from the vehicle's surroundings, and produce an acceleration control signal to drive the vehicle. Jang et al. [57] detail the methodology of the RL-based vehicle controller tested in MVT.

The controller in [57] will be used to produce the simulation results in the "Numerical Experiments" section. This controller was also used in the road experiments reported in the "Field Test Analysis" section. More details about the adopted microcontroller are available in "RL-Based Microcontroller." It is worth pointing out that the controller is assumed to be fully engaged during the simulation test. However, in the field test, the human drivers on the controlled AV are authorized to disengage and reengage the controller according to their onboard observations. The engagement rate is observed as a critical factor affecting the overall system performance.

RL-Based Microcontroller

INTRODUCTION

Here we provide an in-depth overview of the methodologies employed in the RL-based traffic control system designed for the MVT. The research explores the development and implementation of two distinct RL controllers for AVs to mitigate traffic congestion and improve flow dynamics and energy efficiency on highways.

RL FRAMEWORK

The RL framework used in this study encompasses the development of an environment where agents (AVs) interact through a series of states, actions, and rewards. We further consider the partially observable states where agents are only given partial observations of the state, akin to real-world conditions. This scenario is typically modeled as a partially observable MDP (POMDP), defined as

$$\mathcal{P} = (\mathcal{S}, \mathcal{A}, T, R, \gamma, \Gamma, O) \quad (S2)$$

where \mathcal{S} is the set of states representing the possible traffic conditions, \mathcal{A} is the set of possible actions an AV can take, T is the transition probability between states conditioned on actions taken, R is the reward function, $\gamma \in (0, 1)$ is the discount factor, Γ is the set of partial observations of the state, and O maps states to observations. We typically model an agent π using a neural network with parameters θ that outputs the mean and variance of a Gaussian kernel: $(\mu, \sigma^2) = \pi_\theta(o_t)$, where o_t is the observation at time t . An action is then sampled as $a_t \sim \mathcal{N}(\mu, \sigma^2)$ where \mathcal{N} is a Gaussian, leading to a reward r_t and a next observation o_{t+1} . The goal of the optimization process is to maximize with respect to θ the expected cumulative discounted reward $\mathbb{E}_{\tau \sim (\mathcal{P}, \pi_\theta)} [\sum_{t \geq 0} \gamma^t r_t]$ over trajectories τ generated by the POMDP and the agent. Posttraining, the control is rendered deterministic, with actions $a_t = f_\theta(o_t)$ equal to μ in the output of π_θ .

CONTROLLER DESIGN

Two classes of controllers were designed:

- 1) *Acceleration-based controller*: This controller adjusts the acceleration of each AV based on the relative velocity and position of the leading vehicle. The control action a_t at time t is defined by

$$a_t = f_\theta^{\text{accel}}(v_t, \Delta v_t, h_t) \quad (S3)$$

where v_t is the AV's velocity, Δv_t is the velocity difference to the leading vehicle, and h_t is the positional gap.

- 2) *Adaptive cruise control-based controller*: Leveraging adaptive cruise control (ACC) systems, this controller focuses

on maintaining a safe following distance while optimizing speed according to traffic conditions. The target speed v_{target} is dynamically adjusted based on both immediate and upstream traffic data to improve the overall traffic flow and fuel efficiency:

$$v_{\text{target}} = f_\theta^{\text{ACC}}(v_t, \Delta v_t, h_t, v_t^{\text{target}}, h_t^{\text{safe}}) \quad (S4)$$

where v_t , Δv_t , and h_t are defined as previously; v_t^{target} is the AV's target speed computed from traffic density metrics; and h_t^{safe} is a safe following distance. The target speed v_t^{target} given by the speed planner largely contributes to reducing the partial observability of the system by giving the agent significant information about the state of the road network.

SIMULATION AND TRAINING

Before deployment, both controllers underwent rigorous training and validation in simulated environments designed to mimic various traffic patterns and densities. The simulation was designed to replay real-world trajectories collected on the highway, coupled with string-unstable car-following models to replicate realistic wave propagation dynamics. The agent then learns to dissipate waves in this simulation and to optimize its reward function through iterative feedback.

REWARD FUNCTION DESIGN

Critical to training RL agents, the reward function was designed to promote both traffic flow efficiency and safety while driving smoothly and adhering to human social norms. It was defined to penalize high acceleration and deceleration events, close following distances, and deviations from optimal speed planner speeds:

$$R(a_t) = -\alpha |a_t| - \beta |h_t - h_t^{\text{safe}}| - \gamma |v_t - v_t^{\text{target}}| \quad (S5)$$

where α, β , and γ are coefficients that balance safety, comfort, and efficiency.

DEPLOYMENT

Following the simulation phase and extensive software and hardware validation and testing, the trained controllers were connected with the speed planner proposed in this article, implemented within a fleet of 100 AVs, and tested in a controlled field operational test (MVT) on public highways. This deployment aimed to evaluate the practical viability of the RL models under real-world conditions, adjusting traffic dynamics in real time to alleviate congestion and enhance flow continuity.

NUMERICAL EXPERIMENTS

We design an array of experiments to numerically evaluate the performance of the proposed VSL framework. We also investigate the robustness of this framework to common limitations in traffic state data that are encountered in practice such as latency and noise.

Simulator

To test our controller, we built a mixed-autonomy numerical simulator that represents the road portion of the I-24 highway shown in Figure 11; see [58] for details on the design of the simulator. The simulator was designed for a single-lane scenario where two types of vehicles were modeled: human-driven vehicles, whose longitudinal behavior is governed by a car-following model, and AVs, whose behavior is governed by the controller described previously. For modeling human behavior, we use the well-known *intelligent driver model* (IDM) [59].

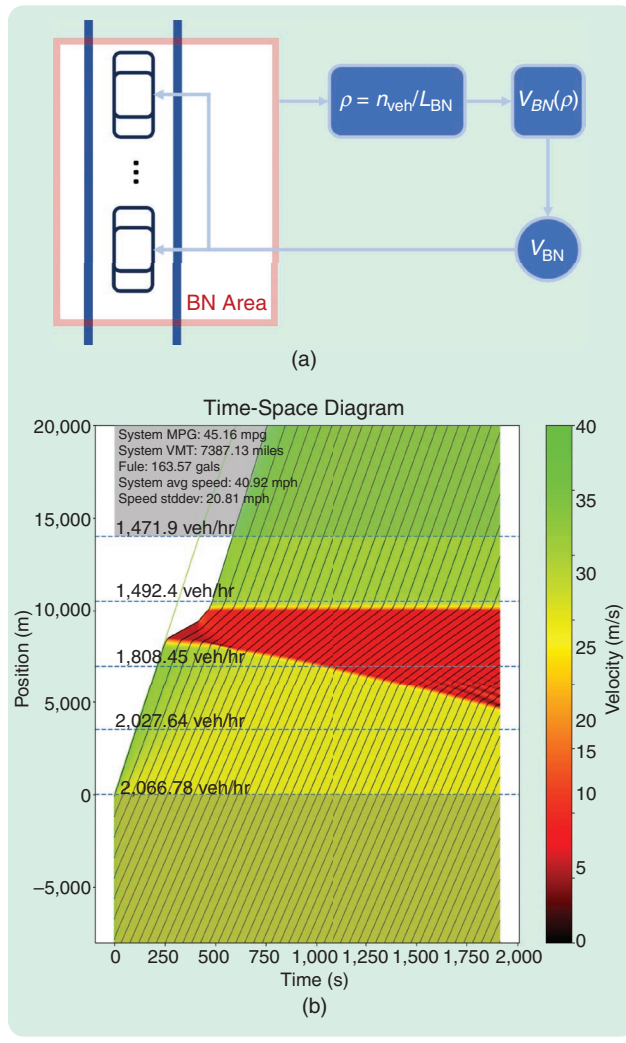


FIGURE 8 The benchmark scenario: (a) a flowchart illustrating the process of the bottleneck simulation and (b) a time-space diagram for the benchmark scenario.

Test Environment

The proposed VSL framework is evaluated on a baseline scenario involving a standing bottleneck in highway merging. The test environment consisted of a 600-meter-long single-lane weaving area where we implemented a forced speed limit to emulate the characteristics of a bottleneck. The simulation worked as follows: At each time step, we calculated the instantaneous density ρ within the bottleneck area using the number of vehicles n_{veh} and the length of the bottleneck area L_{BN} . Then, we derived the corresponding bottleneck speed V_{BN} using an FD, calibrated using field data from I-24. The baseline scenario simulated 1,500 human-driven vehicles, each modeled with the IDM [13], [60], over a span of 2,000 s. Figure 8(a) provides an overview of the process, and Figure 8(b) shows the time-space diagram for the benchmark scenario.

Evaluation Metrics

The effectiveness of the proposed method was evaluated based on several metrics to provide a comprehensive assessment of system performance.

Density

As the major objective, the average density was measured to assess the concentration of vehicles in the traffic flow. This metric is essential for understanding the distribution and accumulation of traffic over different segments of the road.

Throughput

We calculated the throughput at various positions along the road, specifically downstream, in the middle, and upstream of the bottleneck area. Throughput, which is the number of vehicles passing through a point or segment of the road per unit of time, is a direct measure of traffic flow efficiency.

Miles Per Gallon

The system's miles per gallon (MPG) is another key metric for assessing the fuel efficiency of the vehicles within the simulation. A higher MPG indicates better fuel economy and, by extension, improved environmental sustainability.

Vehicle Miles Traveled

We also considered the system's vehicle miles traveled (VMT), a measure of the total distance traveled by all vehicles in the system over the simulation time.

System Average Speed

The system average speed was calculated to evaluate the general speed at which vehicles were able to travel within the domain of the simulation.

Speed Standard Deviation

We also assessed the standard deviation of the speed, providing a measure of the variability in vehicle speeds.

A lower standard deviation indicates more uniform speeds and smoother traffic flow.

Performance Analysis

The primary objective of the RL-based speed planner is to improve the average density upstream bottleneck and nominal flow of traffic. The improvements in other metrics are a consequence of achieving this main objective. The effectiveness of the speed planner is evaluated by comparing the simulation results of the IDM baseline scenario and the speed planner controlled scenario with a 4% AV penetration rate, as shown in Figures 9 and 10 and in Table 1.

In the IDM baseline scenario (Figure 9), the system exhibits a bottleneck upstream density of 48.81 vehicles/km, a bottleneck throughput of 1,492.4 vehicles/hr, a system MPG of 45.16 MPG, and a total VMT of 7,387.13 miles. The fuel consumption stands at 163.57 gallons, with the system average speed being 40.92 mi/h and a speed standard deviation of 20.81 mi/h. The speed planner scenario (Figure 10) demonstrates significant improvements in several key metrics. The bottleneck throughput has dropped by 12.62% to 48.81 vehicles/km. The bottleneck throughput has increased by 5.01% to 1,567.18 vehicles/hr, and the system MPG has seen a substantial rise of 15.41% to 52.12 MPG. Fuel consumption has been reduced by 34.14% to 137.73 gallons, showcasing the eco-friendliness and cost-effectiveness of the speed planner. Most notably, the speed standard deviation has been reduced by a significant 34.36% to 13.66 mi/h, indicating a more uniform and stable traffic flow when the speed planner is in control. However, as the

tradeoff for achieving better fuel efficiency and throughput by homogenizing traffic flow, the system average speed has slightly decreased by 1.76% to 40.2 mi/h, and the system VMT has decreased by 2.82% to 7,178.61 miles.

FIELD TEST ANALYSIS

This section aims to provide a detailed examination of the MVT, the operational traffic experiment with the largest deployment of AVs, and its implications using a dataset [61] created using the I-24 MOTION system [62].

MVT

In mid-November 2022, the CIRCLES Consortium [63] carried out a large-scale traffic experiment on a 14.5-km stretch of I-24 in Nashville, TN, USA, depicted in Figure 11. Over recent years, this network has garnered attention from researchers due to the creation of the I-24 MOTION testbed [62], [64]. Efforts have been made to reconstruct its features, understand the implemented VSL control system [65], [66], and tackle driving characteristics that lead to energy inefficiencies [58], [67], [68], [69].

The large-scale traffic experiment, which we name "MVT," deployed a fleet of 100 vehicles consisting of three market-selling car models, including the Nissan Rogue, Toyota RAV4, and Cadillac XT5, onto the studied network during the morning commute over the course of five days (14–18 November 2022). Each vehicle was equipped with a variety of control algorithms, which we name "MegaController" (details are available in [61]), overriding or modifying the cruise control system, and designed to automatically adjust the longitudinal

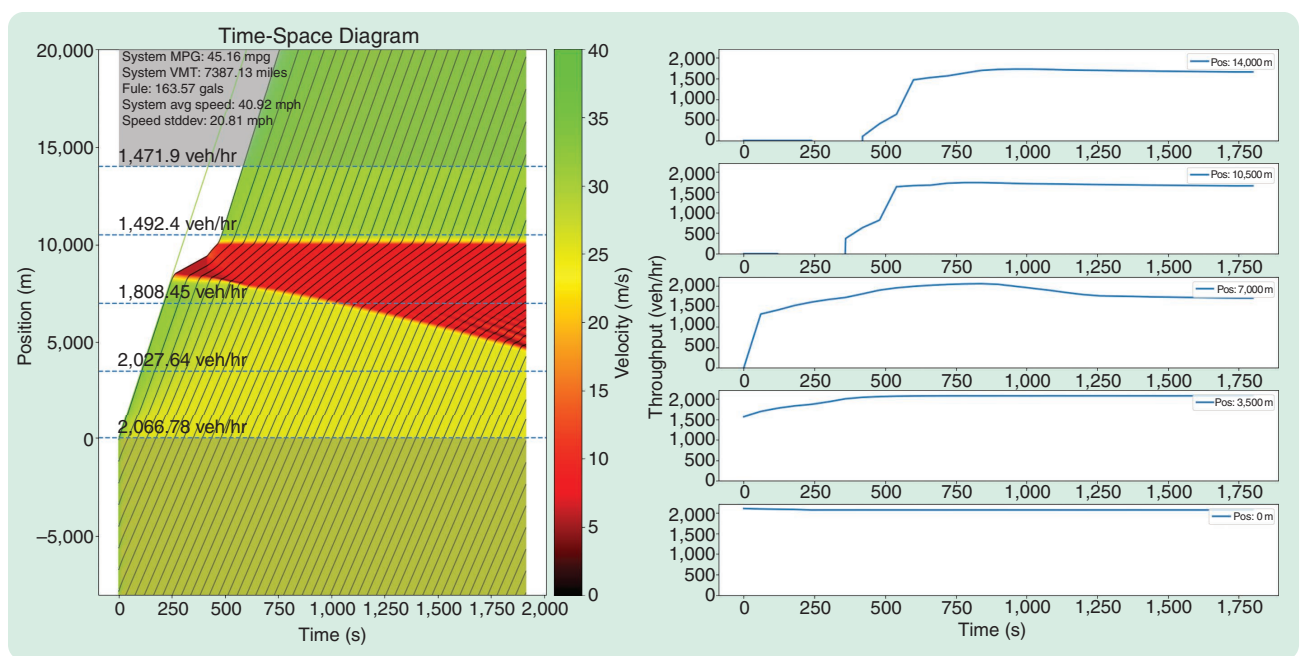


FIGURE 9 The IDM baseline scenario. AV trajectories are shown in black. Bottleneck throughput, 1,492.4 vehicles/hr; bottleneck upstream density, 48.81 vehicles/km; system MPG, 45.16 MPG; system VMT, 7,387.13 miles; fuel consumption, 163.57 gal; system average speed, 40.92 mi/h; and speed standard deviation, 20.81 mi/h.

speed of the vehicle to improve the overall flow of traffic, turning each car into its own “robot traffic manager” [70].

To achieve this large-scale operation, more than 50 CIRCLES [63] researchers from around the world gathered at a

field headquarters in a converted office space in Antioch, TN, USA (Figure 12). Each morning of the experiment, trained drivers drove the control vehicles on the designed routes through the I-24 MOTION testbed [62]. For the

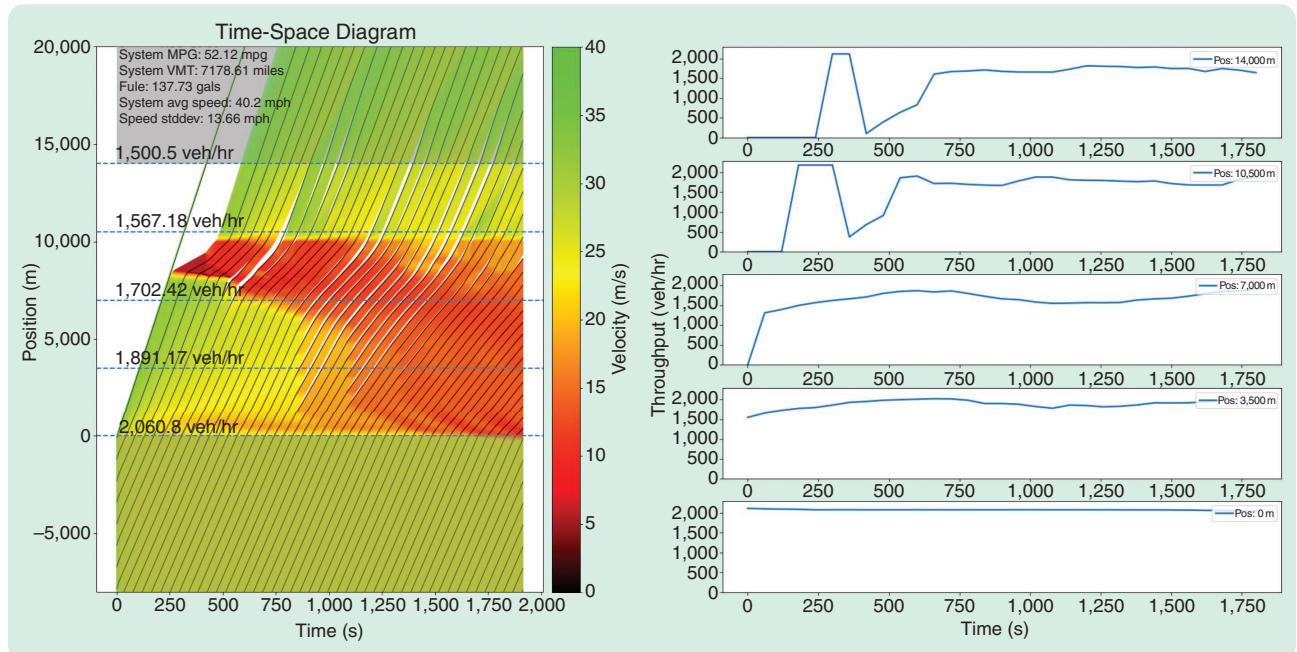


FIGURE 10 The speed planner scenario. AV trajectories are shown as black curves. Bottleneck throughput, 1,567.18 vehicles/hr (+5.01%); bottleneck upstream density, 42.65 vehicles/km (-12.62%); system MPG, 52.12 MPG (+15.41%); system VMT, 7,178.61 miles (-2.82%); fuel consumption, 137.73 gal (-34.14%); system average speed, 40.2 mi/h (-1.76%); and speed standard deviation, 13.66 mi/h (-34.36%).

TABLE 1 Traffic simulation and measurement scenarios.

Scenarios	Upstream Density (vehicles/km)	Bottleneck Throughput (vehicles/hr)	System MPG	System VMT	Fuel Consumption (gal)	Speed Standard Deviation (mi/h)
Simulation baseline	48.81	1,492.4	45.16	7,387.13	163.57	20.81
Simulation controlled	42.65 (-12.62%)	1,567.18 (+5.01%)	52.12 (+15.41%)	7,178.61 (-2.82%)	137.73 (-34.14%)	13.66 (-34.36%)

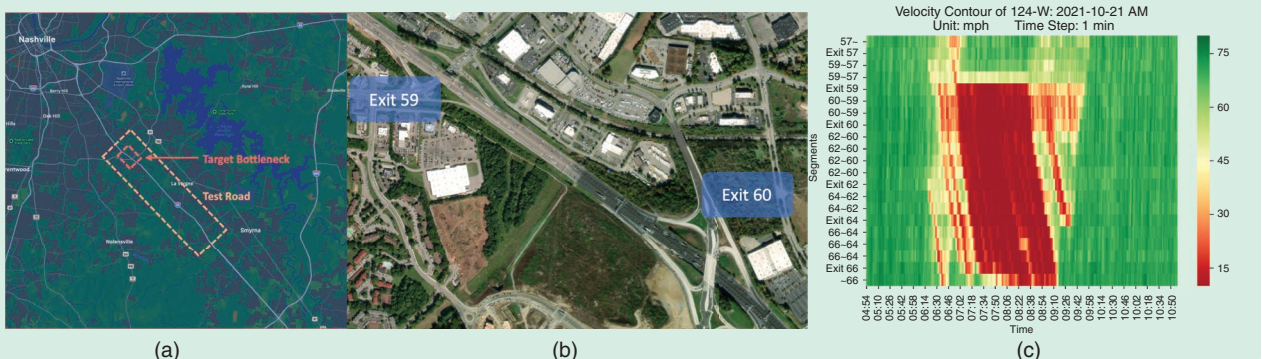


FIGURE 11 The MVT test road: (a) An illustration of the targeted highway network within this study (I-24 westbound in Nashville, TN, USA), seen within the dashed line region. (b) A satellite view of the bottleneck target area between exit 60 and exit 59, Tennessee. (c) A velocity heat map of the morning peak hour during a classical work day, 21 October 2021. (Source: INRIX [2].)

interested reader, we refer to [71] for more details about the organization of the experiment. As the drivers traversed their routes, researchers collected traffic data from both the vehicles and the I-24 MOTION traffic monitoring system.

The hierarchical framework and the speed planner introduced in the “Methodology” section, as part of the “MegaController,” were deployed and tested in MVT. The following section presents the operational analysis based on the I-24 Motion dataset.

Data Processing Stages

Figure 13 provides a comprehensive visualization of the speed planner data processing stages on 18 November

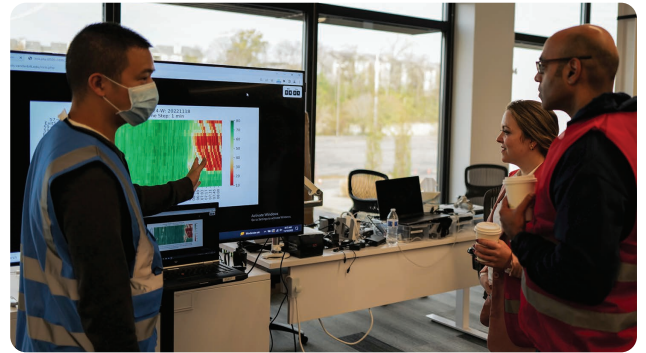


FIGURE 12 Coauthor Jonathan Lee presenting real-time TSE monitoring during MVT at the headquarters in Antioch, TN, USA.

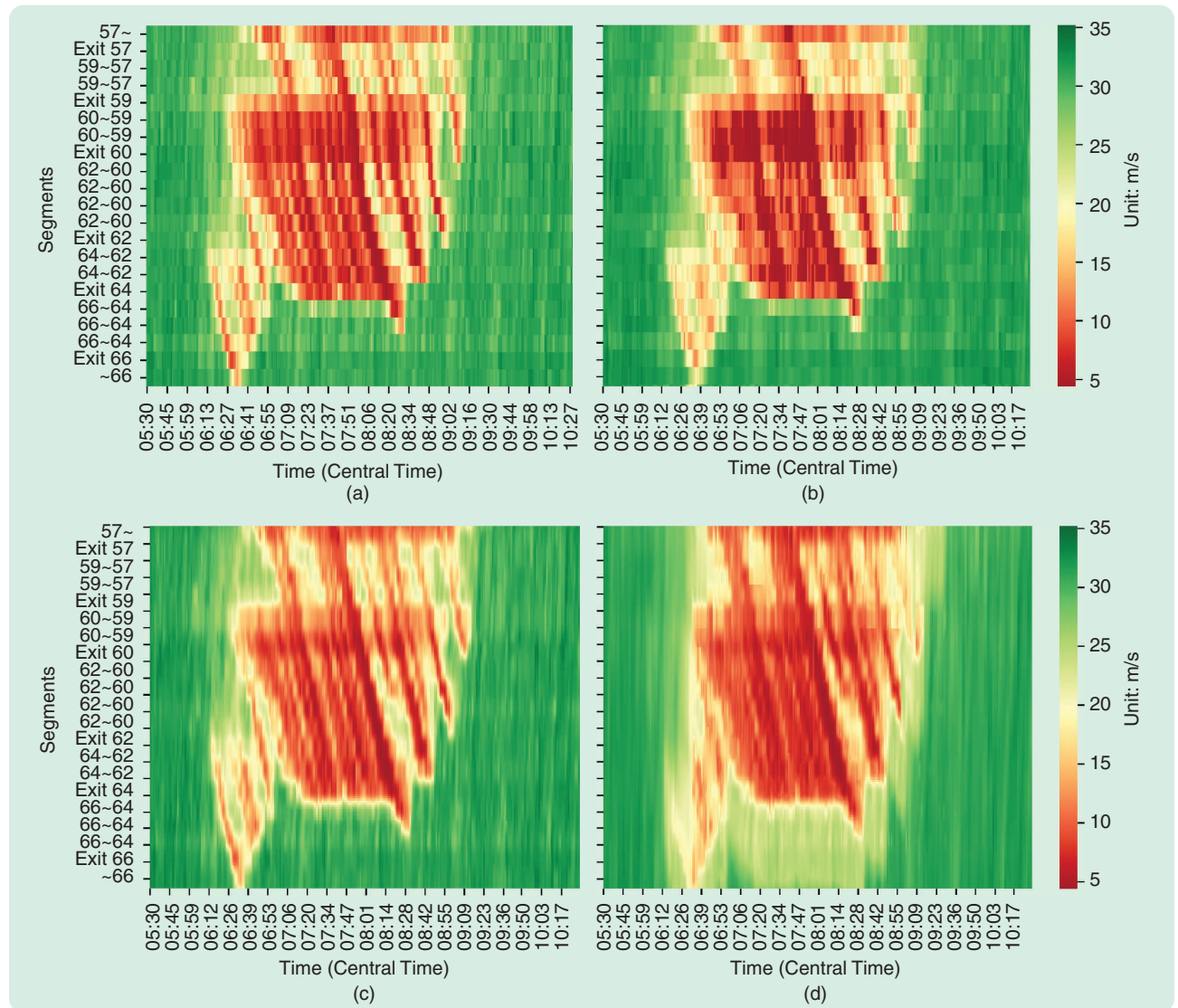


FIGURE 13 A comprehensive visualization of the speed planner data processing stages on 18 November 2022. (a) INRIX: The heat map of the raw INRIX data, illustrating the initial TSE. (b) Prediction: The output heat map of the prediction module, aiming to forecast the traffic condition 3 min ahead to counteract INRIX’s inherent latency. We can see that the prediction captured the location of the standing bottleneck around exit 59 and kept accurate tracking of shockwaves. (c) Fusion: The output heat map of the fusion module, where real-time vehicle observations are integrated with the predicted traffic data, resulting in a high-resolution lane-level TSE. (d) Target: The heat map of the final target speed profile derived from the processed data, guiding vehicle controllers for optimal navigation. A distinct early deceleration zone (buffer area) can be observed upstream of the congestion as the yellow transition zone in the heat map.

2022. The raw INRIX data, as shown in [Figure 13\(a\)](#), serve as the initial TSE. The prediction module, depicted in [Figure 13\(b\)](#), forecasts the traffic condition 3 min ahead to counteract INRIX inherent latency. We can see

that the prediction captured the location of the standing bottleneck around exit 59 and maintained accurate tracking of shockwaves. The fusion module, illustrated in [Figure 13\(c\)](#), integrates real-time vehicle observations

with the predicted traffic data, resulting in a high-resolution lane-level TSE. Finally, [Figure 13\(d\)](#) showcases the heat map of the final target speed profile derived from the processed data, guiding vehicle controllers for optimal navigation. A distinct early deceleration zone (buffer area) can be observed upstream of the congestion, evident as the yellow transition zone in the heat map.

[Figure 14](#) presents the speed surfaces of both the enhanced TSE and the target speed. The overall speed surface appears smoother, especially at the upstream of congestion (exit 62 to exit 66), where our system designs a smooth speed gradient for vehicles about to enter the queue, guiding traffic to decelerate in advance. In [Figure 15](#), we present a comparison of these speed profiles: the raw INRIX data, the predicted INRIX output from our prediction module, and the final target speed profile generated by the speed planner. A buffer area, together with the deceleration area, can be observed on the target profile. The blue scatters overlaying the profiles represent pings from an individual AV sent during the target update interval. These pings provide insights into the real-time behavior of the AVs in relation to the recommended speed profiles. The vehicle exhibits a propensity to adhere to the prescribed target speed profile. The divergence between the target speed and the vehicle ping indicates that the tracking is not enforced due to the necessity of accommodating local microscopic traffic conditions.

Performance Analysis

The performance analysis of the proposed system in MVT is based on I-24 MOTION [62], [64], a state-of-the-art measurement system to collect and analyze vehicle trajectory

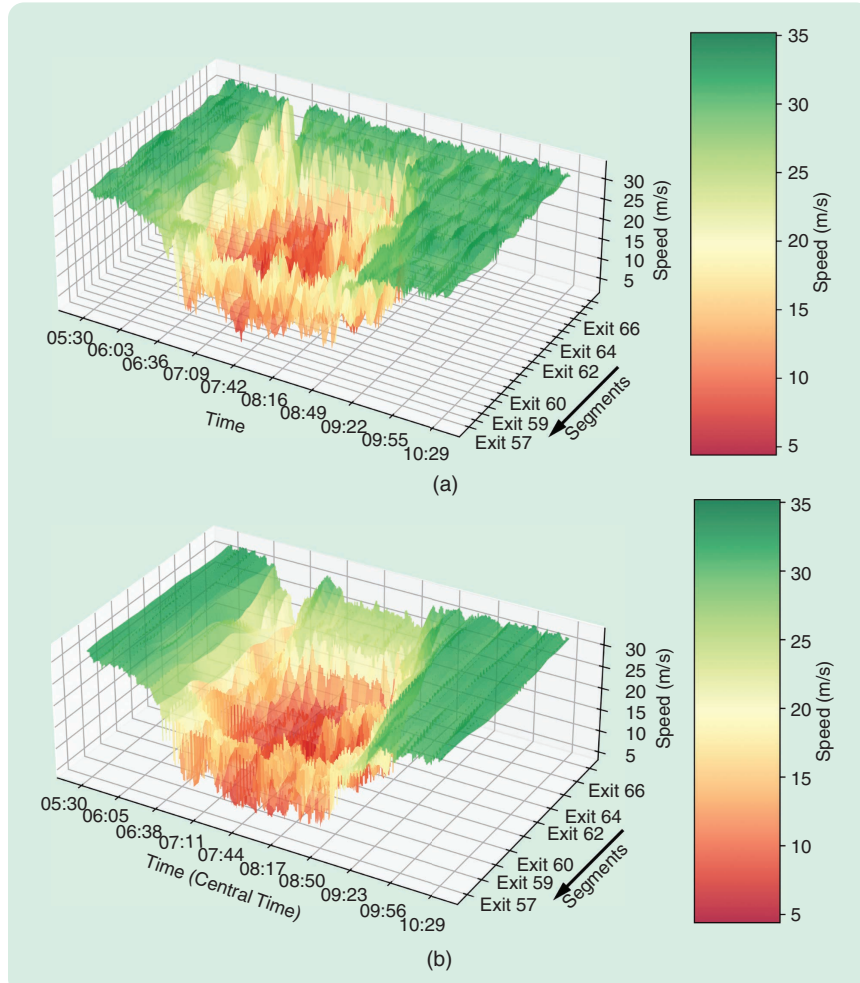


FIGURE 14 The speed surfaces of (a) enhanced TSE and (b) target speed. In (b), the overall speed surface is smoother. Upstream of the congestion (exit 62 to exit 66), our system designs a smooth speed gradient for vehicles about to enter the queue. The goal is to guide the traffic to slow down in advance. (The arrow indicates the traffic flow direction.)

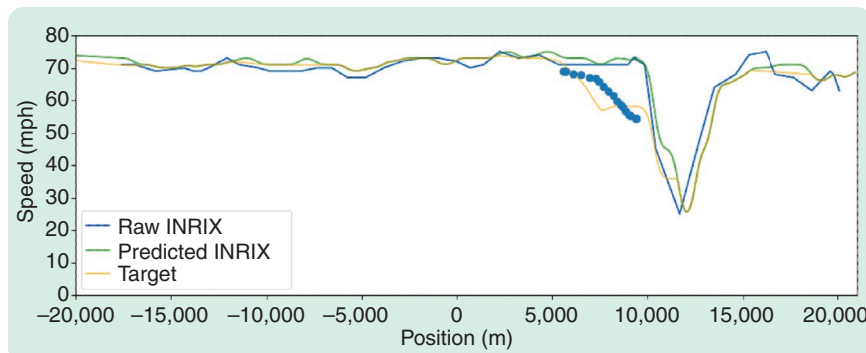


FIGURE 15 A speed profile illustration: raw INRIX, predicted INRIX, and target speed profile. Blue scatters indicate the ping of a single AV during that target update interval.

data on a section of the I-24 highway in Tennessee. The I-24 MOTION system extracts vehicle trajectory datasets from the video images captured by 276 high-resolution traffic cameras. These datasets contain the position of each vehicle on the highway, as well as other supplementary information such as vehicle dimensions and class. The trajectory data are generated using computer vision techniques [72], [73], [74], which analyze the video frames to track the movements of individual vehicles over time. The resulting dataset is then stitched [75], regularized [76], and visualized [77] to create a detailed record of vehicle behavior on the freeway, including speed, acceleration, lane changes, and other maneuvers. Trajectory data are stored in JSON format along with additional metadata such as scene homography, trajectory extraction algorithm settings, and descriptions of data attributes.

The speed planner's performance can be understood through a series of visualizations and analyses that depict its data processing stages, the impact of its deployment, and drivers' behavior when interacting with the system.

Analysis and Interpretation of Improvements

The results of experiments in terms of average density are illustrated in Figures 16–20. The traffic statistics in these

figures are reported in Table 2. Let us recall from the “Designing the Speed Profile” section that the RL-based control is trained by interacting with the mathematical model to improve the average density and consequently avoid contributing to the congestion at the location of the bottleneck. In particular,

$$\begin{cases} \text{Max Reward } (\rho_b) \\ \rho_b l_b \stackrel{\text{def}}{=} \int_{x_b - l_b}^{x_b} FD(\rho(t, x)) dx \end{cases} \quad (17)$$

where the parameters of the policy are designed to minimize the average density at the location of the bottleneck (see also Figure 6). It should be noted that by our assumption on the underlying macroscopic model, the objective of the optimal criteria is equivalent to maximization of theoretical (nominal) throughput (flow); that is, $f(\rho) = \rho v_{\max}(1 - \rho / \rho_{\max})$. Here we discuss the effectiveness of the control in achieving the goal.

Along with this objective, we define several metrics for comparison purposes with the benchmark day (Monday, 14 November 2021; first row in Table 2) and explain the behavior of traffic dynamics. The behavior of the drivers in engaging/disengaging the controller significantly affects the result. The last column of Table 2, which shows the valid penetration rate referring to the

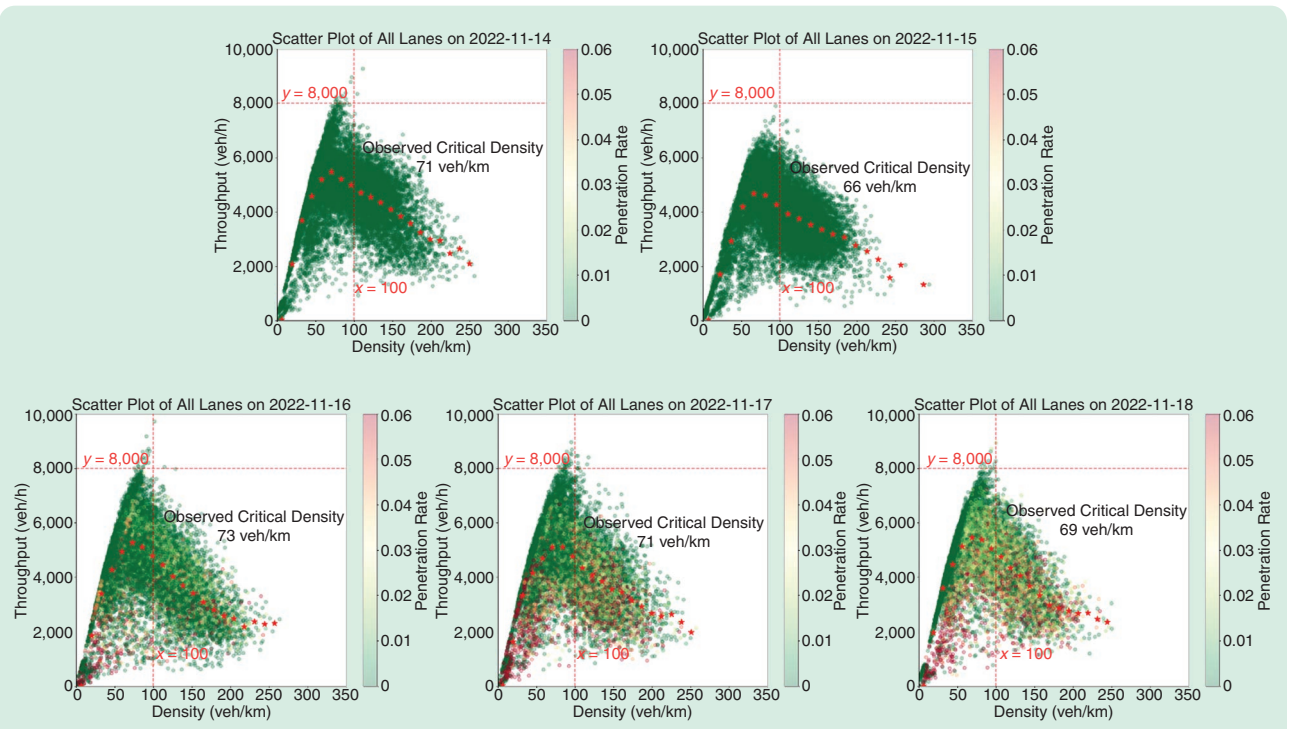


FIGURE 16 Scatters of FD colored by the penetration rate of controlled vehicles with speed planner engaged. Red stars are the mean values for measurement points binned by density (x-axis). In the order of days of the MVT week: (a) Monday, 80+ Nissans running stock ACC without connection to speed planner, which is considered as the human baseline. (b) Tuesday, no controlled vehicles on the road due to inclement weather. (c) Wednesday, 80+ Nissans deployed with speed planner engaged on the westbound route and stock ACC elsewhere. (d) Thursday, 80+ Nissans deployed with speed planner engaged. High server latency was observed. (e) Friday, 97 Nissans deployed with speed planner engaged. Jang et al. [57] provide a detailed deployment timeline on the vehicle side.

proportion of AVs in the traffic flow with an absolute value of the difference between the actual speed and the speed planner's recommended speed of less than 5m/s, shows that the *penetration rate of AVs is significantly higher on Friday* compared with other days. Therefore, for comparison purposes with the benchmark day, we consider the last day (Friday, 18 November 2022; last row in Table 2).

The "Average Density" column in Table 2 shows the overall average of the density, which shows about 8% improvement in the presence of control. To have a better understanding of the performance of the controllers, we investigate the performance on the upstream and downstream of the bottleneck separately, which shows 7% and

10% improvement, respectively. While this information remarkably contributes to the evaluation of the performance of the designed control, the main data are the density at the location of the bottleneck, which the speed planner is trained to improve. The corresponding statistics are shown in the "Congestion Formation Density at BN" column in Table 2. In fact, we may observe a drastic improvement of over 52%.

Figures 19 and 20 illustrate the histogram distribution of the density. The position 9,800–11,000 meters is the location of the bottleneck. The results of the experiments show that the density distribution at the bottleneck downstream, that is, at 11,000–12,300 meters, and at the congestion time from 06:48 to 07:35 a.m., is remarkably

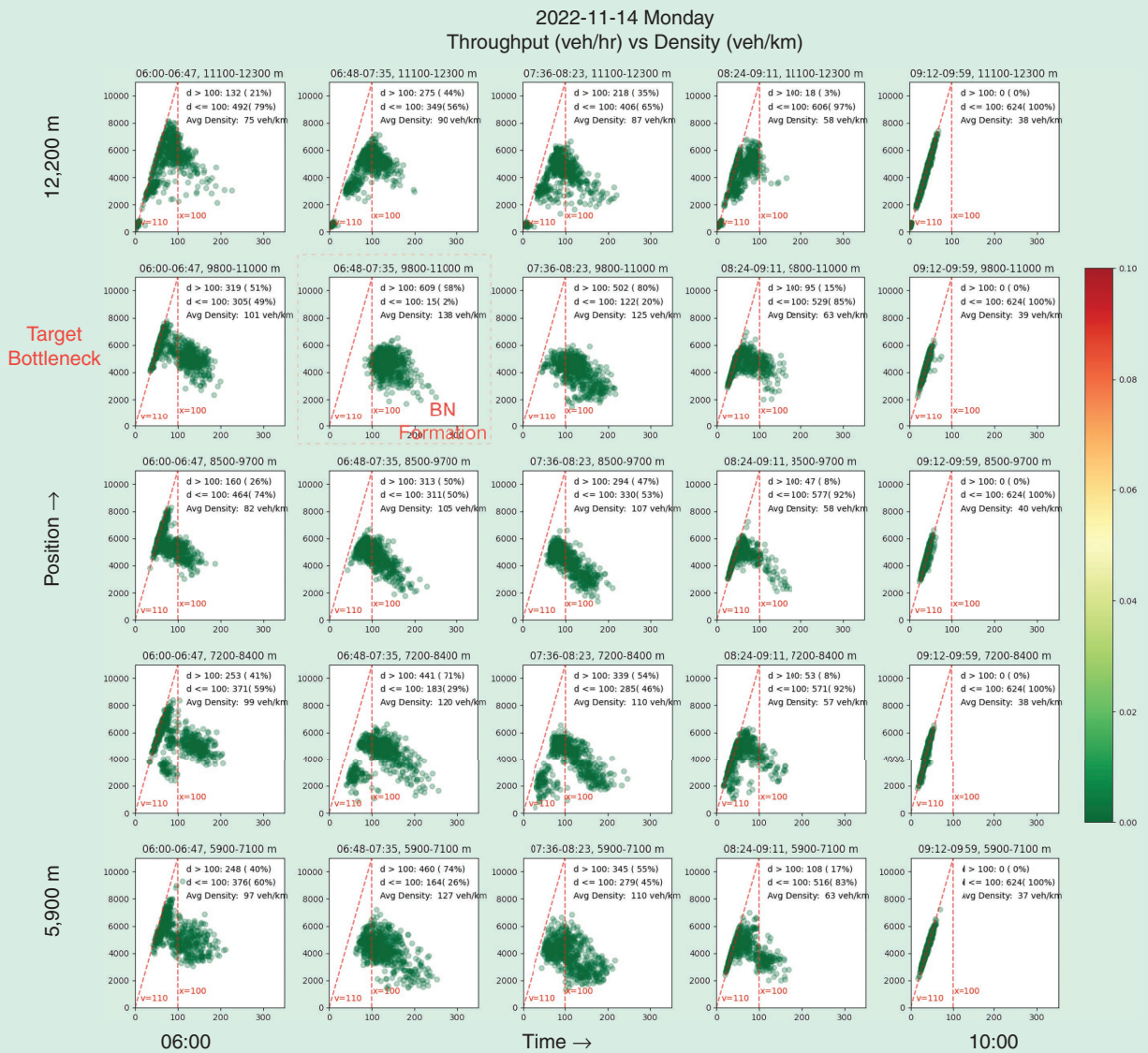


FIGURE 17 The FD scatter grid of Monday divided by time–space windows, colored by the penetration rate of controlled vehicles with speed planner engaged.

improved. Then, later on, the density remains mostly the same, which seems reasonable given that the control is mostly designed to improve the density at the location of the bottleneck.

At the location of the bottleneck and during all the congestion time from 06:48 to 08:23 a.m., the density is drastically improved, which is consistent with the speed planner objective function.

At the bottleneck upstream, that is, at the position 8,500–9,700 meters, the controller causes a slightly higher density, which is consistent with the fact that AVs are engaged. However, it should be noted that the increase in the density is very small, which is consistent with RL training.

More importantly, at the bottleneck farther upstream, that is, at the position 7,200–8,400 meters, the density is

improved, which implies that the deployment of the controller is not creating a persistent bottleneck upstream.

Deployment Impact

Figure 16 illustrates the density-throughput scatters of the MVT weekdays, colored by the penetration rate of controlled vehicles with the speed planner engaged. The density and throughput are calculated using Edie's definition [1] with a 100 m 60 s window. This choice creates a balance between granularity and the ability to capture meaningful traffic patterns obtained by experiment. The variations in the scatter plots across different days provide insights into the system's behavior under different conditions. Figures 17 and 18 further divide it into subscatter for Monday (stock ACCs, the native ACC controller without connection

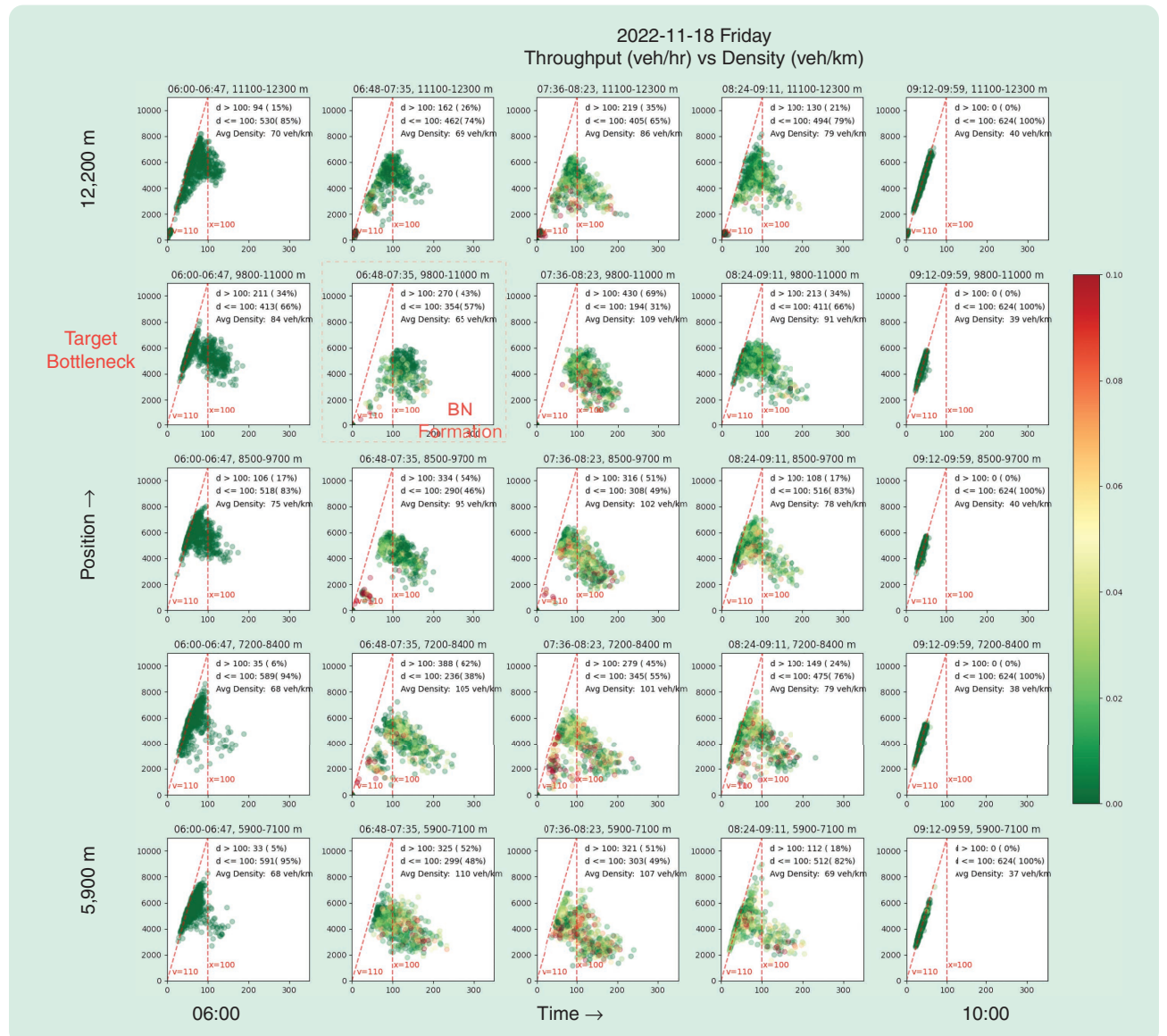


FIGURE 18 The FD scatter grid of Friday divided by time-space windows, colored by the penetration rate of controlled vehicles with speed planner engaged.

to speed planner) and Friday (with controlled vehicles), respectively. These grids, divided by time–space windows and colored by the penetration rate of controlled vehicles with the speed planner engaged, showcase the system impact at different times and locations. On observing the scatter plots, it is evident that congestion often began before our vehicles entered the roadway. This early onset of congestion led to near-saturated traffic conditions, making it challenging to produce significant improvements. Such conditions underscore the complexities inherent in operational traffic scenarios and highlight the need for future experiments to consider these dynamics.

Driver Engagement Analysis

In operational field tests, the performance of the overall system is intricately linked to driver behavior, especially in the context of controlled vehicles. Figures 21 and 22 reflect the controller engagement pattern on 18 November 2022.

The patterns indicate varied levels of driver trust and willingness to activate the controller. While many drivers chose to activate the controller on the westbound route, individual differences in engagement patterns are evident. Some drivers chose not to activate the controller throughout the experiment, while others displayed varied preferences based on the traffic conditions.

Furthermore, even when the controller is activated, the system performance can be influenced by the degree to which vehicle controllers adhere to the assigned target speed. Figure 23 presents a scatter plot comparing the ACC speed setting output by the vehicle controller to both the target speed assigned by the speed planner and the background speed from INRIX. From the correlation coefficients provided in Figure 23, it is evident that the ACC speed setting has a slightly higher correlation with the background speed (0.5659) than with the target speed (0.5604). This suggests that while the vehicle controllers are

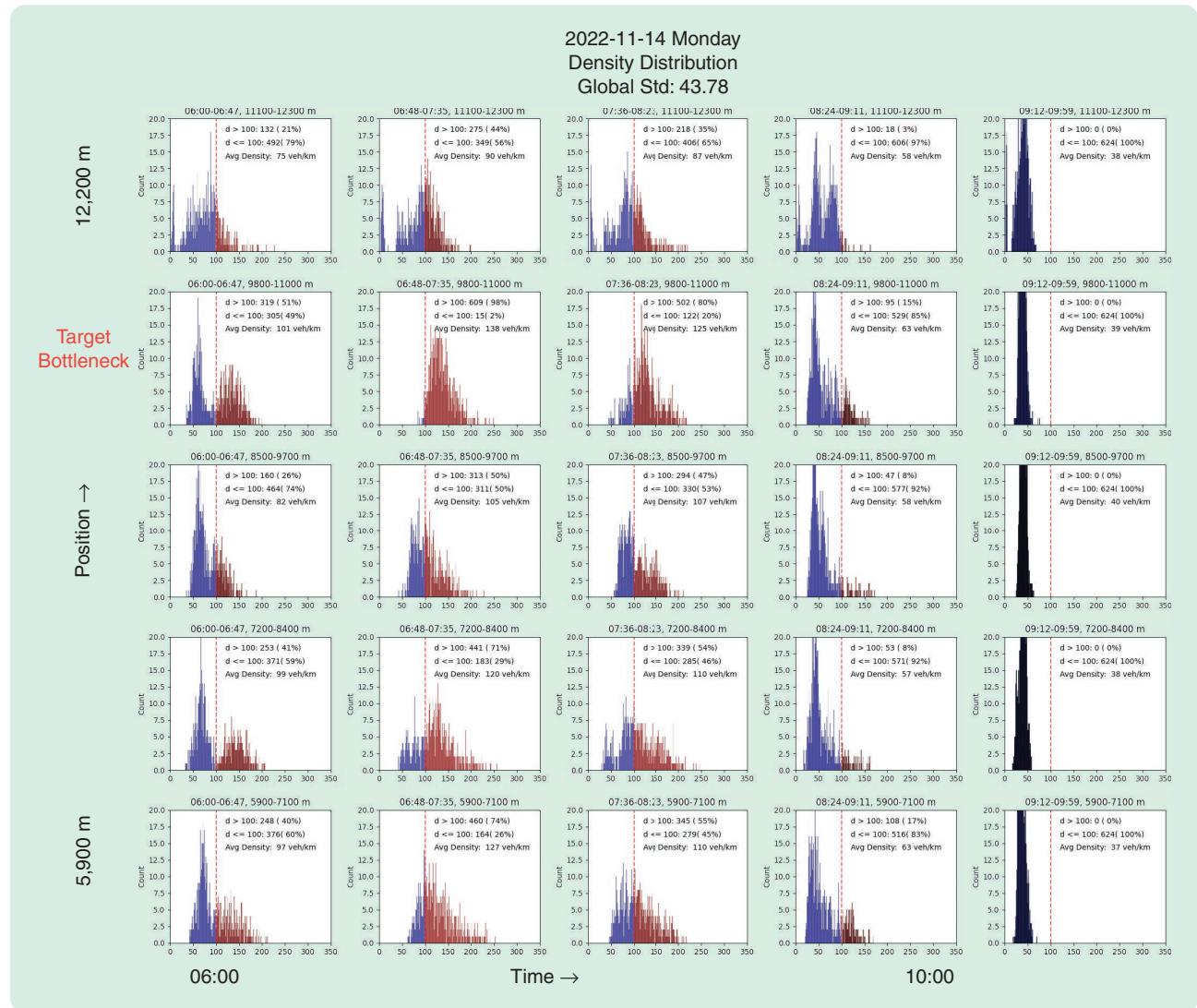


FIGURE 19 A histogram of the density distribution on Monday divided by time–space windows.

influenced by the speed planner recommendations, they tend to align more closely with the prevailing traffic conditions as represented by INRIX. This indicates that the vehicle controller tested in MVT might prioritize harmonizing

with the immediate traffic environment to ensure safety and smooth driving experiences. A challenge emerges when our vehicles, following the speed planner recommendations, drive at speeds significantly different from

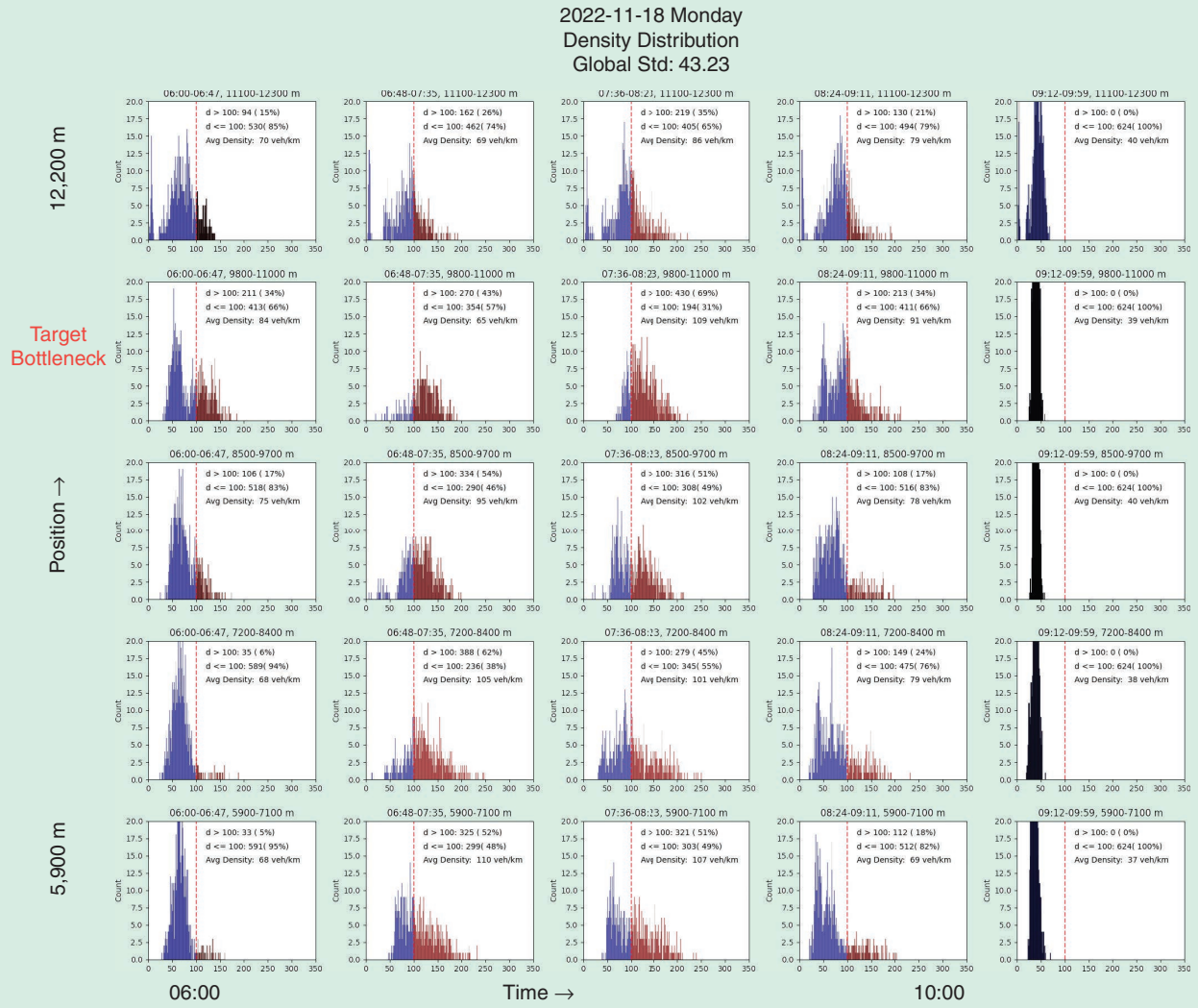


FIGURE 20 A histogram of the density distribution on Friday divided by time–space windows.

TABLE 2 The traffic density metrics by control scenario.

Date	Control	Average Density	Density Std	Average Density Upstream BN (vehicles/km)	Average Density Downstream BN (vehicles/km)	Congestion Formation Density BN (vehicles/km)	Valid PR
Monday, 14 November	No	82.57	43.78	83.33	81.44	138.21	0%
Tuesday, 15 November	No	99	41.12	102.61	93.59	143.76	0%
Wednesday, 16 November	80+ AVs	86.45	48.16	84.07	90.02	114.84	0.67%
Thursday, 17 November	80+ AVs	91.18	40.38	91.2	91.15	136.43	1.02%
Friday, 18 November	100 AVs	76.17	43.23	78.07	73.33	65.77	1.98%

BN: bottleneck; PR: penetration rate.

surrounding traffic. Even if the recommended speeds are optimized for overall traffic flow, driving much slower or faster than nearby vehicles might lead to social acceptance issues. Such discrepancies can make drivers feel out of sync with the general traffic, potentially leading to discomfort or reduced trust in the system.

CONCLUSION

The development and deployment of the speed planner in the MVT system represent a significant step forward in the realm of traffic management and vehicle control. Through a hierarchical framework, the system effectively integrates macro-TSE from external sources like INRIX with micro-observations from probe vehicles, offering a comprehensive view of the traffic environment.

Our performance analysis, as detailed in the preceding sections, underscores the system's capability to process and predict traffic data, fuses it with real-time vehicle observations, and derives optimal target speed profiles. The visualizations provide a clear representation of the data processing stages, from raw INRIX data to the final target speed profile. The system design ensures smoother speed gradients, especially in congestion-prone areas, aiming to enhance overall traffic flow.

However, as the driver engagement analysis highlighted, the effectiveness of such systems is closely tied to driver behavior. The extent to which drivers trust and engage with the controller, as well as their adherence to the recommended speeds, can significantly influence the system's performance. The potential social acceptance challenges, especially when

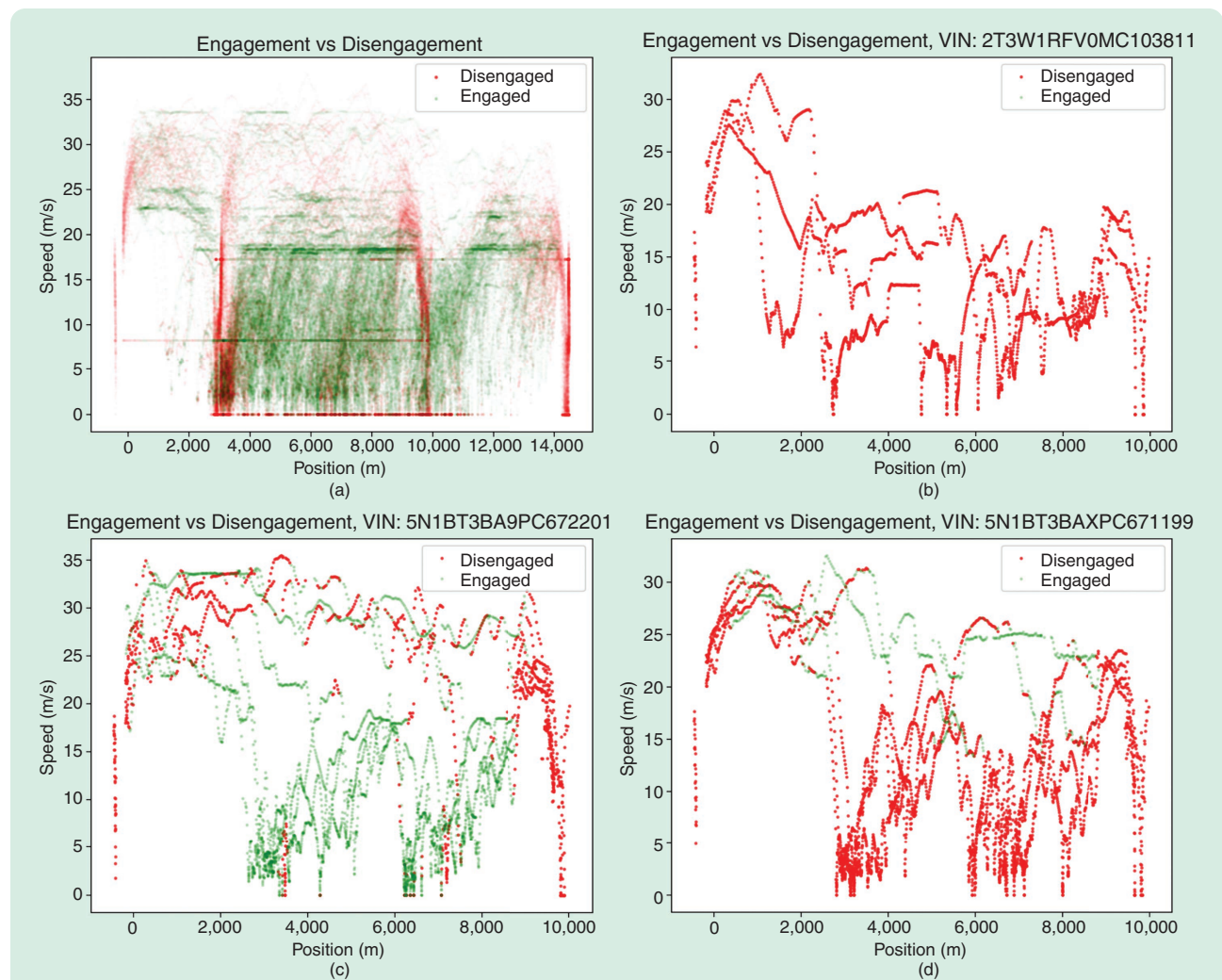


FIGURE 21 Scatters reflecting the controller engagement pattern on 18 November 2022: (a) The overall controller engagement trend. Mostly, drivers followed the instructions and activated the controller on the westbound route, especially in the congested sections. Four vertical red lines show the terminal ramps for two designed routes, where drivers take over the controls to exit and reenter the highway. However, the individual differences are noteworthy: (b) An individual driver who did not activate the controller during the whole experiment. (c) An individual driver who activated the controller during the congestion period and took over the control in the free-flow period. (d) An individual driver who had the opposite preference from the driver in (c). The controller was only activated in some free-flow periods.

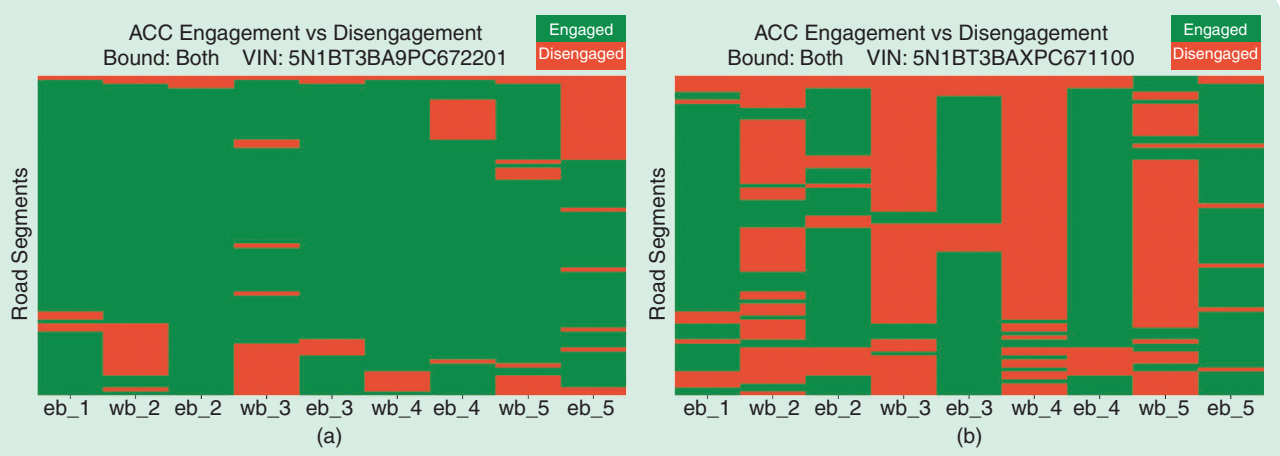


FIGURE 22 A heat map of two drivers' engagement on each run indicated by each column based on the data on 18 November: (a) "Good student" drivers were trained to keep their ACC controller engaged on westbound route as much as possible and keep it engaged when they feel comfortable to do so on the eastbound route. The heat map indicates the driver followed the training properly by keeping the controller engaged for most of the time on both bounds. (b) For "bad students," the heat map indicates that the driver had adopted the opposite pattern from what was trained, remaining engaged only on the eastbound route and disengaged most of the time on the westbound route.

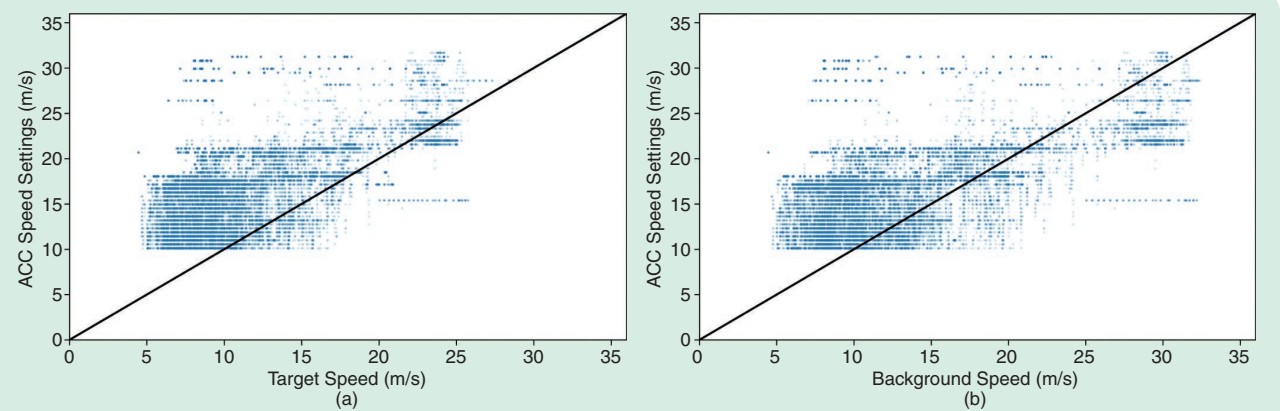


FIGURE 23 The scatter of the ACC speed setting output by the vehicle controller to (a) the target speed assigned by speed planner (correlation coefficient, 0.5604) and (b) the traffic background speed, INRIX (correlation coefficient, 0.5659).

our vehicles drive at speeds divergent from surrounding traffic, underline the importance of considering human factors in designing and deploying automated systems.

In conclusion, while the speed planner showcases promising capabilities in optimizing traffic flow and vehicle control, its full potential can only be realized with a holistic approach that considers both technological advancements and human-centric factors. Future work should focus on enhancing system robustness, improving driver trust and engagement, and addressing potential social acceptance issues to ensure seamless integration of such systems into our daily commutes.

ACKNOWLEDGMENT

This material is based upon work supported by the National Science Foundation under Grants CNS-1837244 (A. Bayen), CNS-1837652 (D. Work), CNS-1837481 (B. Piccoli), CNS-1837210 (G. Pappas), CNS-1446715 (B. Piccoli),

CNS-1446690 (B. Seibold), CNS-1446435 (J. Sprinkle and R. Lysecky), CNS-1446702 (D. Work), and CNS-2135579 (D. Work, A. Bayen, J. Sprinkle, and J. Lee) and by the French CNRS under Grants IEA SHYSTRA and PEPS JCJC (A. Hayat). This material is based upon work supported by the U.S. Department of Energy's Office of Energy Efficiency and Renewable Energy under the Vehicle Technologies Office Award CID DE-EE0008872. The views expressed herein do not necessarily represent the views of the U.S. Department of Energy or the U.S. Government. The authors are grateful for the additional support provided by C3AI, Amazon AWS, Siemens, Toyota, GM, Nissan, Caltrans, CCTA, and the Tennessee Department of Transportation.

AUTHOR INFORMATION

Han Wang (hanw@berkeley.edu) is a Ph.D. candidate at the Department of Civil and Environmental Engineering and

an M.S. degree candidate at the Department of Electrical Engineering and Computer Sciences, University of California, Berkeley, Berkeley, CA 94720 USA. His research interests include the decentralized control of massive AV platforms and driving assistance utilizing computer vision techniques. He is a Graduate Student Member of IEEE.

Zhe Fu (zhefu@berkeley.edu) is a Ph.D. candidate in transportation engineering and an M.S. candidate at the Department of Electrical Engineering and Computer Sciences, University of California, Berkeley, Berkeley, CA 94720 USA. She has research affiliations with the Institute of Transportation Studies, Berkeley Artificial Intelligence Research, California Partners for Advanced Transportation Technology, and Berkeley Deep Drive. Her research interests include traffic control and machine learning in mixed-autonomy environments. She is a Graduate Student Member of IEEE.

Jonathan W. Lee (jonny5@berkeley.edu) received his B.S. degree in engineering physics from the University of California, Berkeley, and his M.S. and Ph.D. degrees in mechanical engineering from Rice University. At Sandia National Laboratories (2011–2013), he completed his postdoctoral appointment studying electrical and material properties via molecular dynamics simulations. He subsequently served as a senior data scientist and product manager on various teams at Uber Technologies, Inc. (2014–2019). Since 2019, he has served as an engineering manager at the University of California, Berkeley, Berkeley, CA 94720 USA, and the program manager and chief engineer of CIRCLES.

Hossein Nick Zinat Matin (h-matin@berkeley.edu) is a postdoctoral researcher at the University of California, Berkeley, Berkeley, CA 94720 USA. His research interests include PDEs, control, and their applications in the theory of traffic flow. He is a Member of IEEE.

Arwa Alanqary (arwa@berkeley.edu) received her B.S. degree in mechanical engineering from Alfaisal University in 2017 and her M.S. degree in computational science and engineering from Massachusetts Institute of Technology in 2019. She is currently a Ph.D. student in electrical engineering and computer sciences at the University of California, Berkeley. Her research interests include optimal control and optimization and learning in multi-agent systems. She is a Graduate Student Member of IEEE.

Daniel Urieli (daniel.urieli@gm.com) received his Ph.D. degree in artificial intelligence (AI) from the University of Texas at Austin, where he developed AI agents that won the Power Trading Agent Competition, as well as the simulated robot soccer league in the international RoboCup competition. He is a staff researcher at General Motors, Herzliya 4672513, Israel where he cofounded the autonomous driving research group and led research on applying AI for congestion reduction and electric vehicle energy management.

Sharon Hornstein (sharon.hornstein@gm.com) is a researcher at General Motors R&D, Herzliya 4672513, Israel. She received her B.Sc., M.Sc., and Ph.D. degrees in mechan-

ical engineering from the Technion, Israel. Her research interests include the dynamic modeling of nonlinear systems.

Abdul Rahman Kreidieh (aboudy@berkeley.edu) is a Ph.D. student at the Department of Civil and Environmental Engineering, University of California, Berkeley, Berkeley, CA 94720 USA.

Raphael Chekroun (raphael.chekroun@minesparis.psl.eu) is a research scientist at Valeo, 75017 Paris, France, and a Ph.D. candidate in the Center for Robotics, Mines Paris, PSL University, 75017 Paris, He worked as a visiting scholar at the University of California, Berkeley, with the CIRCLES consortium. His research interests include AI for autonomous driving and its application to traffic flow regulation.

William Barbour (william.w.barbour@vanderbilt.edu) is research scientist at the Institute for Software Integrated Systems, Vanderbilt University, Nashville, TN 37212 USA. He is a co-principle investigator on the I-24 MOTION test-bed and works on other large transportation systems projects across the state of Tennessee. His technical focus is on intelligent transportation systems, AI, and data science.

William A. Richardson (william.a.richardson@vanderbilt.edu) is graduate student researcher at Vanderbilt University, Nashville, TN 37212 USA.

Dan Work (dan.work@vanderbilt.edu) is a Chancellor Faculty Fellow and professor in civil and environmental engineering and computer science at the Institute for Software Integrated Systems, Vanderbilt University, Nashville, TN 37212 USA. He has held research appointments at the University of Illinois at Urbana-Champaign (2010–2017), the Institute for Pure and Applied Mathematics (2015 and 2020), Microsoft Research Redmond (2009), and Nokia Research Center Palo Alto (2007–2009). His research interests broadly include transportation cyberphysical systems, with many applications in highway traffic sensing and control.

Benedetto Piccoli (piccoli@camden.rutgers.edu) is a university professor and, since 2009, the Joseph and Loretta Lopez Chair Professor of Mathematics with the Department of Mathematical Sciences, Rutgers University–Camden, Camden, NJ 08102 USA. He also served as vice chancellor for research. He received his Ph.D. degree in applied mathematics from the Scuola Internazionale Superiore di Studi Avanzati (SISSA), Trieste, Italy, in 1994. He was a researcher with SISSA from 1994 to 1998; an associate professor with the University of Salerno from 1998 to 2001; and a research director with the Istituto per le Applicazioni del Calcolo “Mauro Picone” of the Italian Consiglio Nazionale delle Ricerche, Rome, Italy, from 2001 to 2009.

Benjamin Seibold (seibold@temple.edu) is a professor of mathematics and physics and the director of the Center for Computational Mathematics and Modeling, Temple University, Philadelphia, PA 19122 USA. His research areas, funded by NSF, DOE, DAC, USACE, USDA, and PDA, include computational mathematics (high-order methods for

differential equations, CFD, and molecular dynamics) and applied mathematics and modeling (traffic flow, invasive species, many-agent systems, and radiative transfer).

Jonathan Sprinkle (jonathan.sprinkle@vanderbilt.edu) has been a professor of computer science at Vanderbilt University, Nashville, TN 3721 USA, since 2021. Prior to joining Vanderbilt, he was the Litton Industries John M. Leonis Distinguished Associate Professor of Electrical and Computer Engineering at the University of Arizona and the interim director of the Transportation Research Institute. From 2017 to 2019 he served as a program director in cyber-physical systems and smart and connected communities at the National Science Foundation in the CISE Directorate.

Alexandre M. Bayen (bayen@berkeley.edu) is the associate provost for Moffett Field program development, the Liao-Cho Professor of Engineering, and a professor of electrical engineering and computer science and of civil and environmental engineering (courtesy) at the University of California, Berkeley, Berkeley, CA 94720 USA. He is a visiting professor at Google, Mountain View, CA 94043 USA. He is also a faculty scientist in mechanical engineering at the Lawrence Berkeley National Laboratory, Berkeley, CA 94720 USA. From 2014 to 2021, he served as the director of the Institute of Transportation Studies at the University of California, Berkeley.

Maria Laura Delle Monache (mldellemonache@berkeley.edu) is an assistant professor in the Department of Civil and Environmental Engineering at the University of California, Berkeley, Berkeley, CA 94720 USA. Her research interests lie at the intersection of transportation engineering, mathematics, and control and focus on modeling and control of mixed-autonomy large-scale traffic systems.

REFERENCES

- [1] L. C. Edie, "Discussion of traffic stream measurements and definitions," in *Proc. 2nd Int. Symp. Theory Traffic Flow*, London, Jun. 25–27, 1963, pp. 139–154.
- [2] G. Cookson and B. Pishue, "Inrix global traffic scorecard—appendices," *INRIX Res.*, 2017. Accessed: Oct. 26, 2023. [Online]. Available: <https://www.verkeerskunde.nl/Uploads/2017/2/INRIX--2016--Global-Traffic-Scorecard-Report-Appendices--English-FINAL.PDF>
- [3] S. Siri, C. Pasquale, S. Sacone, and A. Ferrara, "Freeway traffic control: A survey," *Automatica*, vol. 130, Aug. 2021, Art. no. 109655, doi: [10.1016/j.automatica.2021.109655](https://doi.org/10.1016/j.automatica.2021.109655).
- [4] A. Ferrara, S. Sacone, and S. Siri, *Freeway Traffic Modelling and Control*. New York, NY, USA: Springer, 2018.
- [5] W. Schwarting, J. Alonso-Mora, and D. Rus, "Planning and decision-making for autonomous vehicles," *Annu. Rev. Control Rob. Auton. Syst.*, vol. 1, no. 1, pp. 187–210, 2018, doi: [10.1146/annurev-control-060117-105157](https://doi.org/10.1146/annurev-control-060117-105157).
- [6] X.-Y. Lu and S. E. Shladover, "Review of variable speed limits and advisories: Theory, algorithms, and practice," *Trans. Res. Rec.*, vol. 2423, no. 1, pp. 15–23, 2014.
- [7] H. Nick Zinat Matin and R. B. Sowers, "Near-collision dynamics in a noisy car-following model," *SIAM J. Appl. Math.*, vol. 82, no. 6, pp. 2080–2110, 2022, doi: [10.1137/21M1454055](https://doi.org/10.1137/21M1454055).
- [8] C. M. Gisolo, D. Monache, M. Laura, F. Ferrante, and P. Frasca, "Non-linear analysis of stability and safety of optimal velocity model vehicle groups on ring roads," *IEEE Trans. Intell. Transp. Syst.*, vol. 23, no. 11, pp. 20,628–20,635, Nov. 2022, doi: [10.1109/TITS2022.3192323](https://doi.org/10.1109/TITS2022.3192323).
- [9] S. C. Vishnoi et al., "CAV traffic control to mitigate the impact of congestion from bottlenecks: A linear quadratic regulator approach and microsimulation study," *J. Auton. Transp. Syst.*, vol. 1, no. 2, pp. 1–37, 2024, doi: [10.1145/3636464](https://doi.org/10.1145/3636464).
- [10] H. N. Z. Matin and M. L. Delle Monache, "Near collision and controllability analysis of nonlinear optimal velocity follow-the-leader dynamical model in traffic flow," in *Proc. 62nd IEEE Conf. Decis. Control (CDC)*, Piscataway, NJ USA: IEEE, 2023, pp. 8057–8062, doi: [10.1109/CDC49753.2023.10384086](https://doi.org/10.1109/CDC49753.2023.10384086).
- [11] A. Hayat et al., "Traffic smoothing using explicit local controllers," 2023, *arXiv:2310.18151*.
- [12] B. Van Arem, C. J. Van Driel, and R. Visser, "Effects of adaptive cruise control systems on highway traffic flow capacity," *Transp. Res. Rec.*, vol. 1800, no. 1, pp. 78–84, 2001.
- [13] X. Gong and A. Keimer, "On the well-posedness of the" Bando-follow the leader" car following model and a time-delayed version," *Netw. Heterogen. Media*, vol. 18, no. 2, pp. 775–798, 2023, doi: [10.3934/nhm.2023033](https://doi.org/10.3934/nhm.2023033).
- [14] H. N. Zinat Matin, Y. Yeo, X. Gong, and M. L. Delle Monache, "On the analytical properties of a nonlinear microscopic dynamical model for connected and automated vehicles," *IEEE Control Syst. Lett.*, vol. 8, pp. 1607–1612, 2024, doi: [10.1109/LCSYS.2024.3412156](https://doi.org/10.1109/LCSYS.2024.3412156).
- [15] R. E. Stern et al., "Dissipation of stop-and-go waves via control of autonomous vehicles: Field experiments," *Transp. Res. C: Emerg. Technol.*, vol. 89, pp. 205–221, Apr. 2018, doi: [10.1016/j.trc.2018.02.005](https://doi.org/10.1016/j.trc.2018.02.005).
- [16] M. L. Delle Monache et al., "Feedback control algorithms for the dissipation of traffic waves with autonomous vehicles," in *Proc. Comput. Intell. Optim. Methods Control Eng.*, 2019, pp. 275–299.
- [17] A. R. Kreidieh, C. Wu, and A. M. Bayen, "Dissipating stop-and-go waves in closed and open networks via deep reinforcement learning," in *Proc. 21st Int. Conf. Intell. Transp. Syst. (ITSC)*, 2018, pp. 1475–1480, doi: [10.1109/ITSC.2018.8569485](https://doi.org/10.1109/ITSC.2018.8569485).
- [18] M. L. Delle Monache and P. Goatin, "Scalar conservation laws with moving constraints arising in traffic flow modeling: An existence result," *J. Differ. Equ.*, vol. 257, no. 11, pp. 4015–4029, 2014, doi: [10.1016/j.jde.2014.07.014](https://doi.org/10.1016/j.jde.2014.07.014).
- [19] P. Goatin, "Dissipation of stop-and-go waves in traffic flows using controlled vehicles: A macroscopic approach," *IEEE Control Syst. Lett.*, vol. 8, pp. 628–633, 2024, doi: [10.1109/LCSYS.2024.3401092](https://doi.org/10.1109/LCSYS.2024.3401092).
- [20] P. Goatin and B. Piccoli, "A multi-scale multi-lane model for traffic regulation via autonomous vehicles," 2024, *arXiv:2404.17192*.
- [21] H. N. Z. Matin and M. L. Delle Monache, "On the existence of solution of conservation law with moving bottleneck and discontinuity in flux," 2023, *arXiv:2310.00537*.
- [22] V. Giannmarino, S. Baldi, P. Frasca, and M. L. Delle Monache, "Traffic flow on a ring with a single autonomous vehicle: An interconnected stability perspective," *IEEE Trans. Intell. Transp. Syst.*, vol. 22, no. 8, pp. 4998–5008, Aug. 2021, doi: [10.1109/TITS.2020.2985680](https://doi.org/10.1109/TITS.2020.2985680).
- [23] A. Bayen, M. L. Delle Monache, M. Garavello, P. Goatin, and B. Piccoli, *Control Problems for Conservation Laws With Traffic Applications: Modeling, Analysis, and Numerical Methods*. New York, NY, USA: Springer Nature, 2022.
- [24] P. Goatin, C. Daini, M. L. Delle Monache, and A. Ferrara, "Interacting moving bottlenecks in traffic flow," *Netw. Heterogen. Media*, vol. 18, no. 2, pp. 930–945, 2022, doi: [10.3934/nhm.2023040](https://doi.org/10.3934/nhm.2023040).
- [25] C. Daini, P. Goatin, M. L. Delle Monache, and A. Ferrara, "Centralized traffic control via small fleets of connected and automated vehicles," in *Proc. Eur. Control Conf. (ECC)*, Piscataway, NJ USA: IEEE, 2022, pp. 371–376, doi: [10.23919/ECC55457.2022.9838305](https://doi.org/10.23919/ECC55457.2022.9838305).
- [26] T. Liard, R. Stern, and M. L. Delle Monache, "A PDE-ODE model for traffic control with autonomous vehicles," *Netw. Heterogen. Media*, vol. 18, no. 3, pp. 1190–1206, 2023, doi: [10.3934/nhm.2023051](https://doi.org/10.3934/nhm.2023051).
- [27] L. Li, Y. Lv, and F.-Y. Wang, "Traffic signal timing via deep reinforcement learning," *IEEE/CAA J. Autom. Sin.*, vol. 3, no. 3, pp. 247–254, Jul. 2016, doi: [10.1109/JAS.2016.7508798](https://doi.org/10.1109/JAS.2016.7508798).
- [28] P. Fernandes and U. Nunes, "Platooning of autonomous vehicles with intervehicle communications in sumo traffic simulator," in *Proc. 13th Int. IEEE Conf. Intell. Transp. Syst.*, 2010, pp. 1313–1318, doi: [10.1109/ITSC.2010.5625277](https://doi.org/10.1109/ITSC.2010.5625277).
- [29] B. Khondaker and L. Kattan, "Variable speed limit: An overview," *Transp. Lett.*, vol. 7, no. 5, pp. 264–278, 2015, doi: [10.1179/1942787514Y.0000000053](https://doi.org/10.1179/1942787514Y.0000000053).
- [30] A. Vahidi and A. Eskandarian, "Research advances in intelligent collision avoidance and adaptive cruise control," *IEEE Trans. Intell. Transp. Syst.*, vol. 4, no. 3, pp. 143–153, Sep. 2003, doi: [10.1109/TITS.2003.821292](https://doi.org/10.1109/TITS.2003.821292).
- [31] L. D. Baskar, B. D. Schutter, and J. Hellendoorn, "Traffic control and intelligent vehicle highway systems: A survey," *IET Intelligent Transport Syst.*, vol. 5, no. 1, pp. 38–52, 2011, doi: [10.1049/iet-its.2009.0001](https://doi.org/10.1049/iet-its.2009.0001).

- [32] V. Milanes and S. E. Shladover, "Cooperative adaptive cruise control in real traffic situations," *IEEE Trans. Intell. Transp. Syst.*, vol. 15, no. 1, pp. 296–305, Feb. 2014, doi: [10.1109/TITS.2013.2278494](https://doi.org/10.1109/TITS.2013.2278494).
- [33] A. Ferrara, G. P. Incremona, E. Birliba, and P. Goatin, "Multi-scale model-based hierarchical control of freeway traffic via platoons of connected and automated vehicles," *IEEE Open J. Intell. Transp. Syst.*, vol. 3, pp. 799–812, 2022, doi: [10.1109/OJITS.2022.3217001](https://doi.org/10.1109/OJITS.2022.3217001).
- [34] M. Bunting, R. Bhadani, and J. Sprinkle, "Libpanda: A high performance library for vehicle data collection," in *Proc. Workshop Data-Driven Intell. Cyber-Phys. Syst.*, 2021, pp. 32–40, doi: [10.1145/3459609.3460529](https://doi.org/10.1145/3459609.3460529).
- [35] R. Bhadani et al., "Strym: A python package for real-time CAN data logging, analysis and visualization to work with USB-CAN interface," in *Proc. 2nd Workshop Data-Driven Intell. Cyber-Phys. Syst. Smart Cities Workshop (DI-CPS)*, Piscataway, NJ USA: IEEE, 2022, pp. 14–23, doi: [10.1109/DI-CPS56137.2022.00009](https://doi.org/10.1109/DI-CPS56137.2022.00009).
- [36] S. Elmudani, M. Nice, M. Bunting, J. Sprinkle, and R. Bhadani, "From CAN to ROS: A monitoring and data recording bridge," in *Proc. Workshop Data-Driven Intell. Cyber-Phys. Syst.*, 2021, pp. 17–21, doi: [10.1145/3459609.3460531](https://doi.org/10.1145/3459609.3460531).
- [37] M. Nice, M. Bunting, D. Work, and J. Sprinkle, "Middleware for a heterogeneous CAV fleet," in *Proc. Cyber-Phys. Syst. Internet Things Week*, 2023, pp. 86–91, doi: [10.1145/3459609.3460531](https://doi.org/10.1145/3459609.3460531).
- [38] C. Chen, A. Skabardonis, and P. Varaiya, "Systematic identification of freeway bottlenecks," *Transp. Res. Rec.*, vol. 1867, no. 1, pp. 46–52, 2004, doi: [10.3141/1867-06](https://doi.org/10.3141/1867-06).
- [39] B. Asadi, C. Zhang, and A. Vahidi, "The role of traffic flow preview for planning fuel optimal vehicle velocity," *Dyn. Syst. Control Conf.*, vol. 44182, pp. 813–819, Jan. 2010, doi: [10.1115/DSCC2010-4083](https://doi.org/10.1115/DSCC2010-4083).
- [40] S. Cui, B. Seibold, R. Stern, and D. B. Work, "Stabilizing traffic flow via a single autonomous vehicle: Possibilities and limitations," in *Proc. IEEE Intell. Veh. Symp. (IV)*, Piscataway, NJ USA: IEEE, 2017, pp. 1336–1341, doi: [10.1109/IVS.2017.7995897](https://doi.org/10.1109/IVS.2017.7995897).
- [41] A. R. Kreidieh, Z. Fu, and A. M. Bayen, "Learning energy-efficient driving behaviors by imitating experts," in *Proc. IEEE 25th Int. Conf. Intell. Transp. Syst. (ITSC)*, Piscataway, NJ USA: IEEE, 2022, pp. 2689–2695, doi: [10.1109/ITSC55140.2022.9922352](https://doi.org/10.1109/ITSC55140.2022.9922352).
- [42] Z. Fu, A. R. Kreidieh, H. Wang, J. W. Lee, M. L. Delle Monache, and A. M. Bayen, "Cooperative driving for speed harmonization in mixed-traffic environments," in *Proc. IEEE Intell. Veh. Symp. (IV)*, Piscataway, NJ USA: IEEE, 2023, pp. 1–8, doi: [10.1109/IV55152.2023.10186598](https://doi.org/10.1109/IV55152.2023.10186598).
- [43] C. F. Daganzo, *Fundamentals of Transportation and Traffic Operations*. Leeds, West Yorkshire, England: Emerald Group Publishing Limited, 1997.
- [44] G. F. Newell, "Nonlinear effects in the dynamics of car following," *Oper. Res.*, vol. 9, no. 2, pp. 209–229, 1961, doi: [10.1287/opre.9.2.209](https://doi.org/10.1287/opre.9.2.209).
- [45] B. D. Greenshields, J. R. Bibbins, W. Channing, and H. H. Miller, "A study of traffic capacity," *Highway Res. Board Proc.*, vol. 14, no. 1, pp. 448–477, 1935.
- [46] A. Coursey et al., "FT-AED: Benchmark dataset for early freeway traffic anomalous event detection," 2024, *arXiv:2406.15283*.
- [47] M. L. Puterman, *Markov Decision Processes: Discrete Stochastic Dynamic Programming*. Hoboken, NJ, USA: John Wiley & Sons, 2014.
- [48] J.-P. Lebacque, J.-B. Lesort, and F. Giorgi, "Introducing buses into first-order macroscopic traffic flow models," *Transp. Res. Rec.*, vol. 1644, no. 1, pp. 70–79, 1998, doi: [10.3141/1644-08](https://doi.org/10.3141/1644-08).
- [49] L. Leclercq, S. Chanut, and J.-B. Lesort, "Moving bottlenecks in Light-hill-Whitham-Richards model: A unified theory," *Transp. Res. Rec.*, vol. 1883, no. 1, pp. 3–13, 2004, doi: [10.3141/1883-01](https://doi.org/10.3141/1883-01).
- [50] F. Giorgi, L. Leclercq, and J.-B. Lesort, "A traffic flow model for urban traffic analysis: Extensions of the LWR model for urban and environmental applications," in *Transportation and Traffic Theory in the 21st Century*. Leeds, West Yorkshire, England: Emerald Group Publishing Limited, 2002, pp. 393–415.
- [51] C. Lattanzio, A. Maurizi, and B. Piccoli, "Moving bottlenecks in car traffic flow: A PDE-ODE coupled model," *SIAM J. Math. Anal.*, vol. 43, no. 1, pp. 50–67, 2011, doi: [10.1137/090767224](https://doi.org/10.1137/090767224).
- [52] D. Monache, M. Laura, and P. Goatin, "Stability estimates for scalar conservation laws with moving flux constraints," *Networks Heterogen. Media*, vol. 12, no. 2, pp. 245–258, 2017, doi: [10.3934/nhm.2017010](https://doi.org/10.3934/nhm.2017010).
- [53] T. Liard and B. Piccoli, "Well-posedness for scalar conservation laws with moving flux constraints," *SIAM J. Appl. Math.*, vol. 79, no. 2, pp. 641–667, 2019, doi: [10.1137/18M1172211](https://doi.org/10.1137/18M1172211).
- [54] T. Liard and B. Piccoli, "On entropic solutions to conservation laws coupled with moving bottlenecks," *Commun. Math. Sci.*, vol. 19, no. 4, pp. 919–945, 2021, doi: [10.4310/CMS.2021.v19.n4.a3](https://doi.org/10.4310/CMS.2021.v19.n4.a3).
- [55] M. J. Lighthill and G. B. Whitham, "On kinematic waves. II. A theory of traffic flow on long crowded roads," *Proc. R. Soc. London Ser. A*, vol. 229, no. 1178, pp. 317–346, 1955.
- [56] P. I. Richards, "Shock waves on the highway," *Oper. Res.*, vol. 4, no. 1, pp. 42–51, 1956, doi: [10.1287/opre.4.1.42](https://doi.org/10.1287/opre.4.1.42).
- [57] K. Jang et al., "Reinforcement learning based oscillation dampening: Scaling up single-agent RL algorithms to a 100 AV highway field operational test," 2024, *arXiv:2402.17050*.
- [58] N. Lichtlé, E. Vinitsky, M. Nice, B. Seibold, D. Work, and A. M. Bayen, "Deploying traffic smoothing cruise controllers learned from trajectory data," in *Proc. Int. Conf. on Robotics and Automation (ICRA)*, Piscataway, NJ USA: IEEE, 2022, pp. 2884–2890, doi: [10.1109/ICRA46639.2022.9811912](https://doi.org/10.1109/ICRA46639.2022.9811912).
- [59] M. Treiber, A. Hennecke, and D. Helbing, "Congested traffic states in empirical observations and microscopic simulations," *Phys. Rev. E*, vol. 62, no. 2, 2000, Art. no. 1805, doi: [10.1103/PhysRevE.62.1805](https://doi.org/10.1103/PhysRevE.62.1805).
- [60] S. Albeaik et al., "Limitations and improvements of the intelligent driver model (IDM)," *SIAM J. Appl. Dyn. Syst.*, vol. 21, no. 3, pp. 1862–1892, 2022, doi: [10.1137/21M1406477](https://doi.org/10.1137/21M1406477).
- [61] J. W. Lee et al., "Traffic control via connected and automated vehicles: An open-road field experiment with 100 CAVs," 2024, *arXiv:2402.17043*.
- [62] D. Gloudemanns et al., "I-24 motion: An instrument for freeway traffic science," *Transp. Res. C: Emerg. Technol.*, vol. 155, Oct. 2023, Art. no. 104311, doi: [10.1016/j.trc.2023.104311](https://doi.org/10.1016/j.trc.2023.104311).
- [63] "Circles." Circles. Accessed: Aug. 16, 2024. [Online]. Available: <https://circles-consortium.github.io/>
- [64] D. Gloudemanns et al., "Interstate-24 motion: Closing the loop on smart mobility," in *Proc. IEEE Workshop Des. Autom. CPS IoT (DESTION)*, Piscataway, NJ USA: IEEE, 2020, pp. 49–55, doi: [10.1109/DESTION50928.2020.00014](https://doi.org/10.1109/DESTION50928.2020.00014).
- [65] Y. Zhang, M. Quinones-Grueiro, W. Barbour, C. Weston, G. Biswas, and D. Work, "Quantifying the impact of driver compliance on the effectiveness of variable speed limits and lane control systems," in *Proc. IEEE 25th Int. Conf. Intell. Transp. Syst. (ITSC)*, 2022, pp. 3638–3644, doi: [10.1109/ITSC55140.2022.9922471](https://doi.org/10.1109/ITSC55140.2022.9922471).
- [66] Y. Zhang et al., "Cooperative multi-agent reinforcement learning for large scale variable speed limit control," in *Proc. IEEE Int. Conf. Smart Comput. (SMARTCOMP)*, 2023, pp. 149–156, doi: [10.1109/SMArtComp58114.2023.00036](https://doi.org/10.1109/SMArtComp58114.2023.00036).
- [67] N. Kardous et al., "A rigorous multi-population multi-lane hybrid traffic model and its mean-field limit for dissipation of waves via autonomous vehicles," 2022, *arXiv:2205.06913*.
- [68] A. Hayat et al., *A Holistic Approach to the Energy-Efficient Smoothing of Traffic via Autonomous Vehicles*. Cham, Switzerland: Springer International Publishing, 2022, pp. 285–316.
- [69] J. W. Lee et al., "Integrated framework of vehicle dynamics, instabilities, energy models, and sparse flow smoothing controllers," in *Proc. Workshop Data-Driven Intell. Cyber-Phys. Syst.*, New York, NY, USA: Association for Computing Machinery, 2021, pp. 41–47, doi: [10.1145/3459609.3460530](https://doi.org/10.1145/3459609.3460530).
- [70] Z. Fu, K. Manke, and A. M. Bayen, "Massive CAV experiment in Nashville pits machine learning against traffic jams." Informs. Accessed: May 6, 2023. [Online]. Available: <https://pubsonline.informs.org/do/10.1287/orms.2023.02.05/full/>
- [71] M. Ameli et al., "Design, preparation, and execution of the 100 AV field test for the circles consortium: Methodology and implementation of the largest mobile traffic control experiment to date," 2024, *arXiv:2404.15533*.
- [72] D. Gloudemanns et al., "So you think you can track?" 2023, *arXiv:2309.07268*.
- [73] D. Gloudemanns, Y. Wang, G. Gumm, W. Barbour, and D. B. Work, "The interstate-24 3d dataset: A new benchmark for 3D multi-camera vehicle tracking," 2023, *arXiv:2308.14833*.
- [74] D. Gloudemanns and D. B. Work, "Vehicle tracking with crop-based detection," in *Proc. 20th IEEE Int. Conf. Mach. Learn. Appl. (ICMLA)*, Piscataway, NJ USA: IEEE, 2021, pp. 312–319, doi: [10.1109/ICMLA52953.2021.00055](https://doi.org/10.1109/ICMLA52953.2021.00055).
- [75] Y. Wang, J. Ji, W. Barbour, and D. B. Work, "Online min cost circulation for multi-object-tracking on fragments," in *Proc. IEEE Int. Intell. Transp. Syst. Conf. (ITSC)*, Piscataway, NJ USA: IEEE, 2023, pp. 2803–2810, doi: [10.1109/ITSC57777.2023.10422670](https://doi.org/10.1109/ITSC57777.2023.10422670).
- [76] Y. Wang et al., "Automatic vehicle trajectory data reconstruction at scale," 2022, *arXiv:2212.07907*.
- [77] G. Zachár, "Visualization of large-scale trajectory datasets," in *Proc. Cyber-Phys. Syst. Internet Things Week*, New York, NY, USA: Association for Computing Machinery, 2023, pp. 152–157, doi: [10.1145/3576914.3587710](https://doi.org/10.1145/3576914.3587710).

Traffic Control via Connected and Automated Vehicles (CAVs)

AN OPEN-ROAD FIELD EXPERIMENT WITH 100 CAVs



©SHUTTERSTOCK.COM/VIDEOFLOW

JONATHAN W. LEE , HAN WANG, KATHY JANG , NATHAN LICHTLÉ, AMAURY HAYAT, MATTHEW BUNTING, ARWA ALANQARY, WILLIAM BARBOUR, ZHE FU, XIAOQIAN GONG, GEORGE GUNTER, SHARON HORNSTEIN, ABDUL RAHMAN KREIDIEH, MATTHEW W. NICE, WILLIAM A. RICHARDSON, ADIT SHAH, EUGENE VINITSKY, FANGYU WU, SHENGQUAN XIANG, SULAIMAN ALMATRUDI, FAHD ALTHUKAIR, RAHUL BHADANI, JOY CARPIO, RAPHAEL CHEKROUN, ERIC CHENG, MARIA TERESA CHIRI, FANG-CHIEH CHOU, RYAN DELORENZO, MARSALIS GIBSON, DEREK GLOUDEMANS, ANISH GOLLAKOTA, JUNYI JI, ALEXANDER KEIMER, NOUR KHOUDARI, MALAIKA MAHMOOD, MIKAIL MAHMOOD, HOSSEIN NICK ZINAT MATIN, SEAN MCQUADE, RABIE RAMADAN, DANIEL URIELI , XIA WANG, YANBING WANG, RITA XU, MENGSHA YAO, YILING YOU, GERGELY ZACHÁR, YIBO ZHAO, MOSTAFA AMELI, MIRZA NAJAMUDDIN BAIG, SARAH BHASKARAN, KENNETH BUTTS, MANASI GOWDA, CAROLINE JANSEN, JOHN LEE, LIAM PEDERSEN, RILEY WAGNER, ZIMO ZHANG, CHANG ZHOU, DANIEL B. WORK , BENJAMIN SEIBOLD , JONATHAN SPRINKLE , BENEDETTO PICCOLI , MARIA LAURA DELLE MONACHE , and ALEXANDRE M. BAYEN

The CIRCLES project aims to reduce instabilities in traffic flow, which are naturally occurring phenomena due to human driving behavior. Also called “phantom jams” or “stop-and-go waves,” these instabilities are a significant source of wasted energy. Toward this goal, the CIRCLES project designed a control system, referred to as the MegaController by the CIRCLES team, that could be deployed in real traffic. Our field experiment, the MegaVanderTest (MVT), leveraged a heterogeneous fleet of 100 longitudinally controlled ve-

hicles as Lagrangian traffic actuators, each of which ran a controller with the architecture described in this article. The MegaController is a hierarchical control architecture that consists of two main layers. The upper layer is called the *Speed Planner* and is a centralized optimal control algorithm. It assigns speed targets to the vehicles, conveyed through the LTE cellular network. The lower layer is a control layer, running on each vehicle. It performs local actuation by overriding the stock adaptive cruise controller, using the stock onboard sensors. The Speed Planner ingests live data feeds provided by third parties as well as data from our own control vehicles and uses both to perform the speed assignment. The architecture of the Speed Planner

Digital Object Identifier 10.1109/MCS.2024.3498552

Date of current version: 14 January 2025



DISCLAIMER

The views expressed herein do not necessarily represent the views of the U.S. Department of Energy or the U.S. Government.

demonstrate the potential of an AV and highway system for societal benefit [1]. The consortium partners included the University of California (UC) Berkeley, California Partners for Advanced Transit and Highways (PATH) and General Motors (GM), among several others. In the implementation of Demo '97 on Interstate 15 in San Diego [2], CA, USA, the consortium introduced and/or brought to realization concepts such as adaptive cruise control (ACC), vehicle-to-vehicle (V2V) communication, and cooperative ACC (CACC) [3], [4], [5]. The demonstrations involved high-speed platooning, made possible by V2V and CACC, as well as infrastructure sensor integration. Moreover, it laid the foundation for modern automated highway system (AHS) architectures, emphasizing the importance of V2V and vehicle-to-infrastructure (V2I) communications [6]. Some of the key challenges and barriers faced at the time included scalability due to infrastructure, reliable communication systems, and accurate vehicle positioning. Its eventual demise came in the late 1990s with tightening of research budgets at the U.S. Department of Transportation (DOT).

» *Generation Two:* In the 2000s, the Defense Advanced Research Projects Agency (DARPA) introduced the DARPA Grand Challenge. In the first Grand Challenge (2004), a US\$1 million prize was offered to any team whose autonomous vehicle could complete a 150-mi course in the Mojave Desert; no teams were

allows for the modular use of standard control techniques, such as optimal control, model predictive control (MPC), kernel methods, and others. The architecture of the local controller allows for the flexible implementation of local controllers. Corresponding techniques include deep reinforcement learning (RL), MPC, and explicit controllers. Depending on the vehicle architecture, all onboard sensing data can be accessed by the local controllers or only some. Likewise, control inputs vary across different automakers, with inputs ranging from torque or acceleration requests for some cars to electronic selection of adaptive cruise control (ACC) setpoints in others. The proposed architecture technically allows for the combination of all possible settings proposed previously, that is {Speed Planner algorithms} \times {local Vehicle Controller algorithms} \times {full or partial sensing} \times {torque or speed control}. Most configurations were tested throughout the ramp up to the MegaVandertest (MVT).

The promise of generating societal benefits from autonomous vehicle technology has long been capturing the imagination of researchers, legislators, and popular culture. Its footprints can be seen in the earliest stages of modern automated vehicle (AV) research and development in the United States. AV technology advancements, spanning over three decades of work, are sometimes broken down into three generations.

» *Generation One:* In the 1990s, the Federal Highway Administration (FHWA) established the National Automated Highway System Consortium (NAHSC) to

Summary

In November 2022, the CIRCLES project deployed 100 longitudinally-controlled connected and automated vehicles in live traffic to demonstrate a reduction of traffic flow instabilities. To this end, a modular and hierarchical control algorithm was designed, featuring a server-side Speed Planner and a vehicle-side Vehicle Controller. The modular nature of these components allowed multiple approaches to be developed and tested, while the hierarchical nature allowed for downstream information to be utilized locally. Furthermore, the controller architecture facilitated the use of a heterogeneous vehicle fleet, where certain vehicle makes and models required unique design choices to overcome real-world challenges. This paper introduces the architectural design philosophy, details the specific controller designs, and presents specific implementation details for the actual experiment.

successful. The second Grand Challenge (2005) doubled the prize money, and five teams were successful in completing the course [7]. The third Grand Challenge (2007) moved to an urban environment. The DARPA Grand Challenge competitions were notable for creating a renewed interest in autonomous vehicles and directly supporting efforts to commercialize successful technologies [8] in the following decade.

» *Generation Three:* In the 2010s, many major automotive manufacturers (such as GM, BMW, Audi, and Tesla) and technology companies (such as Google/Waymo, Uber, and Lyft) began developing autonomous vehicle technology for commercialization purposes. The investments have generated an industrial ecosystem centered on hardware, software, and services designed to advance fully autonomous driving. Today, multiple companies are testing AVs on numerous public roads in the United States, with Waymo most notably operating an autonomous ride-share service in Phoenix, San Francisco, and Los Angeles without a safety driver in the vehicle and Cruise operating autonomous shuttles in San Francisco. At the same time, Level 1 and Level 2 AV technologies, including ACC, are now widely available in the commercial market. These commercial systems predominantly focus on safety and driver comfort [9] rather than improved transportation system efficiency [10].

Many experiments involved using CACC within platooning experiments to improve fuel efficiency on highways [11]. In 2009, the Safe Road Trains for the Environment (SARTRE) [12] three-year project was funded by the European Commission to investigate the benefits of platooning (following previous European projects, such as PROMOTE CHAUFFEUR I + II or Konvoi), where a leading bus or truck driven by a professional driver controls a following platoon of a few heavy or light vehicles, achieving up to 16% energy savings [13] on public highways. In other works, Energy ITS [14] deployed a platoon of three fully automated trucks in Japan in 2008. In 2011, nine teams developed CACC controllers with V2V communication and compared them in urban and highway settings as part of the Grand Cooperative Driving Challenge (GCDC) [15], [16] held in The Netherlands and later reiterated in a 2016 edition [17]. Between 2015 and 2017, the California PATH program has been involved in CACC truck platooning experiments on public highways [18]. More recently, the European ENSEMBLE project [19] investigated multibrand truck platooning to integrate V2V technologies in all European brands of trucks.

Additional studies have experimentally demonstrated the benefits of vehicle platooning. In [20] and [21], CACC platoons were developed and deployed on commercially available vehicles using linear control theory and string stability. These CACC platoons were shown to outperform ACC vehicles in terms of disturbance dissipation.

Ref. [22] showed in simulations that a moderate penetration rate of CACC vehicles can significantly increase network capacity. The research in [23] demonstrated that CACC control allows for safe platooning at low following distances and high speeds, thus improving traffic throughput. Furthermore, [24] indicated that energy consumption in freight trucks could be reduced by driving at low following distances due to decreased air resistance. Recent experiments in [25] built upon these prior CACC studies by employing MPC V2I communication, showing that vehicle platoons can enhance throughput on arterial roadways with traffic lights.

Our work brings full circle the nascent imaginings from the early 1990s. The Generation One promise of automating highways for societal benefit began to manifest in the late 2010s within our team and in several groups around the world. In 2016, a group led by coauthors Delle Monache, Piccoli, Seibold, Sprinkle, and Work replicated the Sugiyama experiment [26] of string instability in a ring road; in what is known as the “Arizona ring experiment,” they further demonstrated that phantom jams can be reduced using partially AV technologies and specially designed algorithms [27]. This work was followed shortly by coauthor Bayen’s lab at UC Berkeley with the development of Flow, a software package to interface then-state-of-the-art microsimulation software with deep-RL libraries [28], [29], [30], [31], [32], [33]. With Flow, the UC Berkeley team was able to independently train an AV controller to replicate the findings of the Arizona ring experiment [34] and generalize them to a variety of other settings, such as freeway and urban traffic [30]. (Note the distinction in terminology between “autonomous vehicle” and “automated vehicle,” specifically because our past and present work focuses on automated longitudinal control as Lagrangian traffic controllers.)

In 2019, coauthors Bayen, Piccoli, Seibold, Sprinkle, and Work united to form the Congestion Impacts Reduction via CAV-in-the-loop Lagrangian Energy Smoothing (CIRCLES) Consortium (see <https://circles-consortium.github.io/>) [36], [37], [38], joined shortly thereafter by coauthors Lee and Delle Monache, each leading various aspects of the CIRCLES project. The CIRCLES project seeks to extend these prior research efforts to real traffic. To achieve our goals, our group designed a modular hierarchical control framework, consisting of a centralized Speed Planner and decentralized Vehicle Controllers, and implemented it on 100 vehicles in a large-scale field operational test, dubbed the *MegaVanderTest (MVT)*. Our aim is to deploy flow-smoothing ACC-enabled AVs that don’t require explicit communication and are mixed within highway traffic in an unstructured way, contrary to many of the CACC truck platooning experiments previously mentioned. As many modern vehicles come equipped with ACC technology, the focus of this work is to modify the ACC algorithm to become significantly better at flow smoothing, without requiring additional hardware, road infrastructure, or V2V communication capabilities.

This article presents our control system design and subsequent analysis of field test results. Diverse candidates for each module of the framework are developed utilizing cross-disciplinary knowledge and tools, including ordinary differential equation/partial differential equation (ODE/PDE)-based flow control [39], [40], deep-RL [41], stabilization theory [42], functional analysis [43], optimal control on microscopic and macroscopic systems [44], [45], approximation theory [46], mean-field limits [47], nonentropic solutions to hyperbolic systems [48], MPC via linearly constrained quadratic programming (LCQP) [49], kernel smoothing [50], traffic flow theory [51], variable speed limit [52], and many other areas. The control system was then evaluated and tested on the open road as part of the MVT, the largest deployment of AVs designed to smooth traffic flow. In this test, we deployed 100 AVs on Interstate 24 (I-24) near Nashville, TN, USA, in November 2022. The experiment coincided with the debut of I-24 Mobility Technology Interstate Observation Network (MOTION) (<https://i24motion.org>) [53], [54], a 4-mi section of I-24 near Nashville, TN, USA, to capture ultrahigh-resolution trajectory data of all vehicles.

The rest of the article is organized as follows. The section “[Design of the Controller Architecture](#)” introduces the *MegaController*, our controller architecture, which consists of several components that operate together. The section “[Design of Controller Components](#)” then details the design and functioning of each of these individual components. The section “[Candidate Controller Selection](#)” explains how controllers are selected for the test, and finally, the section “[Open-Road Field Operational Test](#)” introduces the experimental design for the 100 AV deployment as well as implementation details for the selected controllers and deployment on hardware and data collection procedures. Preliminary findings and insights are presented in the “[Results](#)” section, followed by concluding remarks in the “[Conclusion](#)” section. Furthermore, several sidebars are spread throughout the article, which can serve different roles: giving background about certain parts of the projects, diving into much more detail about certain aspects of the project, or presenting interesting work that happened before or in parallel to the project or that didn’t make it into the final deployment. The sidebars are as follows, in order of appearance: “[Adaptive Cruise Control Modeling](#),” “[Macroscopic ODE/PDE Models](#),” “[Optimal Control of Measure PDEs](#),” “[MPC Controller](#),” “[Optimized Vehicle Trajectory](#),” “[Vehicle Energy Models](#),” “[Trajectory Simulator](#),” “[Car-Following Models](#),” and “[Vehicle Interfacing](#).”

This work presents a modular hierarchical control framework, consisting of a centralized Speed Planner and decentralized Vehicle Controllers, as it was used during the MVT.

DESIGN OF THE CONTROLLER ARCHITECTURE

We introduce the *MegaController*, a control framework depicted in [Figure 1](#), for the mixed-autonomy traffic flow problem. Mixed autonomy refers to the setting in which some vehicles

are automated while other vehicles are manually controlled (level 0 automation). The primary design paradigm of the control framework is to achieve two goals: hierarchy for task allocation and modularity for control flexibility.

We designed a hierarchical structure to efficiently coordinate the control goals between macroscopic traffic flow optimization [57] and microscopic vehicle control [58], [59], [60], [61] and to efficiently solve the computational task allocation problem between the server and vehicle sides. There is an inherent interplay between the two components as the Speed Planner informs the vehicle controller of downstream events, and the vehicles are instrumented to report observations to the server for data aggregation.

Use of Modular Design

A modular structure is used for two important purposes: 1) to facilitate a diversity of controller design approaches and 2) to enable a heterogeneous vehicle fleet with different sensing and actuation capabilities.

As long as each controller utilizes the available interfaces, it is technically straightforward to exchange different controllers when using a modular design. This decision allows us to support a wide range of expertise from our team, who may explore many different designs, each with a different technical focus or approach. While there may be subtleties for stability, convergence, and other properties if integration decisions are made strictly through type matching, our modular approach mitigates a key challenge: the dynamics of the roadway and our ability to control it may not be fully understood until testing begins. Since testing may be possible only at a scale when we can evaluate its impact, we will be very close to the full test deadline when we make final decisions. By embracing a modular approach, we can use data from tests that concluded fewer than 24 h earlier to decide what controller to run during the following test.

The fleet of vehicles used in the MVT represented three different years, makes, and models. The fleet was composed of 2023 Nissan Rogue, 2022 Cadillac XT5, and 2020–2021 Toyota RAV4 vehicles. Trade secrets and design differences between the systems on these vehicles mean that it is not possible to have a uniform system interface for sensing and control. For example, although each car we used has ACC that uses forward-facing radar for safety, the data from those sensors were not available to our system for all vehicle types. Designing a controller that can work on only one vehicle type may give greater controllability but reduces the potential impact of the design when deployed at a societal scale.

Thus, it is a design strength that our system can operate across vehicles with myriad different sensing and control modalities. While the interfaces to the Speed Planner remain the same, different vehicles will have different implementations that have completely unique characteristics compared to other vehicles, similar to textbook design

patterns in software engineering for producer/consumer architectures. This allows the flexibility to adapt to a heterogeneous fleet, theoretically opening the door to many other vehicle configurations and constraints.

In the MegaController design, there are two distinct components as follows:

- » The first component is a server-side *Speed Planner*, which is a centralized planner unit that provides high-level macroscopic speed suggestions based on periodic state updates from the distributed vehicles and external macroscopic data sources, like INRIX employed in this study. The algorithms deployed on the server side are designed to handle computationally heavy data aggregation and macro-state tasks.
- » The second component is a vehicle-side *Vehicle Controller*, which is a networked decentralized controller [62] that commands local actuation of the vehicle. The algorithms deployed here take into

consideration the target speed suggested by the server-side planner unit, the latency of that information, and any observations from the vehicle's onboard sensors.

Borrowing conceptually from object-oriented programming, the interfaces are agreed upon a priori, allowing an abstraction of individual components for ease of design and testing.

Speed Planner

The objective of the Speed Planner is to optimize the overall traffic flow efficiency by providing macroscopic guiding speeds for AV fleets using realtime traffic data from multiple heterogeneous sources. While optimality for our deployment was defined by flow efficiency, our framework allows for arbitrary objective functions.

The data sources at our disposal are the set of recent vehicle ping messages from our AV fleet using our custom hardware and software stack as well as aggregated vehicular

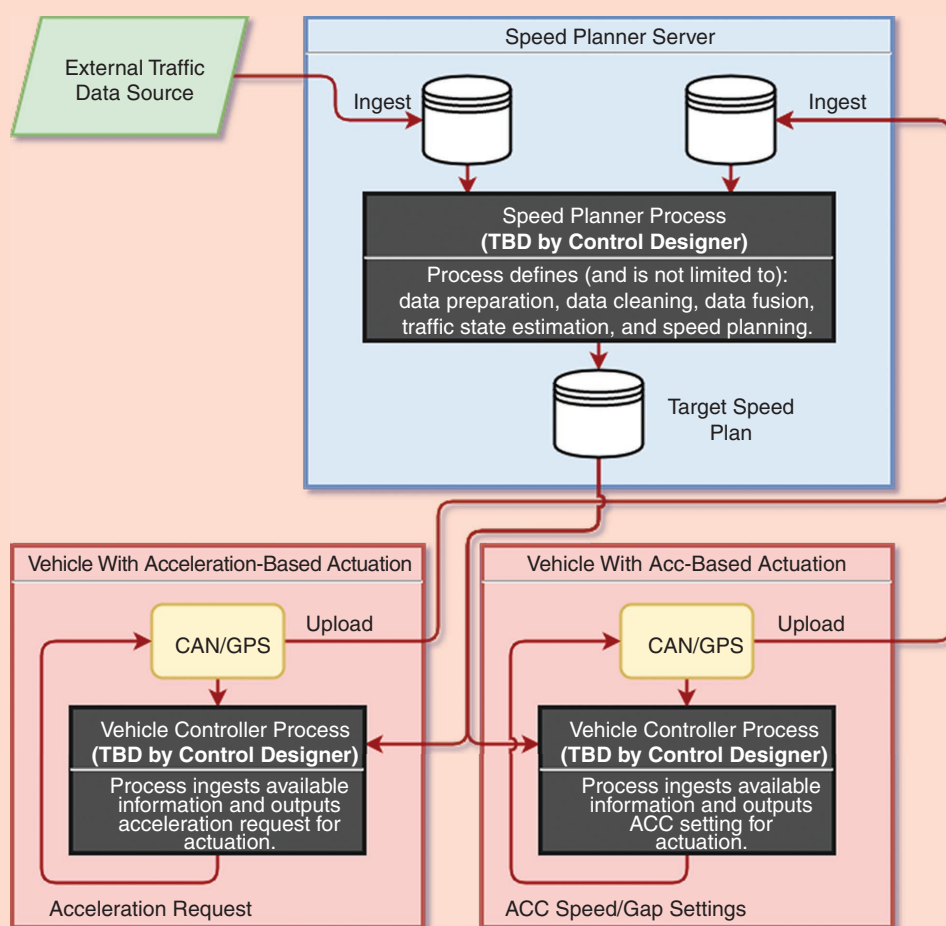


FIGURE 1 The architectural framework of the MegaController. The hierarchical and modular nature of the design allows for greater flexibility in design decisions and dealing with varied sensing and actuation capabilities of the heterogeneous fleet. The blue box represents the centralized Speed Planner unit, and the red boxes represent decentralized vehicle controllers, which are vehicle dependent (that is, each vehicle has a different control architecture and thus requires a different control paradigm). The components work in concert to achieve the higher-level goals of flow smoothing. TBD: to be determined.

velocity data within distinct sections of highway through INRIX, a provider of live data for traffic, parking, and other transportation data. INRIX data have been studied in the literature for their applicability in traffic estimation and validated by researchers for their accuracy using post hoc methods [63]. Utilizing these heterogeneous data sources presented some key challenges and considerations, namely unknown latency of external data sources and differences in spatial and temporal resolution of those data sources when fused with our vehicle message data. Although the specific aggregation algorithm is not publicly known, INRIX data latency is explored in [64], which describes delays between 3 and 5 min, and in some cases, up to 10 min. A summary of data specifications can be found in Table 1.

Targeting the challenges, the two main functions of the Speed Planner are 1) traffic state estimation (TSE) enhancement and 2) the design of the Speed Plan, an ideal target speed profile. The TSE enhancement module is designed to eliminate the effects of inherent latency in the third-party data source and to improve the spatial and temporal resolution of the input traffic data. The target design module generates Speed Plans with the goal of reducing vehicle energy consumption and increasing the overall throughput of the traffic flow. Various approaches are utilized to develop the target design module, including kernel smoothing [50], ODE/PDE-based flow control [39], and vehicle trajectory optimization [58].

Vehicle Controller

The Vehicle Controller enables each car to use traffic information provided by the Speed Planner in context with the local state, such as the distance to the vehicle in front, relative speed, etc. The Vehicle Controller aims to improve the flow of traffic while ensuring the safety of both the AV and other vehicles around it.

Input data for the Vehicle Controller are obtained from the in-vehicle network and may include other inputs, such as the target speeds from the Speed Planner. A subset of data from the controller area network (CAN) bus is made available to the vehicle controller and varies depending on the vehicle make/model/year. Realizing control algorithms on vehicles required new computer hardware, electronics, and software development [65], [66], [67], [68], [69], [70] because of the heterogeneity in vehicle data and control interfaces.

Depending on the vehicle platform, we have explored options including speed-based control [71], [72], acceleration-based control [67], [73], and ACC-based control [41]. Speed-based control was initially explored but then deprecated as acceleration-based control best matched desired goals from algorithm designers. The acceleration-based and ACC-based approaches fit into the overall architectural design. Torque-based control (that is, applying the requisite torque directly to the gears) would be the most prescriptive control with the tightest actuation, but it also requires a level of CAN bus access that prevents the quick return of the vehicle to the

stock state. The majority of the vehicles used in the experiment were stock vehicles that were later returned to the manufacturer, so all changes to enable experimental control needed to be minimal and noninvasive changes to the vehicle. Therefore, for this deployment, our architecture included two types of control capabilities on our heterogeneous fleet, which are summarized in Table 2.

Architectural Details of the Acceleration-Based Controller

While acceleration controllers don't have natural safety enforcement, such as the one speed controllers have, we have found a way to add safety enforcements. Using new approaches in [74], we demonstrated that it was possible to constrain unsafe accelerations when they were passed to the vehicle. This opened the door to the use of acceleration-based control on cars that support it. Acceleration-based control is a natural analog to how most of us drive; we

TABLE 1 A summary table of the data sources for TSE (and subsequent processes). INRIX aggregates data from a fleet of vehicles on the road. The AV Ping data come from our own fleet, where each car posts speeds to the server through an API that contains speed (from CAN) and positioning (from GPS) as well as timing and vehicle identity information.

Data Source	INRIX	AV Ping
Period (s)	60	1
Latency (s)	~180	negligible
Segment length (mi)	~0.5 (varied)	Not applicable
Lateral aggregation	Lane averaged	Lane specific

TABLE 2 A summary table of the sensing and actuation available to our system for the heterogeneous vehicle fleet. *Space gap* refers to the distance between the ego vehicle's front bumper and the leader vehicle's rear bumper. The *minicar* refers to a Boolean indication of whether the ego vehicle's sensors detect the presence of a leader vehicle (an approximate 80–100-m maximum distance). *Relative speed* is the leader vehicle's speed minus the ego vehicle's speed.

Vehicle(s)	Nissan Rogue, Cadillac XT5		
	Toyota RAV4	ACC	
Sensing	Ego position	✓	✓
	Ego speed	✓	✓
	Ego ACC speed setting	✓	✓
	Ego ACC gap setting	✓	✓
	Leader space gap	✓	✗
	Leader minicar	✓	✓
	Leader relative speed	✓	✗

press down on the accelerator pedal when we want to go faster, and we either let off the accelerator or press the brake pedal when we want to go slower.

When making control requests to the car, we provide a desired input over the vehicle's CAN, which is interpreted by the powertrain and ACC subsystems of the car. This desired input is not strictly a direct acceleration command; it is processed by the vehicle's ACC system, which interprets the commanded acceleration and decides whether it will meet it 1) by actuating the brake, 2) by decreasing acceleration through reducing the throttle, 3) by keeping the throttle constant, or 4) by increasing the throttle. Examples of how these dynamics from step inputs have been observed can be found in [71]. The specific input selected by the car is a function of many different vehicle dynamics and perhaps even trade secrets for reducing the wear and tear of parts, so there is no single mapping or predictive function that easily codifies the transfer function of the system once an acceleration is requested.

Using acceleration-based control *implicitly* adds safety challenges as the controller must ignore all existing acceleration commands from the car—including any acceleration commands that come from the safety subsystems on board. Safety wrappers such as [74] are needed to prevent rear-end collisions, and additional care must be taken to evaluate external sensors. Further, environmental challenges such as lane changes by other vehicles require our system to ensure that our dynamics do not inadvertently cause their own stop-and-go waves. We decompose the behavior of this controller into two modes as follows:

- » A *base controller* prescribes a performance-based desired acceleration under “ideal” conditions. The base controller is designed to output an acceleration that satisfies a specific performance-based goal, for example, reducing energy footprint or minimizing the magnitude of accelerations. In general, care is taken during its design phase to ensure that other aspects of the traffic flow are not negatively impacted. Note that the base controller should still, by design, be safe and collision free, under the assumption that accelerations are actuated perfectly.
- » A *lane-change recovery controller* modulates the base controller's desired acceleration in the event of discontinuities in the lead-vehicle space gap. The acceleration output of the base controller can change dramatically if there is a time discontinuity in the input signals. Most commonly, this appears in the form of a lane change by another vehicle in front of the ego vehicle. Since a lane change is out of the ego vehicle's control, it can theoretically put the ego vehicle into an unsafe state if the objective were to control a time gap with discontinuous input. This mode recognizes that discrete changes in the space gap are not controller failures, so the objective of this controller is to comfortably return the vehicle to a safe state where the base controller can resume actuation.

Architectural Details of the ACC-Based Controller

Another option for controlling vehicles is to update the vehicle's ACC setpoints electronically. This mimics what the driver can do through buttons on the steering wheel and has the benefit of keeping the safety features of the car's ACC systems in the loop. This approach is contrasted with the acceleration-based approach in a few ways, notably the following:

- » The controllability of the system is affected, and the bandwidth of the controller is likely reduced since the stock ACC has its own gains and modes.
- » The multimodel design features of the acceleration-based approach (namely the lane-change recovery controller and safety wrapper) are not needed here as those features are built into the stock ACC algorithm.

To understand the changes in controllability, we explored the vehicle's ACC dynamics with the goal of making design decisions on whether rate limits or other constraints on the input signals would be required for stability or performance reasons. Every vehicle make and model equipped with ACC has its own unique mapping of state space (for example, ego speed, space gap, leader speed, etc.) and ACC inputs (speed setting and gap setting) to actuated acceleration. Architecturally, we take as given that this model is available for the design of the base ACC controller. For a more detailed discussion of ACC and our specific approach to obtaining a model for our algorithm design, see the section “[Design Details of the ACC-Based Controller](#).”

As a result, the only component of the ACC-based controller that requires specific designing is the base controller. Just as with the acceleration-based controller, the base controller is performance based, striving for some performance goal. Similar design philosophies are applied as before. Uniquely different, as noted previously, is that this base controller does not need to explicitly consider safety and vehicle-specific dynamics—the controller design can implicitly account for the vehicle-specific dynamics by utilizing the ACC model in a feedback loop (see “[Adaptive Cruise Control Modeling](#)”).

The MVT deployed 100 vehicles in November 2022 and was the largest coordinated open-road test designed to smooth traffic flow.

DESIGN OF CONTROLLER COMPONENTS

Here, we describe in detail how each of the modular components was designed. The discussion is in a parallel structure to the previous section, with a particular focus on controllers that were actually implemented for deployment. In the life span of the project, we explored many approaches for designing the controller. See “[MPC Controller](#)” and “[Optimized Vehicle Trajectory](#)” for some notable research and designs that were not deployed but contributed key concepts that helped the ultimate implementation.

Design Details of the Speed Planner

Based on the hierarchical framework, [Figure 2](#) (shown later) indicates the implementation of the Speed Planner we tested in the MVT. As introduced in [Table 1](#), INRIX and probe vehicle data are posted to the central database in different frequencies; each vehicle makes its post approximately every 1 s, and a server-side process inserts new data from INRIX approximately every 60 s. It is important to note that while the INRIX data provide a single speed across all lanes, the AV pings provide lane-level speed information.

The sequence of events of a Speed Plan publication can be summarized as follows:

- 1) Each new INRIX update is combined with historical INRIX data and fed into the prediction module.
- 2) All vehicle observations from the previous 60 s are fetched and then fused with the INRIX prediction to obtain a lane-level traffic state estimate.
- 3) The lane-level TSE is smoothed with the forward-kernel average.
- 4) Bottleneck identification is performed with the smoothed lane-level TSE.
- 5) If a standing bottleneck is identified in the lane, a deceleration region is prescribed as a buffer segment.

For all other regions, the smoothed lane-level TSE is used as the lane-level Speed Plan.

6) Publish the Speed Plan for all lanes.

The subsequent sections delve deeper into the intricacies of the TSE enhancement and target design modules, providing a comprehensive understanding of the steps outlined previously. Wang et al. [39] provide an in-depth methodology description of the Speed Planner.

TSE Enhancement

The TSE enhancement module comprises two main components: the INRIX prediction module and the data fusion module. The prediction module's primary role is to minimize the latency issues associated with INRIX realtime data, especially when applied to vehicular control, as opposed to its standard use for general traffic insights. The fusion module complements this by integrating realtime data from our system's probe vehicles, enabling a more detailed lane-level TSE with enhanced time–space precision. A detailed mathematical explanation of the TSE enhancement module for MVT implementation is available in [39].

To achieve a lane-level TSE with superior spatial detail, we further segment the INRIX data into smaller units.

Adaptive Cruise Control Modeling

by Fang-Chieh Chou and Jonathan W. Lee

Adaptive cruise control (ACC) is an advanced driver assistance system that automatically operates vehicles at a set driving speed or keeps a set driving gap with respect to a leading vehicle. The operation of ACC requires a speed setting and a gap setting input by the driver. When there is no leading vehicle, ACC automatically adjusts the vehicle's driving speed to the speed setting preset by the driver. When there is a leading vehicle ahead, the system automatically regulates the gap with respect to the leading vehicle to a separation set by the driver while not driving faster than the speed setting.

An ACC-controlled car can, therefore, be modeled as a dynamical system composed of two control modes: speed-control mode and gap-control mode. The system switches between two modes depending on the proximity and speed of a leading vehicle. When there is no nearby leading vehicle, the system is in speed-control mode, in which the system tracks the speed setting. On the other hand, when the system is in gap-control mode, the system tracks both the leading vehicle speed and the gap setting.

To model an ACC-controlled car, we used parametric models for each control mode. Mathematically, the speed-control mode can be written as

$$a_e = f_p(v_e, v_{ref}) \quad (S1)$$

where a_e is the acceleration of the ego vehicle, v_e is the speed of the ego vehicle, and v_{ref} is the speed setting. $f_p: \mathbb{R} \times \mathbb{R} \rightarrow \mathbb{R}$ is a parametric model of parameters p .

Gap-control mode can be written as

$$a_e = f_g(v_e, v_l, d_{el}, g_{ref}) \quad (S2)$$

where v_l is the speed of the leading vehicle, d_{el} is the space gap between the ego vehicle and the leading vehicle, and g_{ref} is the gap setting. $f_g: \mathbb{R} \times \mathbb{R} \times \mathbb{R} \times \mathbb{R} \rightarrow \mathbb{R}$ is a parametric model of parameters g .

To fit parameters p and q for speed-control mode and gap-control mode, field experiments are carried out using a Nissan Leaf vehicle equipped for data collection. For the speed-control mode, data collection is done with a variety of initial speeds and speed settings so that dynamic responses with different speed changes can be collected. For the gap-control mode, highway driving data under different traffic conditions are collected so that dynamic response over a range of speeds can be covered in the dataset. The collected data are firstly smoothed to reduce sensor noise. Some outliers of abnormal driving conditions (for example, temporally near cut-in and cut-out events) are removed before fitting the models. The model is validated by comparing the dynamic response of the model in simulation to the response of the real system in field experiments. While the models are fitted for the Nissan Leaf, they are assumed to be acceptable approximations for the ACC systems of other vehicles in our AV fleet.

Macroscopic ODE/PDE models

by Xiaoqian Gong

Here, we model the traffic dynamics in the presence of M AVs and N human-driven vehicles in a single lane from the microscopic perspective using systems of ODEs. We assume that only AVs can be controlled and have a greater impact on the vehicle population than human-driven vehicles. Let $T > 0$ be a fixed time horizon, and $I_M = \{1, \dots, M\}$ and $I_N = \{1, \dots, N\}$ are the index sets of AVs and human-driving vehicles, respectively. Denote by $(x, v) \in \mathbb{R}^N \times \mathbb{R}_{\geq 0}^N$ and $(y, w) \in \mathbb{R}^M \times \mathbb{R}_{\geq 0}^M$ the position-velocity vectors of human-driven vehicles and AVs, respectively. To represent the positions and velocities of the M AVs during the time interval $[0, T]$, we define the time-dependent atomic probability measure on $\mathbb{R} \times \mathbb{R}_{\geq 0}$, also referred to as the *empirical measure*, as

$$\mu_M(t) = \frac{1}{M} \sum_{i=1}^M \delta_{(y_i(t), w_i(t))}, \quad t \in [0, T]. \quad (\text{S3})$$

Alternatively, we can represent solutions as a measure supported on absolutely continuous trajectories $t \in [0, T] \mapsto (y_i(t), w_i(t)) \in \mathbb{R} \times \mathbb{R}_{\geq 0}$, $i \in I_M$. Similarly, we use the atomic measure

$$\mu_N(t) = \frac{1}{N} \sum_{j=1}^N \delta_{(x_j(t), v_j(t))}, \quad t \in [0, T] \quad (\text{S4})$$

to track the positions and velocities of the N human-driven vehicles during the time interval $[0, T]$. The dynamics of the $M + N$ vehicles are given as follows:

$$\begin{aligned} \dot{y}_i &= w_i, \\ \dot{w}_i &= (H_1 *_1 (\mu_N + \mu_M) + H_2 * (\mu_N + \mu_M))(y_i, w_i) + u_i, \quad i \in I_M, \\ \dot{x}_j &= v_j, \\ \dot{v}_j &= (H_1 *_1 (\mu_N + \mu_M) + H_2 * (\mu_N + \mu_M))(x_j, v_j), \quad j \in I_N \end{aligned} \quad (\text{S5})$$

where the convolution kernels $H_1: \mathbb{R} \times \mathbb{R}_{\geq 0} \rightarrow \mathbb{R}$ and $H_2: \mathbb{R} \times \mathbb{R} \rightarrow \mathbb{R}$ represent a microscopic model, such as Optimal Velocity [75], Follow-the-Leader [76], or a combination of them [77]. Here, $*_1$ is the convolution concerning the first variable, and $u: [0, T] \rightarrow \mathbb{R}$ are measurable controls for $i \in I_M$ influencing the time evolution of AVs. Given the initial data $(x(0), v(0), y(0), w(0)) = (x_0, v_0, y_0, w_0) \in \mathbb{R}^N \times \mathbb{R}_{\geq 0}^N \times \mathbb{R}^M \times \mathbb{R}_{\geq 0}^M$, the existence and uniqueness of solutions to system (S5) can be proved using the Carathéodory theorem. This is a consequence of the fact that the two convolution kernels H_1 are locally Lipschitz with sublinear growth. For more detailed discussions, we refer the readers to [S1].

Now we consider modeling mixed traffic dynamics when the number of human-driven vehicles is much greater than the number of AVs. This allows us to pass to the mean-field limit of the system (S5) with the number of human-driven vehicles

formally going to infinity, that is, $N \rightarrow \infty$. The mean-field limit of the system (S5) is given by a Vlasov-type PDE coupled with a system of controlled ODEs. The Vlasov-type PDE describes the evolution of the density of human-driven vehicles as a measure, and the ODEs describe the controlled behavior of the M AVs. Specifically, the interaction between M AVs and the human-driven vehicles can be modeled using the following system:

$$\begin{aligned} \dot{y}_i &= w_i, \\ \dot{w}_i &= (H_1 *_1 (\mu + \mu_M) + H_2 * (\mu + \mu_M))(y_i, w_i) + u_i, \quad i \in I_M, \\ \partial_t \mu + v \partial_x \mu + \partial_v ((H_1 *_1 (\mu + \mu_M) + H_2 * (\mu + \mu_M))\mu) &= 0, \end{aligned} \quad (\text{S6})$$

where $(y, w): t \in [0, T] \mapsto (y(t), w(t)) \in \mathbb{R}^M \times \mathbb{R}_{\geq 0}^M$ is the position-velocity vector of the M AVs, μ_M is defined as in (S3) tracking the position and velocity of the M AVs, $H_1: \mathbb{R} \times \mathbb{R}^+ \rightarrow \mathbb{R}$, $H_2: \mathbb{R} \times \mathbb{R} \rightarrow \mathbb{R}$ are locally Lipschitz convolution kernels with sublinear growth, $*_1$ is the convolution with respect to the first variable, and $\mu \in \mathcal{P}(\mathbb{R} \times \mathbb{R}_{\geq 0})$ is a measure on $\mathbb{R} \times \mathbb{R}_{\geq 0}$ representing the density distribution of the human-driven vehicles in position and velocity.

The rigorous limit process connecting the finite-dimensional system of ODEs (S5) to an infinite-dimensional system with coupled Vlasov-type PDEs and ODEs (S6) was proved in [S2] using Wasserstein distance.

In addition, one can use finite-dimensional hybrid systems to model multilane and multiclass traffic dynamics with M AVs and N human-driven vehicles on an open stretch of the road with m lanes. The hybrid nature of the model is based on the vehicles' continuous dynamics and the discrete events due to the vehicle's lane-changing maneuvers. The mean-field limit of the finite-dimensional hybrid system is an infinite-dimensional hybrid system containing a Vlasov-type PDE with a source term, ODEs, and discrete events caused by the lane-changing behavior of the AVs. For the rigorous derivation of the mean-field limit of the finite-dimensional hybrid system, please see [S3].

REFERENCES

- [S1] B. Piccoli and F. Rossi, "Transport equation with nonlocal velocity in Wasserstein spaces: Convergence of numerical schemes," *Acta Appl. Math.*, vol. 124, no. 1, pp. 73–105, 2013, doi: [10.1007/s10440-012-9771-6](https://doi.org/10.1007/s10440-012-9771-6).
- [S2] M. Fornasier, B. Piccoli, and F. Rossi, "Mean-field sparse optimal control," *Philos. Trans. R. Soc. London, Ser. A*, vol. 372, no. 2028, 2014, Art. no. 20130400, doi: [10.1098/rsta.2013.0400](https://doi.org/10.1098/rsta.2013.0400).
- [S3] X. Gong, B. Piccoli, and G. Visconti, "Mean-field of optimal control problems for hybrid model of multilane traffic," *IEEE Control Syst. Lett.*, vol. 5, no. 6, pp. 1964–1969, Dec. 2021, doi: [10.1109/LC-SYS.2020.3046540](https://doi.org/10.1109/LC-SYS.2020.3046540).

After generating the INRIX prediction, it is merged with realtime data from the system's controlled vehicles. Given that each AV communicates with the server at a rate of 1 Hz, we receive approximately 60 pings records from each vehicle for every Speed Plan generation. These records help determine the average speed of each vehicle over the previous update period, which then updates the TSE for the respective subsegment. Assuming that our drivers consistently stick to their designated lanes (a behavior largely confirmed through systematic data review), we can generate lane-specific TSE estimates by combining vehicle data with the broader INRIX speed data. When it comes to data fusion, we give precedence to data from our vehicles over INRIX data, considering the inherent characteristics of both sources. Our vehicles gather and relay perception data through a system that is both observable and controllable, with quantifiable error and latency as detailed in [79]. In contrast, the INRIX realtime application programming interface (API) employs averaging techniques to forecast over a given period. This method might introduce

inaccuracies at specific points within that timeframe, which could impact our control execution. The INRIX system, in essence, operates as a somewhat opaque system, with its error and latency aspects largely inferred from provider descriptions. In this article, we adopt the following notation to represent the discrete TSE:

$$\{(x_j, \bar{v}_j), j \in \mathcal{J}\} \quad (1)$$

where j represents the index of road segments, x_j is the post-mile coordination of the central road segment j , and \bar{v}_j is the average speed of the corresponding road segment j . Wang et al. [39] details the procedure of data fusion applied in MVT.

Target Design

This section introduces the target design's main modules, namely the kernel-based smoothing and the learning-based buffer design. The kernel smoothing processes the enhanced TSE at each time step using a chosen kernel to improve the

Optimal Control of Measure PDEs

by Xiaoqian Gong

In this section, our goal is to investigate the optimal control problem (OCP) of multiclass traffic consisting of AVs and human-driven vehicles in a single lane. In applications, it aims to minimize congestion, energy consumption, or travel delays by adding controls on AVs rather than controlling all vehicles in the population.

Let us again assume that we have a small number of M AVs that have a large impact on the vehicle population and a fixed large number of N human-driven vehicles that have a small impact on the vehicle population. Let $T > 0$ be a fixed time horizon. We choose controls $u \in L^1((0, T), \mathcal{U})$, where \mathcal{U} is a fixed nonempty compact subset of R^M . We model the situation by solving the following finite-dimensional optimization problem:

$$\min_{u \in L^1((0, T), \mathcal{U})} F_N(u) = \int_0^T \left\{ L(y_N(t), w_N(t), \mu_N(t)) + \sum_{i=1}^M \frac{|u_i(t)|}{M} \right\} dt, \quad (S7)$$

where $L(\cdot)$ is a suitable continuous map in its arguments, μ_N is the atomic probability measure tracking the positions x and velocities v of the N human-driven vehicles as defined in (S4), and the position-velocity vectors (y_N, w_N) and (x, v) satisfy the dynamics (S5) with given initial datum $(x(0), v(0), y_N(0), w_N(0)) = (x_0, v_0, y_{N,0}, w_{N,0}) \in R^N \times R_{\geq 0}^N \times R^M \times R_{\geq 0}^M$ and control $u \in L^1((0, T), \mathcal{U})$. Note that we added the subscript N to the AVs' position-velocity vector (y, w) , indicating the dependence of the AVs' positions and velocities on the number of human-driven vehicles N . The existence of optimal control for the finite-dimensional optimization problem (S7) was proved in [S4].

The mean-field limit of the finite-dimensional system (S5) was given by system (S6) coupled with Vlasov-type PDEs and ODEs when the number of human-driven vehicles goes to infinity, that is, $N \rightarrow \infty$. Correspondingly, we introduce the following infinite-dimensional optimization problem:

$$\min_{u \in L^1((0, T), \mathcal{U})} F(u) = \int_0^T \left\{ L(y(t), w(t), \mu(t)) + \sum_{i=1}^M \frac{|u_i(t)|}{M} \right\} dt, \quad (S8)$$

where $L(\cdot)$ is a suitable continuous map in its arguments, and (y, w, μ) is the unique solution to system (S6) with the given initial condition $(y^0, w^0, \mu^0) \in R^M \times R_{\geq 0}^M \times \mathcal{P}(R \times R_{\geq 0})$ (μ^0 is compactly supported) and control $u \in L^1((0, T), \mathcal{U})$.

It turns out that the cost functional F_N in (S7) Γ -converges to the functional F in (S8) as $N \rightarrow \infty$. This leads to the existence of optimal controls for the infinite-dimensional OCP (S8). In fact, the solutions of the finite-dimensional OCP (S7) converge to the optimal controls for the infinite-dimensional OCP (S8). For more details, please see [S4].

Furthermore, for multilane and multiclass traffic dynamics, we can study the mean-field limit of an OCP of a finite-dimensional hybrid system, which is given by an OCP of an infinite-dimensional hybrid system. The existence of optimal control for the OCP associated with the infinite-dimensional hybrid system is again due to a Γ -convergence result. For a more detailed discussion, please see [S4].

REFERENCE

- [S4] X. Gong, B. Piccoli, and G. Visconti, "Mean-field limit of a hybrid system for multi-lane multi-class traffic," 2021, arXiv:2007.14655.

fuel consumption caused by the shockwave in a high-density traffic flow. The buffer design utilizes RL to form a buffer area upstream of the standing bottleneck with the goal of improving throughput at the bottleneck. The target speed suggested by the RL is employed in a mathematical model of traffic, represented by a strongly coupled partial and ordinary differential equation (PDE-ODE). The outcome of this mathematical model is an identification of traffic density $(t, x) \mapsto \rho(t, x)$. The kernel smoothing then receives this information for learning the velocity of the next time step.

In the kernel smoothing module, we rely on enhanced TSE data to synchronize the driving speeds of AVs. In particular, vehicles are assigned target speed profiles contingent on traffic state information, which is shared and common among all AVs.

At any fixed time step t , the desired speed profile $\mathbf{v}: \mathbb{R}_+ \times \mathbb{R} \rightarrow \mathbb{R}_+$ is extracted from enhanced TSE by utilizing kernel methods. First, we preprocess the sparse TSE data by interpolating the discrete data pairs (x_i, \bar{v}_i) to a continuous speed profile $(t, x) \in \mathbb{R}_+ \times \mathbb{R} \mapsto v(t, x)$ as an approximation of the average speed of higher-granularity traffic at a position x and at time t . Then, for any fixed time $t = t_*$, we obtain the desired speed by applying a kernel function $K(\cdot)$ at a position $x = x_\alpha$ as follows:

$$\mathbf{v}(t_*, x_\alpha) = \frac{\int_{x=x_\alpha}^{x_\alpha+w} K(x_\alpha, x) v(t_*, x) dx}{\int_{x=x_\alpha}^{x_\alpha+w} K(x_\alpha, x) dx} \quad (2)$$

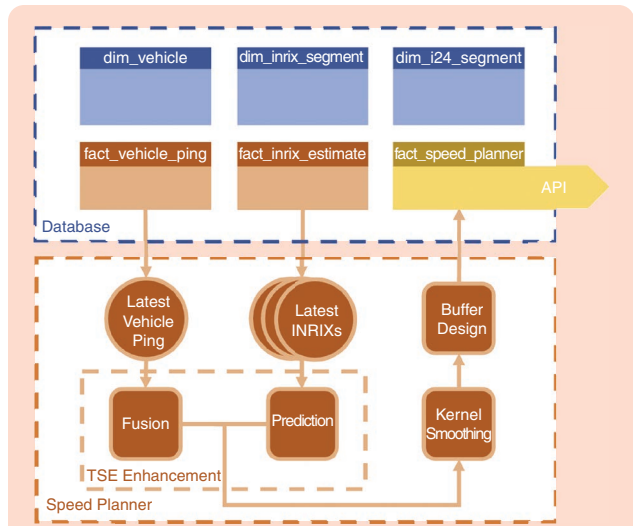


FIGURE 2 The data pipeline and major function modules of the Speed Planner. At the beginning of each update, the Speed Planner extracts a combination of macroscopic TSE and vehicle observations from the corresponding factual tables (`fact_inrix_estimate` and `fact_vehicle_ping`) in the database to calculate the target speed profile. The raw TSE is used as the input of the prediction module, of which the output is fused with vehicle observations. The fusion is then smoothed and used in the buffer design module, of which the output is saved into the database (`fact_speed_planner`) and published as the target speed profile.

where w is the width of the estimation window. Many different kernel functions, such as Gaussian kernel, triangular kernel, quartic kernel, uniform kernel, etc., can be chosen. For the purposes of this article, we consider a uniform kernel. The desired speed profile at a position x_α is accordingly defined as follows:

$$\mathbf{v}(t_*, x_\alpha) = \frac{\int_{x=x_\alpha}^{x_\alpha+w} v(t_*, x) dx}{w}. \quad (3)$$

When human drivers observe a gap between their vehicle and the one preceding, they tend to accelerate to close the distance. Our proposed desired speed profile aims to slow down *in advance*, although not excessively, to create a gap from the preceding vehicle. This approach takes into account the information provided by the TSE, which indicates the presence of congestion in the nearby downstream area. The proposed desired speed profile is adaptive to traffic states and offers relative robustness as it requires only one parameter, w , to tune.

Congestion induces a reduction in system efficiency due to the uneven distribution of traffic density in the time-space domain.

For buffer design, we consider the interval $\mathcal{I} \subset \mathbb{R}$ as the region of interest. In addition, we consider a subregion $\mathcal{I}_c \subset \mathcal{I}$ as a congested area. The idea is to determine the controlled vehicle target speed at a time step t_* , denoted by $\mathbf{u}(t_*, x)$, such that the density $\rho(t, x)$ for $x \in \mathcal{I}_c$ and $t \geq t_*$ is distributed uniformly through the region \mathcal{I} . Determining the controlled vehicle's target speed will be done in the following steps: 1) designing a target speed $\mathbf{u}(t_*, x)$, given the input $\mathbf{v}(t_*, x)$ from the kernel smoothing step; 2) identifying the density $(t, x) \in \mathbb{R}_+ \times \mathcal{I} \mapsto \rho(t, x)$, given the target speed of the controlled vehicle, employing a strongly coupled PDE-ODE model of traffic flow; and 3) an evaluation step in which using the density, the speed profile will be updated by smoothing kernel.

Article [39] provides details of the procedure introduced in the previous paragraphs.

Vehicle Controller

Recall that in the architectural design of the controller, the vehicle controller layer features two distinct methods for actuating the vehicle: acceleration-based control and ACC-based control. Here, we will discuss component implementations prepared for both options.

Acceleration-Based Controller: Base Control

The acceleration-based controller requires a baseline controller to use under normal and emergency operating conditions and a lane-change recovery controller to behave smoothly when cut-ins and cut-outs take place.

The base controller is an explicit, mathematically defined controller designed to reach and keep an ideal target speed without being trapped in the stop-and-go

wave. These two goals are somewhat antagonistic; a naive approach consisting of following the ideal target speed (unless it is unsafe to do so) may result in braking at the same time and with a comparable amplitude as the leading car when caught in the wave.

To address this, the base controller has an anticipation mechanism based on a paradigm that can be summarized as “act swiftly but slightly,” which reduces variability in acceleration. It is composed of three key components: *target*, *anticipation*, and *safety*. The target component infers an ideal target speed for each specific AV based on inputs from the Speed Planner and from the local data available. The anticipation component is an MPC module that aims to anticipate the leader’s behavior based on its current acceleration. This enhances the controller’s ability to follow the target speed effectively. The safety component is a safety module, which has priority over all the other components and ensures that the AV remains safe at all times. Since

CFMs never represent traffic perfectly (see, for instance, [80] and [81]), it is important that the safety module, at least, is independent of the mathematical model used to model vehicle behavior.

The mathematical expression of the commanded acceleration is given by

$$a_{\text{cmd}} = \min(a_{\text{safe}}, a_{\text{target}}, a_{\text{MPC}}) \quad (4)$$

where a_{safe} , a_{target} , and a_{MPC} correspond to the *safety*, *target*, and MPC-based *anticipation* components. The safety component is given by

$$\begin{aligned} a_{\text{safe}}(t) &= -k(v(t) - v_{\text{safe}}(t)) + v_{\text{safe}}(t) \\ v_{\text{safe}}(t) &= \sqrt{2|a_{\text{min}}| \left(h(t) - s_0 + \frac{1}{2} \frac{v_{\text{lead}}^2(t)}{|a_{\text{min}}|} \right)} \end{aligned} \quad (5)$$

where k is a positive parameter, v is the velocity of the ego vehicle, s_0 is the safety distance, h is the space gap, v_{lead} is

MPC Controller

by Fangyu Wu

Stop-and-go waves, characterized by periods of motion followed by abrupt halts, present significant challenges in traffic control and vehicular automation. To address this issue, we consider MPC, a popular optimal control method [78]. The appeal of MPC lies in its ability to translate a typically discrete-time control task into a finite-dimensional optimization problem.

At each discrete time step i , the optimization problem obtains an estimate of the initial state of the plant. It then computes an optimal sequence of control over a specified planning horizon. Only the first control sequence is dispatched for actuation, with this cycle repeating until task completion.

We denote the state and input of the plant as $\mathbf{x} \in \mathbb{R}^n$ and $\mathbf{u} \in \mathbb{R}^m$, respectively. The discrete-time dynamics are expressed as $\mathbf{x}_{i+1} = f(\mathbf{x}_i, \mathbf{u}_i)$, where $f: \mathbb{R}^n \times \mathbb{R}^m \rightarrow \mathbb{R}^n$. The initial state, \mathbf{x}_0 , equals \mathbf{x}_{init} . The control task imposes the following state and actuation constraints: $\mathbf{x} \in \mathcal{X}$, $\mathbf{u} \in \mathcal{U}$.

The objective of MPC is to minimize the cost function $I = \sum_{i=0}^{N-1} \ell(\mathbf{x}_i, \mathbf{u}_i) + \ell_f(\mathbf{x}_N)$. This function measures the cumulative effect of state and control inputs, with $\ell, \ell_f: \mathbb{R}^n \times \mathbb{R}^m \rightarrow \mathbb{R}$. Analytically, the MPC entails solving the following optimization at each time step:

$$\begin{aligned} \min_{\mathbf{x}_i, \mathbf{u}_i} & \sum_{i=0}^{N-1} \ell(\mathbf{x}_i, \mathbf{u}_i) + \ell_f(\mathbf{x}_N) \\ \text{subject to } & \mathbf{x}_0 = \mathbf{x}_{\text{init}}, \\ & \mathbf{x}_{i+1} = f(\mathbf{x}_i, \mathbf{u}_i), \quad i = 0, \dots, N-1, \\ & \mathbf{x}_i \in \mathcal{X}, \quad i = 1, \dots, N, \\ & \mathbf{u}_i \in \mathcal{U}, \quad i = 0, \dots, N-1. \end{aligned} \quad (\text{S9})$$

Upon each iteration, the MPC accepts \mathbf{x}_{init} as input and generates \mathbf{u}_0 as output. This feedback control process continues in a receding horizon manner until the task is terminated.

For the CIRCLES project, our team has developed an MPC that adopts an LCQP formulation, as demonstrated in [49]. This control method primarily focuses on the longitudinal dynamics of the ego vehicle, defined as the vehicle controlled by the algorithm. The state comprises the vehicle’s position and velocity, and the control input is its acceleration.

The imposed state constraints ensure that the ego vehicle neither collides with nor overtakes the predicted position of the lead vehicle. They also enforce a maximum road speed limit. Concurrently, input constraints set upper and lower bounds on acceleration. The MPC’s objective is to minimize the sum of the L^2 norm on acceleration. This objective leads to a standard convex quadratic programming problem, which is solvable by widely available solvers.

The primary challenge associated with employing MPC for wave attenuation lies in accurately predicting the lead vehicle’s longitudinal position across a substantial planning horizon. To optimally smooth traffic waves, it is imperative that this planning horizon aligns with both the spatial and temporal scales of the wave.

To overcome this challenge, our approach incorporates a realtime map service for long-term prediction and leverages instantaneous acceleration extrapolation for short-term forecasting. This dual predictive strategy serves two critical functions; the long-term predictions guide the ego vehicle to effectively dampen the traffic waves, while the short-term forecasts act as safeguards, preventing potential collisions with the lead vehicle.

Optimized Vehicle Trajectory

by Arwa AlAnqary

To gain more insights into the car-following task and to create a baseline for the performance benchmark of control algorithms, we propose an optimal control formulation of the problem. We consider a mixed-autonomy platoon of vehicles driving in a single lane following a leader with a prespecified trajectory over a fixed interval $[0, T]$. The aim is to find the optimal control signal for all AVs in the platoon to minimize the platoon's energy consumption.

OCP

We consider a mixed-autonomy platoon of M AVs, N *human vehicles* (HVs), and a leader vehicle. The AVs are controlled in their acceleration, the HVs' acceleration is governed by a *car-following model (CFM)* $A: \mathbb{R}^2 \times \mathbb{R}_{\geq 0}^2 \rightarrow \mathbb{R}$, and the leader trajectory of the leader is specified by its position $x_l(t)$ and velocity $v_l(t)$. We index the vehicles in the platoon from front to back with $i = 0$ being the leader vehicle. Let $\mathbf{u}(t)$, $\mathbf{x}(t)$, $\mathbf{v}(t)$, $\in \mathbb{R}^{N+M}$ be the control, position, and velocity vectors, respectively.

Given initial value vectors \mathbf{x}_0 and \mathbf{v}_0 , the platoon dynamics are governed by the following system of ODEs:

$$\begin{aligned}\dot{\mathbf{x}}_i(t) &= \mathbf{v}_i(t), & i \in I \setminus \{0\}, \\ \dot{\mathbf{v}}_i(t) &= A(\mathbf{x}_i(t), \mathbf{x}_{i-1}(t), \mathbf{v}_i(t), \mathbf{v}_{i-1}(t)) & i \in I_h, \\ \dot{\mathbf{v}}_i(t) &= \mathbf{u}_i(t) & i \in I_a\end{aligned}\quad (S10)$$

where $I = \{0, 1, \dots, M + N\}$, I_a , and I_h are the sets of indices of the AVs and HVs, respectively.

We use Bando-Follow-the-Leader CFM [75] for the HVs in the platoon. The model describes the acceleration of the vehicle as a function of its space gap, velocity, and relative velocity. For parameters α , β , k , d , and car length l , we have

$$A(x_l, x, v_l, v) = \alpha(V(x_l - x - l) - v) + \beta \frac{v_l - v}{(x_l - x - l)^2} \quad (S11)$$

where

$$V(h) = v_{\max} \frac{\tanh(kh - d) + \tanh(l + d)}{1 + \tanh(l + d)}. \quad (S12)$$

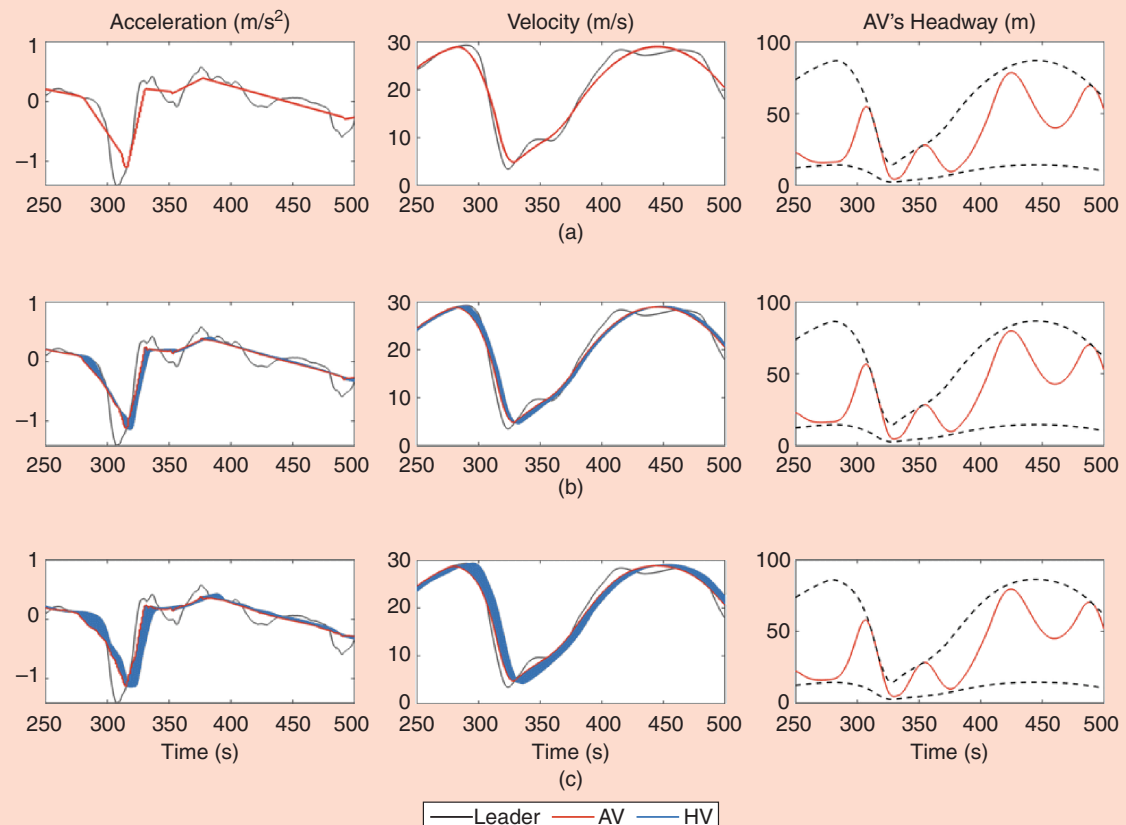


FIGURE S1 Trajectories of different platoons following the considered leader. Platoon size: (a) 0 HVs, (b) 10 HVs, and (c) 20 HVs. The dashed lines in the space gap plots represent the feasible space gap profile. By introducing one AV behind the leader, we can achieve up to a 10% reduction in energy consumption compared to the fully human-driven platoon.

(Continued)

Optimized Vehicle Trajectory (Continued)

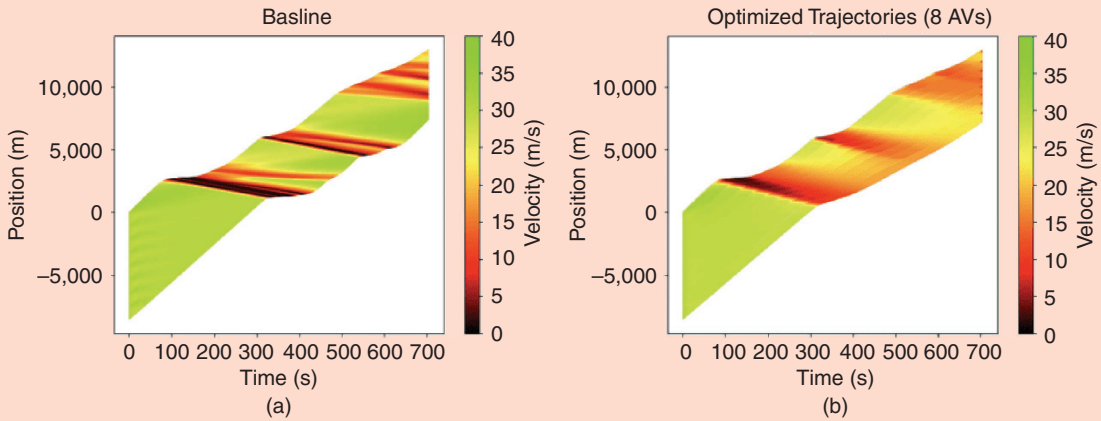


FIGURE S2 (a) and (b) Time–space diagrams showing the effect of introducing eight AVs with trajectories optimized (b) using the proposed approach and (a) comparing it with a baseline of a full human-driven platoon. The introduction of the AVs dampens the propagation of stop-and-go waves that appear in the leader’s trajectory. It also achieves a 24% reduction in fuel consumption compared to the baseline.

Next, we define the set of admissible controllers as the set of functions $\mathbf{u}: [0, T] \mapsto \mathbf{R}$ that satisfy certain conditions: 1) the controllers can be applied only to the AVs, and they are bounded; 2) the AVs cannot drive backwards; and 3) the AVs remain within an allowable space gap envelope.

Lastly, we define the objective functional of the OCP as the L^2 norm of the acceleration of all the vehicles in the platoon. We use this as a simple proxy of the fuel consumption of the vehicles.

Based on the aforementioned, we formulate the following OCP:

$$\inf_{\mathbf{u}} \int_0^T \sum_{i \in I_a} \mathbf{u}_i^2(t) + \sum_{i \in I_h} (\mathbf{A}(\mathbf{x}_{i-1}(t), \mathbf{x}_i(t), \mathbf{v}_{i-1}(t), \mathbf{v}_i(t)))^2 dt \quad (\text{S13})$$

where (\mathbf{x}, \mathbf{v}) satisfies (S10) and $\forall i \in I_a, \forall t \in [0, T]$

$$\begin{aligned} h_{\min} \mathbf{v}_i(t) + d_{\min} &\leq \mathbf{x}_{i-1}(t) - \mathbf{x}_i(t) - l, \\ h_{\max} \mathbf{v}_i(t) + d_{\max} &\geq \mathbf{x}_{i-1}(t) - \mathbf{x}_i(t) - l, \\ \mathbf{v}_i(t) &\geq 0 \end{aligned} \quad (\text{S14})$$

the leader vehicle velocity, $a_{l,\min}$ is the minimal possible leader vehicle acceleration (so maximal deceleration), and a_{\min} is the minimal possible ego acceleration.

The target component is defined by

$$a_{\text{target}}(t) = -k(v(t) - v_{\text{target}}(t)) \quad (6)$$

where v_{target} is an inferred ideal speed obtained either from the Speed Planner when available or by integrating local measurements.

where h_{\min} and h_{\max} are bounds on the allowable time gap, and d_{\min} and d_{\max} are the allowable minimum and maximum space gap at zero velocity.

To solve this optimization problem, we parameterize the controls using piecewise constant functions. This renders a finite-dimensional optimization problem that we solve by means of gradient descent. We compute the analytical gradients of the problem using the adjoint formulation. For further details, see [58].

NUMERICAL SIMULATION

We apply the proposed approach to a platoon with one AV following an empirical leader trajectory. This trajectory exhibits stop-and-go waves. We show the simulation results in Figure S1. By introducing one AV, we achieve up to a 10% reduction in fuel consumption compared to the baseline of a full human-driven platoon. We apply the same approach sequentially to multiple AVs in a larger platoon. In Figure S2, we show the time–space diagrams for the baseline platoon compared to one with eight AVs, which achieves a 24% reduction in fuel consumption.

The MPC-based anticipation component a_{MPC} is given by

$$a_{\text{MPC}}(t) = \begin{cases} a_{\min, \text{brake}}(h(t), v(t), v_{\text{lead}}(t), a_{\text{lead}}(t)), & \text{if } P_1 > 0, a_{\text{lead}}(t) < 0 \\ \frac{a_{\text{lead}} v(t)}{v_{\text{lead}}(t)}, & \text{if } P_1 \leq 0 \text{ and } P_2 \geq 0, a_{\text{lead}}(t) < 0 \\ a_{\text{lead}} - \frac{(v(t) - v_{\text{lead}}(t))^2}{2(h(t) - s_0)}, & \text{if } P_1 \leq 0 \text{ and } P_2 < 0, a_{\text{lead}}(t) < 0 \\ a_{\text{lead}} - \frac{(v(t) - v_{\text{lead}}(t))^2}{2(h(t) - s_0)}, & \text{if } P_2 < 0, a_{\text{lead}}(t) \geq 0, \\ \min(a_{\max}, a_{\text{lead}}(t)(1 + k_2(v_{\text{lead}}(t) - v(t)))), & \text{otherwise} \end{cases} \quad (7)$$

where, as in (5), h is the space gap, s_0 is the safety distance, k_2 is a positive constant, a_{lead} is the leader vehicle acceleration, and a_{\max} is the maximal possible acceleration of the ego vehicle. The terms $a_{\min.\text{brake}}$, P_1 , and P_2 are given by

$$\begin{aligned} a_{\min.\text{brake}}(h(t), v(t), v_{\text{lead}}(t), a_{\text{lead}}(t)) \\ = - \left(h(t) - s_0 + \frac{1}{2} \frac{v_{\text{lead}}^2(t)}{a_{\text{lead}}(t)} \right)^{-1} \frac{(v(t))^2}{2}, \\ P_1 = a_{\min.\text{brake}}(h(t), v(t), v_{\text{lead}}(t), a_{\text{lead}}(t)) - \frac{a_{\text{lead}}(t)v(t)}{v_{\text{lead}}(t)}, \\ P_2 = v_{\text{lead}}(t) - v(t). \end{aligned} \quad (8)$$

Further details of this controller can be found in [82].

Acceleration-Based Controller: Lane Change

The design of the lane-change recovery controller relies on global traffic information as well as local traffic states, such as the space gap to the leader vehicle and the relative velocity. The event of the lane changing of the leader vehicle creates a discontinuity in the observed local state. Such discontinuities can translate to sudden large jumps in the controller output, causing large jerk values. This sudden jump in the controller output might be necessary to avoid collision (for example, if a vehicle cuts-in in front of the AV and has low relative velocity). However, in many cases, these jumps are by-products of the discontinuity in the observation and can be avoided without creating additional safety threats. To remedy this effect of lane changes in such conditions, we designed a simple lane-change handling mechanism that treats the main acceleration-based controller as opaque and makes minimal assumptions about it. Essentially, the mechanism works by detecting the event of lane changing, assessing the safety conditions created by the event, and (when appropriate) smoothing the output of the controller.

We assume discrete observations with a fixed frequency. At step k , we denote the ego velocity v_k , the relative velocity Δv_k , the space gap s_k , the output of the main controller a_k , and the actual acceleration input to the vehicle u_k . If the lane-change mechanism is not active, we have $u_k = a_k$.

To design this mechanism, we make a few natural assumptions about the behavior of the underlying controller. We assume that the controller is a continuous and nondecreasing function of the leader's states (that is, the space gap s_k and relative velocity Δv_k). We also assume that the main controller encodes its own safety measures as the lane-change handling mechanism does not provide any additional safety measures. Beyond these assumptions, the exact form of the main controller is treated as opaque.

We impose multiple criteria for the lane-change handling mechanism to take effect as follows:

- 1) A lane-change event is detected—this is done by detecting a discontinuity in the space gap to the leader vehicle.
- 2) The lane-change event is significant—this is measured by the amount of jerk it causes.

- 3) The lane-change event does not cause safety threats—this is measured by the *time to collision* (TTC) (if $\Delta v_k < 0$) or time gap (if $\Delta v_k \geq 0$) at the lane-change event.

When the lane-change mechanism is activated, it smooths the acceleration by taking a convex combination of the main controller output at the current step and the actual acceleration command in the previous step as follows:

$$u_k = a_k u_{k-1} + (1 - a_k) a_k. \quad (9)$$

Here, $0 \leq a_k < 1$ is a smoothing factor where larger values mean smoother acceleration change. Here, we consider a time-varying a_k whose value is a nondecreasing function of the relative velocity and time headway at step k . The rationale for this modeling choice is to make the smoothing effect stronger the less critical the situation is (that is, larger space gap and relative velocity). The smoothing factor has the following functional form:

$$a_k = c \cdot \left(f_1 \left(\frac{s_k}{\Delta v_k} \right) \right) + (1 - c) \cdot f_2(\Delta v_k, s_k). \quad (10)$$

It depends on the time headway through the function

$$f_1 \left(\frac{s_k}{\Delta v_k} \right) = \tanh \left(t^* \cdot \frac{s_k}{\Delta v_k} \right) \quad (11)$$

where the parameter t^* is chosen such that the function is close to the one when the time headway $s_k / \Delta v_k \geq h_{\text{safe}}$, where h_{safe} is an acceptable safety time headway. The smoothing factor depends on the relative velocity through the function

$$f_2(\Delta v_k, s_k) = \begin{cases} \frac{1}{2} \tanh \left(\Delta v^* \cdot \frac{s_k}{|\Delta v_k|} \right) + \frac{1}{2} & \Delta v_k < 0 \\ \frac{1}{2} \tanh(\Delta v_k) + \frac{1}{2} & \Delta v_k \geq 0 \end{cases} \quad (12)$$

where the parameter Δv^* is selected such that the function value is close to zero when the TTC ($s_k / |\Delta v_k| \leq C_{\text{safe}}$, where C_{safe} is an acceptable safety TTC). Concretely, we use $h_{\text{safe}} = 2s$, $C_{\text{safe}} = 4.5s$, $t^* = 1.32$, and $\Delta v^* = 10.3$. The parameter $c = 0.75$ is chosen by testing on multiple trajectories and lane-change scenarios.

Finally, the lane-change mechanism is deactivated when the main controller acceleration becomes close enough to the output acceleration

$$|a_k - u_k| \leq \epsilon. \quad (13)$$

An example of this mechanism is depicted in Figure 3. In the figure, the dashed red line indicates the lane-change event (cut-in) happening at around 14 s. The acceleration profile of the main controller (shown in gray in the bottom left panel) decelerates heavily in reaction to the lane change. This event is detected and considered safe by the lane-change recovery controller, which remained active for 2.9 s, during which time it smoothed the acceleration profile significantly and removed the unnecessary jerk caused by the lane change.

Design Details of the ACC-Based Controller

The ACC-based controller is the version of the controller that was ultimately deployed on 97 of the 100 vehicles

during the final MVT. The crucial distinction between the ACC-based controller and the acceleration-based controller introduced in the prior section is the controller's output. The ACC-based controller, rather than providing an acceleration to actuate, provides output setpoints for the AV's native ACC system, which controls the AV's longitudinal movements based on those setpoints. We use the stock ACC system's safety assurances and lane-change handling. Thus, while this provides a less direct form of control, it is more robust in ensuring the safety and smoothness of the ride. For more information on how the ACC works, please refer to the section "Adaptive Cruise Control Modeling." For context on the simulator that was developed for training this algorithm, please refer to "Trajectory Simulator."

The ACC-based controller is an RL controller that is trained using Proximal Policy Optimization [83]. Elements of training the Markov decision process (MDP) problem [84] (Figure 4) are described below.

Observation Space

The observation space includes the following:

- » v , the velocity of the AV
- » v_s , the target speed given by the Speed Planner
- » l , a "minicar" flag that indicates whether there is a leader vehicle detected, nominally within 80 m (dubbed as such due to the miniature car icon that appears in the dashboard when the leader is detected)
- » s , the current ACC speed setting
- » g , the current ACC gap setting.

Action Space

The action space includes the following:

- » The requested ACC speed setting, which our onboard computer will realize in a series of button presses (see Figure 5), dictates the maximum speed at which the ACC can drive.
- » The requested ACC gap setting, which the onboard computer will realize with priority over the speed setting, takes on three bars between one and three, with each bar indicating a higher allowable gap. Each bar roughly corresponds to constant time gaps of 1.2, 1.5, and 2.0 s.

In addition, a clipping mechanism was used to ensure controller safety and social acceptability, particularly in the

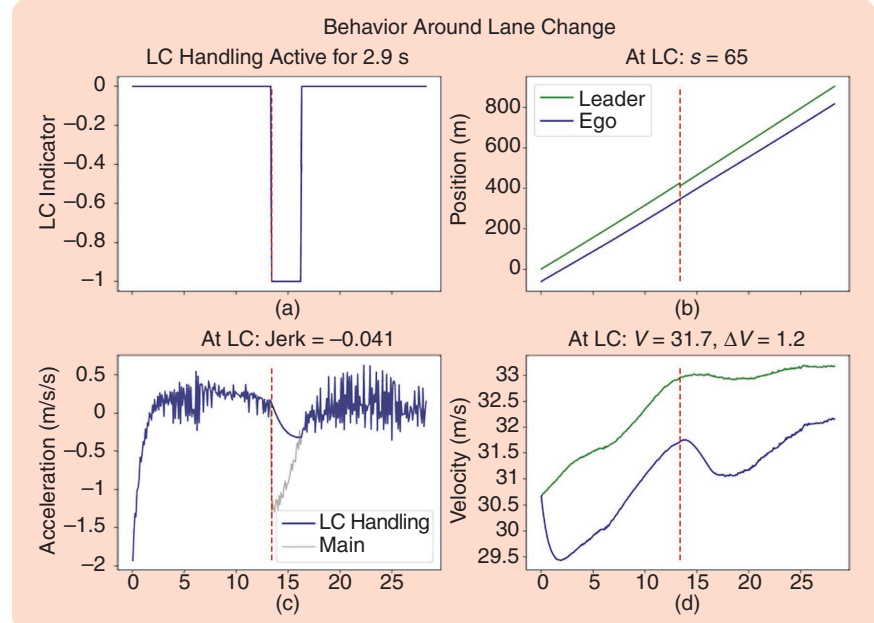


FIGURE 3 An example of the effect of the lane-change (LC) handling mechanism on a real-world trajectory in the event of a cut-in. (a) The lane-change event is detected and considered safe, so the lane-change recovery controller was active for 2.9 s. (b) A car cuts-in in front of the ego vehicle at a headway of 65 m. (c) The main controller's commanded acceleration drops sharply due to the lane-change event, causing a large jerk value, but the lane-change controller smooths out this drop in the acceleration. (d) The relative velocity is large enough at the lane change, allowing the controller to be active.

absence of leader state information. The post facto lower and upper bounds placed on the speed setting output are based on the average speed of the ego vehicle during the last 1 s (10 time steps, with 0 mi/h and null observations omitted) as follows:

$$v_{\text{lower}} = \frac{1}{10} \sum_{i=1}^{10} v_i - 15 \text{ mi/h},$$

$$v_{\text{upper}} = \frac{1}{10} \sum_{i=1}^{10} v_i + 5 \text{ mi/h} \quad (14)$$

where v_{lower} and v_{upper} are the lower and upper bounds of the clip, respectively. The final clip is executed as follows:

$$v_{\text{clip}} = \min(\max(v_{\text{action}}, v_{\text{lower}}), v_{\text{upper}})$$

$$v_{\text{final}} = \min(\max(v_{\text{clip}}, 20 \text{ mi/h}), 73 \text{ mi/h}) \quad (15)$$

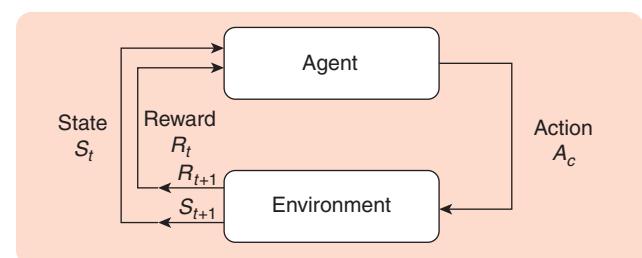


FIGURE 4 The Markov decision process (MDP) that RL is based on. An agent exists in an environment and repeatedly chooses an action based upon a state and receives rewards, which then inform the agent of the value of the state and action pair.

where v_{final} is the final speed setting command, and v_{action} is the unnormalized speed output, or action, from the neural net. The 73 mi/h maximum speed accounts for modest speeds in excess of the posted speed limit of 70 mi/h.

Reward Function

The reward function is as follows:

$$r_t = 1 - c_1 a_t^2 - c_2 (v_t^{av} - v_t^{sp})^2 - \frac{c_3}{n} \sum_{i=1}^n E_t^i - c_4 \mathbb{1}_{h_t^{av} \leq h_{\min} \vee h_t^{av} \geq h_{\max}} \quad (16)$$

where $c_1 - c_4$ are coefficients; a_t^2 is an acceleration penalty; $(v_t^{av} - v_t^{sp})^2$ is a squared penalty on the difference between the Speed Planner's suggested speed and the actual speed; $(1/n) \sum_{i=1}^n E_t^i$ is instantaneous fuel consumption according to the energy models described in "Vehicle Energy Models;" and the last indicator term is an intervention penalty that is invoked if the space gap is less than the minimum space gap or greater than the maximum space gap.

Further details on the development and design decisions for the state and reward representations and the intermediate and final policies are given in depth in [41].

CANDIDATE CONTROLLER SELECTION

In the months leading up to the MVT open-road test, our team developed a multitude of candidate controllers, as seen in previous sections and sidebars. To pare down the list of candidate controllers to be considered for real-world deployment in November 2022, various (Speed Planner and ACC-based vehicle controller) combinations were assessed over a range of simulation scenarios. The simulation and testing framework follows from [87] and features an updated simulation methodology described in "Trajectory Simulator."



FIGURE 5 A photograph of a Nissan Rogue's steering wheel buttons that control the vehicle's ACC. The ACC system is turned on by manually pressing the blue icon on the far right. Through our vehicle interfacing efforts, we are able to electronically press the + and – buttons to toggle the ACC speed, setting up 1 mi/h and down 1 mi/h, respectively, or hold them to increment by 5 mi/h. The three ACC gap settings are rotated through by pressing the button on the bottom right.

Simulation scenarios included shockwaves, bottlenecks, and free-flow. Shockwave and free-flow scenarios follow precisely from the simulator described in "Trajectory Simulator" and differ only in the leader trajectory (one being stop-and-go and the other being all high speed). The bottleneck scenario features a dynamically imposed speed limit in a spatial region of the domain. The speed limit is inversely related to the vehicle density of the region, and the scaling parameter is tuned to historically observed speeds in the I-24 region. The bottleneck region is meant to model a weaving area where the close proximity of on-ramps and off-ramps results in increased lane-change frequency.

The key performance indicators (KPIs) used to assess the controllers include fuel economy, throughput, and network speed. Fuel economy is the overall miles per gallon of all vehicles, and it is computed by applying the energy model (see "Vehicle Energy Models") and computing

$$\text{fuel economy} = \frac{\sum_{t=0}^T \sum_{i=1}^n E_t^i}{\sum_{i=1}^n x^i} \quad (17)$$

where the numerator is the total fuel consumed by all vehicles over all simulation times, and the denominator is the total distance traveled by all vehicles. The throughput is measured by counting the number of vehicles crossing various positions along the highway, normalized by time. For the shockwave and free-flow simulations, this is taken to be the straight average of the time average of five equispaced measurement locations. For the bottleneck, this is taken to be the steady state (or final value) at the measurement location just downstream of the bottleneck region. The network speed KPI is defined as the total distance traveled by all vehicles divided by the total driving time of all vehicles.

At the time of our self-imposed "controller freeze" (that is, the time at which substantial changes to controllers are no longer allowed), there were two Speed Planner variants and 12 vehicle controller variants. The KPI performance for each of these controllers is shown in Figure 6. The Speed Planner variants are Kernel Smooth (just the first three steps described in the Speed Planner) and Kernel Smooth with RL Buffer (all steps described in the Speed Planner). The vehicle controller variants include the following:

- » **Simple:** This is a hand-designed logic-based controller that largely adheres to the Speed Planner suggestion.
- » **MicroAccel:** This is the main controller described in the section "AccelerationBased Controller: Base Control" with modifications to output ACC set-points. This controller itself has six variants, with different parameter choices.
- » **RL:** This is the RL controller described in the section "Design Details of the ACCBased Controller." This controller has five variants, with different training meta-parameter choices.

- » *HybridRL*: An additional variant was also created, which blends two RL variants together, according to the speed planner speed suggestion.

In the shockwave scenario, an ideal controller should maximize fuel economy improvements and remain neutral on throughput and network speed. In the bottleneck

Vehicle Energy Models

by Nour Khoudari, Sulaiman Almatrudi, Rabie Ramadan, Joy Carpio, Mengsha Yao, Kenneth Butts, Jonathan W. Lee, and Benjamin Seibold

The quantification of the energy demand of the vehicles on the road, given their trajectories, requires vehicle-specific energy models that take as an input the velocity profile $v(t)$ and the road grade profile $\theta(t)$ and output the resulting energy/fuel consumption rate $f(t)$. This project requires the quantification of the energy demand of the traffic flow at large, composed of many vehicles, and also the use of RL and optimization techniques that minimize (under certain constraints) the energy demand of traffic. Thus, the energy models used should accurately represent different vehicle types on the road and should average out any local non-convexity behavior due to gear switching to avoid trapping the optimizer in local minima. For that purpose, we use energy models derived from a systematic model-reduction procedure to generate simple fitted models. The procedure starts from the fidelity software Autonomie [85] for a number of vehicles, each of which represents a typical average vehicle of a given class.

VEHICLE PORTFOLIO

To capture the diversity and prevalence of different vehicle types on U.S. roads, we select a representative group of vehicle classes on which we apply the model-reduction process to derive their corresponding simplified energy models. Those vehicle classes are divided into two categories: 1) light-duty vehicles: compact size sedan, midsize sedan, midsize SUV, and pickup and 2) heavy-duty vehicles: Class 4 pickup and delivery and Class 8 tractor. Each vehicle model represents a class of vehicles that have comparable weight (with load assumed half full) and fuel consumption characteristics [S5].

AUTONOMIE AND VIRTUAL CHASSIS DYNAMOMETER

We use the simulation software Autonomie Rev 16SP7 [85] with a library of energy models for several types of vehicles. These include a detailed plant and controller model, whose components are provided in MATLAB and Simulink and can be customized. To build our models, we use 1) physics-based vehicle parameters extracted directly from Autonomie, 2) tuned parameters extracted in an automated fashion by running the Autonomie model on test cycles, and 3) performance maps computed gear by gear on a complete velocity–load phase space of driving by running Autonomie’s customized vehicle models on a virtual chassis dynamometer (VCD) (those maps are vehicle speed to engine speed, vehicle speed and wheel force to engine torque, and engine speed and torque to fuel rate).

SEMIPRINCIPLED ENERGY MODELS

We build an energy model that is semiprincipled in that it has a physics-based part using Autonomie’s extracted physics-based vehicle parameters, but it also relies on the maps obtained from the VCD. Gear scheduling in this model is based on choosing the feasible gear that yields minimal fuel consumption, and the torque converter bypass clutch is assumed to be open in the first gear only. In contrast to Autonomie, which considers hysteresis effects, this model yields the fuel consumption rate (and other outputs) as a direct function of the instantaneous velocity v , acceleration a , and road grade θ .

SIMPLIFIED ENERGY MODELS

A further model-reduction step is conducted by fitting the semi-principled models into simplified models. Those models have a simple polynomial structure that can easily be integrated into optimization and control problems, yet they are highly accurate. The fuel consumption rate function is

$$f(v, a, \theta) = \max \{ \beta, C(v) + P(v)a + Q(v)a^2 + Z(v)\theta \} \quad (\text{S15})$$

where β is the minimum fuel rate set to be zero or a positive constant depending on the fuel cut criteria, $a_+ = \max(-P(v)/2Q(v), a)$, $C(v) = c_0 + c_1v + c_2v^2 + c_3v^3$, $P(v) = p_0 + p_1v + p_2v^2$, $Q(v) = q_0 + q_1v$, and $Z(v) = z_0 + z_1v + z_2v^2$.

In the aforementioned functions, c_0 ensures that fuel is being consumed at idle, the c_1 , c_2 , and c_3 terms can be interpreted as fuel consumed due to friction and air drag, the $P(v)$ term yields fuel demand due to nonzero accelerations, the $Q(v)$ term captures the superlinear trend of the fuel rate with respect to a , and the $Z(v)$ term captures the fuel consumed due to the road grade, with the z_1 term playing the role of the weight force exerted at θ . Both types of models are validated, for all different vehicle types, against Autonomie models as the ground truth on standard U.S. Environmental Protection Agency (EPA) drive cycles [S6] for flat roads and constant road grade drive cycles, and the results showed that the models are highly accurate (within 4% for zero road grades). See [86] for more details on the design of the energy models and corresponding results.

REFERENCES

- [S5] *Autonomie Compiled Vehicles: A Technical Manual for Training in Autonomie*. Lemont, IL, USA: Argonne National Laboratory (ANL), 2020.
- [S6] “Dynamometer drive schedules.” United States Environmental Protection Agency (US EPA). Accessed: Sep. 24, 2023. [Online]. Available: <https://www.epa.gov/vehicle-and-fuel-emissions-testing/dynamometer-drive-schedules>

scenario, an ideal controller should maximize throughput improvements and optionally improve or stay neutral on the other two KPIs. In the free-flow scenario, an ideal controller will not worsen on any of the KPIs. Given these criteria, we determined that the HybridRL vehicle controller paired with the Kernel Smooth with RL Buffer variant of Speed Planner presented the ideal combination for ACC-based vehicles.

OPEN-ROAD FIELD OPERATIONAL TEST

Following the controller selection, this section introduces the implementation details of the selected controllers, the experimental design for the 100 AV deployment, and contemporaneous data collection procedures.

Server-Side Implementation

As indicated in [Figure 3](#), the server-side implementation includes the construction of the database, the API, and the Speed Planner algorithm scripts. The database schema is designed following the star schema data model, consisting of dimension tables (for storing static metadata) and fact

tables (for storing quantitative data). The tables include the following:

- » dim_vehicle for storing the vehicle metadata, route, and lane assignment
- » dim_inrix_segment for storing INRIX road segment data for I-24
- » dim_i24_segment for storing finer-grained road segment data, which support the TSE and Speed Plan profiles after data fusion
- » fact_vehicle_ping for storing the realtime AV ping information
- » fact_vehicle_observation for storing extracted vehicle observations from the AV ping table
- » fact_inrix_estimate for storing realtime INRIX data
- » fact_speed_planner for storing Speed Plan profiles.

The fact_vehicle_ping and fact_inrix_estimate tables are continually being populated with realtime updates at 1 Hz. After processing these input data via the

Trajectory Simulator

by Nathan Lichl  

Establishing a robust, representative, and reliable simulation environment is key for the successful implementation of our wave-smoothing controllers in autonomous vehicles as it ensures their efficient operation across a wide range of traffic conditions. Our simulator [S7] is based on real human driver data collected on the highway [S8] and has been extensively used for designing, training, and evaluating the different types of controls implemented in this work, assessing their safety, energy-reducing performances, robustness, and smoothness. This sidebar describes the procedure by which highway trajectory data were gathered and a simulator was created from the data.

ACQUISITION OF DATA

The trajectory dataset [S8] for our study was recorded on a 14.5-km segment of I-24, located southeast of Nashville, TN, USA. An example recorded speed trajectory profile can be

seen in [Figure S3](#). An instrumented vehicle is used to gather data that log the vehicle controller area network (CAN) data through libpanda [65] and GPS information from an in-built receiver. The CAN data collection comprises measurements like the speed of the vehicle under consideration (ego vehicle), the relative speed of the lead vehicle (the vehicle in front), the instantaneous acceleration, and the space gap (distance from bumper to bumper).

REFINING RAW DATA

Each drive's raw data are stored in two separate files: a CAN data file and a GPS file. The relevant data are extracted from the CAN file and adjusted to match the GPS time, which is recorded at 10 Hz. The high-frequency CAN data are downsampled and interpolated linearly to align with the GPS time, whereas low-frequency CAN data are subjected to linear interpolation to match the 10-Hz GPS time. GPS position

data are used to calculate the distance traveled and direction. As westbound data usually demonstrate more consistent congestion, they are primarily used for training, comprising 60 trajectories, which translates to 8.8 h and 772.3 km of driving.

ANALYZING THE DATASET

The trajectory dataset encapsulates a wide variety of traffic conditions ranging from nearly stationary congested traffic

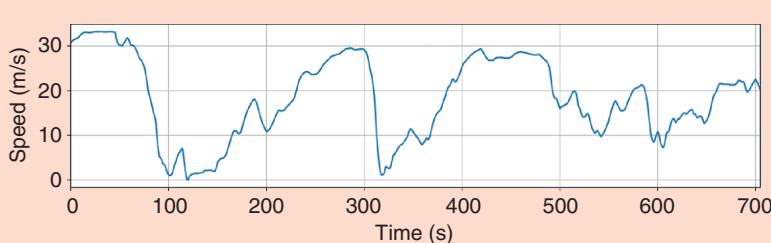


FIGURE S3 Speed versus time for one of the dataset trajectories, exhibiting large acceleration and breaking patterns that can typically lead to stop-and-go waves.

Python-based Speed Planner algorithm, the Speed Plan is written to the `fact_speed_planner` table, which is exposed to the Internet via a PHP-based HTTP API.

Vehicle-Side Implementation

The vehicle-side implementation includes several software libraries and a mix of custom and off-the-shelf hardware components.

In the past decades, vehicles have been gradually increasing the implementation of the open CAN protocol for in-vehicle networking communication between various electrical modules. The usage of the CAN bus lets automotive manufacturers use minimal wiring to design complex systems involving anything from engine diagnostics, infotainment, security, and emissions to (in more recent years) ACC and Lane Keep Assist (LKA). The ACC systems on cars typically involve a sensor module to measure the leading vehicle dynamics and a separate controller module, which communicates with the vehicle's transmission and engine. Since these modules are physically located in

different parts of the vehicle, they communicate using CAN buses, where listening CAN analyzers can record the information. [Figure 7](#) shows the method of tapping into a CAN bus for message reading.

While automotive manufacturers provide information on the structure of the in-vehicle network in the form of wiring diagrams, specific information being sent on the CAN bus is typically a closely guarded secret, likely due to both trade secrets and safety concerns. However, some companies (such as comma.ai [90] and Intrepid Control Systems [91]) are entering the space of custom vehicle autonomy by selling modules that intercept CAN messages between these modules and provide their own inputs based on custom controllers. This is possible only after spending time decoding messages and reverse engineering the protocols needed to inject custom messages. Compared to basic CAN reading, [Figure 7](#) shows the different electrical architecture needed for CAN message interception and injection between original equipment manufacturer (OEM) modules.

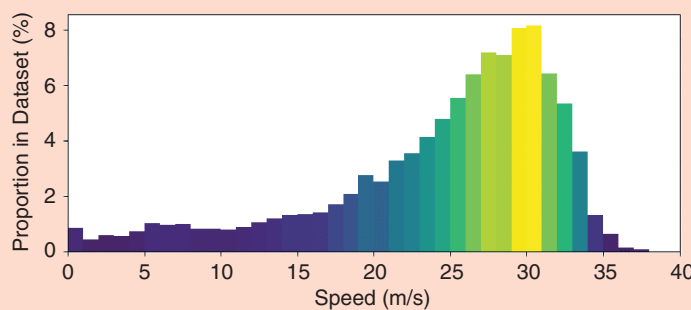


FIGURE S4 The distribution of speeds in the I-24 dataset.

to maximum speed free-flow traffic, including diverse acceleration and deceleration patterns associated with stop-and-go traffic. The example trajectory displayed in [Figure S3](#) demonstrates the ego vehicle's quick transitions between low and high speeds.

While the primary interest lies in mitigating the high-frequency waves that are common in congestion, [Figure S4](#) indicates the tendency of speeds in the training dataset toward the higher end. Despite the possibility of simplifying the learning problem by filtering out high-speed data, congestion zones are often immediately followed by high-speed areas. To ensure our controller's competent behavior at high speeds and during transitions from high-speed to low-speed zones, the training dataset retains both low-speed and high-speed data.

DEVELOPING THE TRAINING AND EVALUATION FRAMEWORK

To exploit the gathered data, a single-lane training environment is designed where an AV follows the trajectory data recorded from human drivers. The human driver is simulated at the front of a vehicle platoon, followed by the AV and then a number of vehicles operating according to the *Intelligent Driver Model (IDM)* (see “[Car-Following Models](#)”). This setup guarantees the growth of waves in congestion due to the string-unstable nature of the chosen IDM parameters. While

a comprehensive microsimulation of I-24 might allow training with more complex vehicle interactions, the proposed simulator focuses on realistic driving dynamics representative of the highway's wave types and drivers' reactions to wave formation. The simulator's efficiency is also commendable as it achieves 2,000 steps per second, whereas a microsimulation of the complete 14-km section would be computationally expensive due to the thousands of vehicles in congestion.

REFERENCES

- [S7] N. Lichtlé, E. Vinitsky, M. Nice, B. Seibold, D. Work, and A. M. Bayen, “Deploying traffic smoothing cruise controllers learned from trajectory data,” in Proc. Int. Conf. Rob. Autom. (ICRA), Philadelphia, PA, USA, 2022, pp. 2884–2890, doi: [10.1109/ICRA46639.2022.9811912](https://doi.org/10.1109/ICRA46639.2022.9811912).
- [S8] M. Nice et al., “The I-24 trajectory dataset (1.1.1).” Zenodo. [Online]. Available: <https://zenodo.org/records/6456348>

In this work, our solution is based on a similar principle; however, additional protocols on the 2023 Nissan Rogue vehicles (which comprise the vast majority of our control fleet) prevented the injection of commands, though CAN data could still be read for realtime controller inputs. Due primarily to supply chain issues and additionally to an inability to inject CAN messages, a custom circuit board was developed, coined *mattHAT*. A *mattHAT* can be seen in Figure 8. The *mattHAT* acted as a CAN interface and also

Car-Following Models

by Nour Khoudari and Benjamin Seibold

CFMs [51], [88] are systems of ODEs describing the dynamics of each vehicle on the road, where drivers react to the changes in the relative positions of the vehicle ahead. The ODEs could describe the vehicle velocity only, and those are first-order models, or the velocity and the acceleration, and those are second-order models. Second-order CFMs are of the form

$$\dot{v}(t) = f(s(t), v(t), \Delta v(t)) \quad (\text{S16})$$

where s is the gap to the vehicle ahead measured in meters, v is the velocity of the vehicle, commonly measured in m/s , and Δv is the velocity difference or the approaching rate to the vehicle ahead, commonly measured in m/s . An elegant CFM is the Optimal Velocity Model (OVM) [75]

$$f(s, v, \Delta v)_{\text{OVM}} = \alpha[V(s) - v] \quad (\text{S17})$$

where the optimal velocity function, $V(s)$, determined by the gap s to the vehicle ahead, is a positive monotonically increasing function, with $s \rightarrow \infty$ asymptote at the speed limit. Some variations of this model were proposed to avoid car collisions; an example is the Optimal Velocity Follow-the-Leader Model (OVM-FtL) as follows:

$$f(s, v, \Delta v)_{\text{OVM-FtL}} = \alpha[V(s) - v] + \beta \left[\frac{\Delta v}{s^v} \right] \quad (\text{S18})$$

where v is a positive exponent, and β is a positive braking coefficient (measured in m^v/s). Another example of second-order CFMs is the IDM, introduced in [89] and suitably adapted and used in this work. The IDM acceleration function is

$$f(s, v, \Delta v)_{\text{IDM}} = a \left[1 - \left(\frac{v}{v_0} \right)^{\delta} - \left(\frac{s^*(v, \Delta v)}{s} \right)^2 \right] \quad (\text{S19})$$

where $s^*(v, \Delta v) = s_0 + vT + (\max\{0, v\Delta v\}/2\sqrt{ab})$. Here, v_0 is the desired velocity on an empty road (measured in m/s), s_0 represents the minimum spacing between vehicles (measured in m), T is the minimum possible time gap to reach the vehicle ahead (measured in s), δ is an acceleration exponent, and a and b are the maximum vehicle acceleration and minimum desired comfortable deceleration, respectively (measured in m/s^2).

provided methods of sending ACC button press commands using custom circuitry. The board was designed to plug into a Raspberry Pi 4. Custom wire harness cables were designed and built for vehicle installation across the 97 Nissan Rogue vehicles, targeting specific CAN buses related to the vehicle's ACC state.

A C++-based library named *libpanda* [65] was developed to operate the *mattHAT*'s CAN interface and button snooper as well as record raw CAN and GPS data. *libpanda* also supports a USB-based GPS module to both record the vehicle's position and synchronize the system's time. A tool named *stry* was also developed to decode and quickly analyze *libpanda*'s recorded data for CAN signal decoding and classification [92],

Vehicle Controller	SHOCKWAVE SCENARIO	Speed Planner					
		Kernel Smooth			Kernel Smooth with RL Buffer		
		Fuel Economy % Increase	Throughput % Increase	Speed % Increase	Fuel Economy % Increase	Throughput % Increase	Speed % Increase
Vehicle Controller	Simple	17.33%	1.18%	-0.32%	24.24%	-0.04%	-5.86%
	MicroAccel-a	9.33%	-0.08%	-0.37%	10.71%	1.18%	-0.75%
	MicroAccel-b	4.56%	0.26%	7.68%	8.87%	2.27%	2.87%
	MicroAccel-c	9.33%	-0.08%	-0.37%	10.71%	1.18%	-0.75%
	MicroAccel-d	9.33%	-0.08%	-0.37%	10.71%	1.18%	-0.75%
	MicroAccel-e	9.33%	-0.08%	-0.37%	10.71%	1.18%	-0.75%
	MicroAccel-f	12.20%	1.02%	0.37%	14.94%	0.35%	0.45%
	KL-a	14.31%	-1.11%	-1.42%	13.29%	-1.32%	-1.69%
	RL-b	12.58%	-1.10%	-1.87%	11.63%	-1.45%	-1.87%
	RL-c	-2.76%	0.82%	0.37%	-1.42%	0.36%	0.15%
	RL-d	3.24%	0.26%	0.67%	-0.53%	0.11%	-0.27%
	RL-e	23.18%	2.84%	-2.19%	18.47%	2.04%	-1.69%
	HybridRL	22.96%	2.75%	-2.29%	17.49%	1.69%	-2.14%

(a)

Vehicle Controller	BOTTLENECK SCENARIO	Speed Planner					
		Kernel Smooth			Kernel Smooth with RL Buffer		
		Fuel Economy % Increase	Throughput % Increase	Speed % Increase	Fuel Economy % Increase	Throughput % Increase	Speed % Increase
Vehicle Controller	Simple	6.85%	13.57%	8.78%	8.44%	14.34%	12.63%
	MicroAccel-a	4.90%	12.77%	4.21%	3.97%	13.16%	3.87%
	MicroAccel-b	1.81%	13.55%	8.16%	-0.60%	13.16%	7.99%
	MicroAccel-c	4.90%	12.77%	4.21%	3.97%	13.16%	3.87%
	MicroAccel-d	4.90%	12.77%	4.21%	3.97%	13.16%	3.87%
	MicroAccel-e	4.90%	12.77%	4.21%	3.97%	13.16%	3.87%
	MicroAccel-f	1.26%	13.16%	3.35%	1.09%	12.39%	3.18%
	KL-a	4.23%	9.30%	4.47%	3.45%	9.30%	4.64%
	RL-b	3.83%	9.30%	4.55%	3.36%	9.30%	4.64%
	RL-c	0.88%	13.16%	3.18%	0.88%	13.16%	3.18%
	RL-d	0.91%	12.77%	3.78%	1.08%	8.82%	4.81%
	RL-e	8.22%	14.34%	8.08%	8.72%	14.73%	8.68%
	HybridRL	2.95%	14.73%	9.19%	2.92%	14.74%	9.19%

(b)

Vehicle Controller	FREEFLOW SCENARIO	Speed Planner					
		Kernel Smooth			Kernel Smooth with RL Buffer		
		Fuel Economy % Increase	Throughput % Increase	Speed % Increase	Fuel Economy % Increase	Throughput % Increase	Speed % Increase
Vehicle Controller	Simple	1.13%	-0.56%	-2.14%	-2.79%	-1.24%	-1.81%
	MicroAccel-a	14.50%	9.15%	-11.63%	14.52%	5.21%	-11.53%
	MicroAccel-b	13.78%	4.49%	-12.73%	13.80%	5.90%	-11.83%
	MicroAccel-c	14.50%	5.13%	-11.63%	14.52%	5.21%	-11.53%
	MicroAccel-d	14.50%	5.13%	-11.63%	14.52%	5.21%	-11.53%
	MicroAccel-e	14.50%	5.13%	-11.63%	14.52%	5.21%	-11.53%
	MicroAccel-f	15.68%	0.33%	-15.38%	15.81%	0.63%	-15.20%
	KL-a	21.27%	2.50%	-25.19%	20.39%	2.05%	-22.38%
	RL-b	32.78%	2.33%	-23.78%	25.27%	3.47%	-21.54%
	RL-c	-0.19%	1.49%	0.43%	-0.03%	1.80%	0.26%
	RL-d	0.05%	0.12%	-0.86%	0.05%	0.12%	-0.86%
	RL-e	29.47%	1.41%	-34.28%	25.13%	2.35%	-27.52%
	HybridRL	-0.19%	1.49%	0.43%	-0.03%	1.80%	0.26%

(c)

FIGURE 6 A summary of controller assessments prior to MVT deployment. Candidate controller components to the MegaController were simulated under three scenarios (top: shockwave; middle: bottleneck; and bottom: free flow) and evaluated against key performance indicators (KPIs) (fuel economy, throughput, and network speed) relative to a baseline simulation of homogeneous human drivers. The Speed Planner candidates are shown across the top, and the vehicle controllers are shown in rows. The key performance indicators are shown in columns. Results are color-coded from improved (green) to neutral (white) to worsened (red).

[93], [94]. To allow control designers to easily make use of libpanda, the Robot Operating System (ROS) was installed on the Raspberry Pi. A set of ROS nodes was designed in the software project named `can_to_ros` [66], [69], which abstracts various sensors and actuators into a set of ROS topics. A tool named `bagpy` was also developed to quickly process and plot the recorded ROS data in the format of bag files [95]. With the infrastructure of ROS in place, control designers could use modeling software like MATLAB's Simulink to design controllers and generate code to greatly ease controller integration.

libpanda also features a set of auxiliary services to manage the vehicle at scale. A method to automatically perform over-the-air (OTA) updates was implemented so that

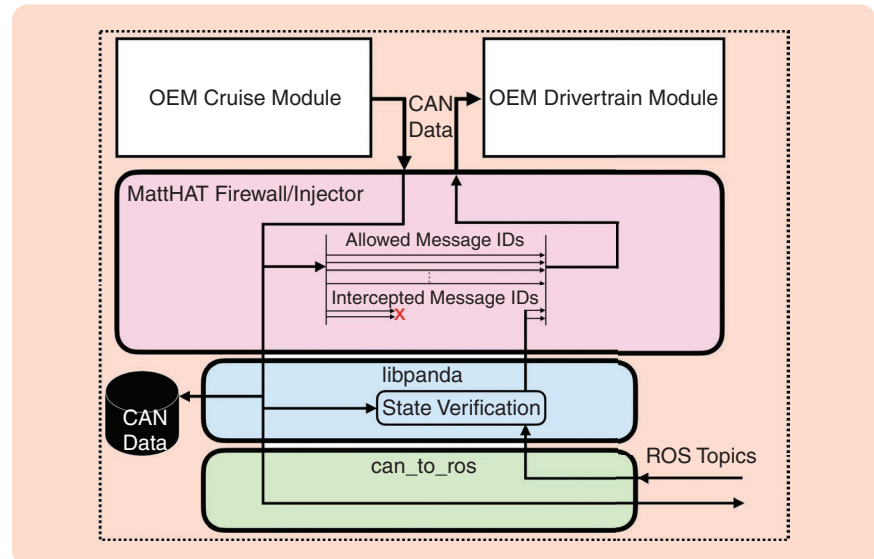


FIGURE 7 CAN firewall and message injection with ROS. A special CAN interface called the mattHAT firewalls messages between OEM modules at the hardware level and can replace blocked messages with third-party messages from software with libpanda. libpanda provides direct CAN recording as well as verification of CAN data to be sent by checking the OEM's CAN states. CAN messages can be read and sent through ROS topics provided by adapters in `can_to_ros`.

Vehicle Interfacing

by Matthew Bunting

The set of hardware involves both off-the-shelf and custom components assembled as a stack of printed circuit boards. Figure S5 shows the relationship of hardware components installed in each car.

HARDWARE

A Raspberry Pi 4 served as the main computer to run controllers. This was chosen due to its wide open source support and its availability and low cost. The operating system was 64-bit Raspbian Lite. We chose Raspbian instead of other Linux distributions since it was the only actively fully supported version from the hardware manufacturer.

Attached to the Raspberry Pi was an x728 battery-backup uninterrupted power supply (UPS). An experiment lifecycle began with turning on the car and therefore providing power to the Raspberry Pi and then ended when the vehicle parked and shut off at our headquarters. The UPS would continue to provide power to the Pi and signal that the Pi should stop the processing of the custom control and upload the experiment's data over Wi-Fi.

To provide Internet to the Pi during an experiment, needed for receiving control setpoints, a separate mobile hotspot was connected to the Pi's ethernet. Our chosen hotspot was an industrial-grade Cradlepoint IBR900 and IBR600. This hardware setup was shown to be effective for societal-scale experiments [79].

A uBlox M8 series USB GPS module provided the system with positional tracking. This sensor was also used to

synchronize the Raspberry Pi's system clock to GPS time to ensure that later data processing would involve minimal manual realignment.

The mattHAT (Hardware Attached on Top) served as the interface for the vehicles, with the majority being 2023 Nissan Rogue vehicles. The only standard interface on vehicles is the *Onboard Diagnostics (OBD)* port; however, this provides useful yet minimal data like the *Vehicle Identification Number (VIN)*. While modern vehicles have a rich set of sensors and actuators using the standardized CAN bus for communication, they are minimally documented to prevent third parties from interpreting sensors and from sending actuation commands. This leads to a significant effort to decode CAN signals. While off-the-shelf CAN decoders exist, our solution had to be custom to send low-level electrical signals to operate the stock ACC unit. This was possible for the Nissan Rogue by applying an electrical resistance to spoof button presses, requiring a custom circuit. The mattHAT was designed with these three communication components in mind to read the VIN over OBD, read vehicle sensors and state information over specific CAN buses, and send low-level ACC control commands.

SOFTWARE

libpanda is a low-level C++ library to operate the mattHAT (Hardware Attached on Top), written with a focus on

(Continued)

Vehicle Interfacing (*Continued*)

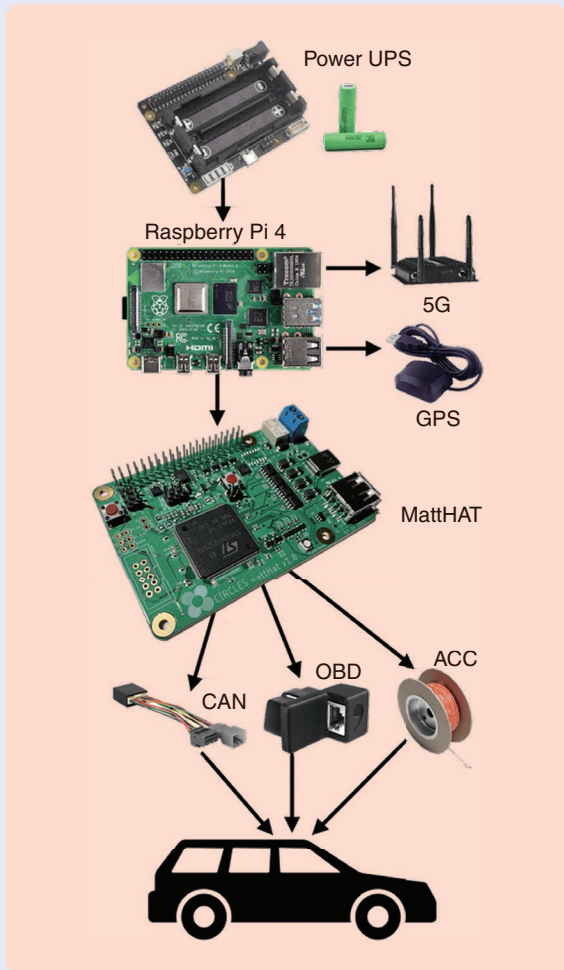


FIGURE S5 The set of hardware installed in each vehicle.

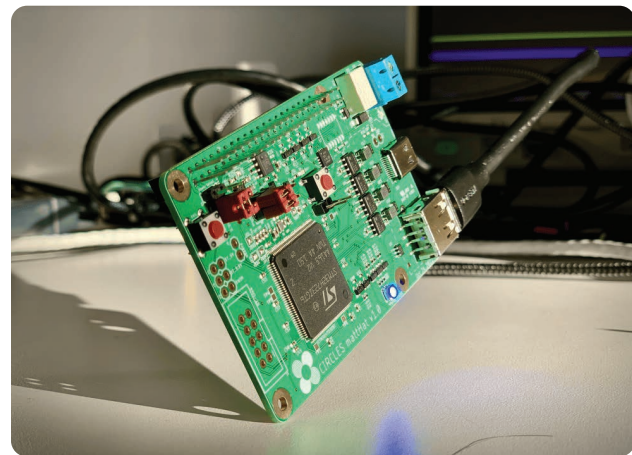


FIGURE 8 The mattHAT. This custom-designed circuit board was rapidly manufactured for both CAN interfacing and ACC button command spoofing.

data timeliness and low CPU usage [S9]. libpanda abstracted the vehicle interface in the form of an observer design pattern to easily write software for reading CAN and GPS data and to send control commands, either through CAN message injection or through the mattHAT's ACC interface. In addition to the low-level operation of the vehicle, libpanda also features a set of utilities to manage the Raspberry Pi for functions like automatic data upload, *over-the-air* (OTA) updates, and reporting system status.

Using libpanda, a Robot Operating System (ROS) node was designed to translate the various vehicle functions into the form of ROS topics. A project named `can_to_ros` provided prewritten middleware so that controller designers could use tools like MATLAB's Simulink to generate code in the form of C++ to control the vehicle [S10]. `can_to_ros` was also expanded to handle a heterogeneous fleet due to the mixture of models and make of vehicles [S11], [68]. In conjunction with `can_to_ros` and libpanda, data analysis tools named `bagpy` [95] and `strym` [92] were used to quickly analyze and decode the recorded data. Data from the signal decoding and system characterization process for a 2020 Toyota RAV4 have also been made publicly available [71].

REFERENCES

- [S9] M. Bunting, R. Bhadani, and J. Sprinkle, "Libpanda: A high performance library for vehicle data collection," in *Proc. Workshop Data-Driven Intell. Cyber-Phys. Syst.*, 2021, pp. 32–40.
- [S10] S. Elmadiani, M. Nice, M. Bunting, J. Sprinkle, and R. Bhadani, "From CAN to ROS: A monitoring and data recording bridge," in *Proc. Workshop Data-Driven Intell. Cyber-Phys. Syst.*, 2021, pp. 17–21.
- [S11] M. Nice, M. Bunting, D. Work, and J. Sprinkle, "Middleware for a heterogeneous CAV fleet," in *Proc. Cyber-Phys. Syst. Internet Things Week*, 2023, pp. 86–91, doi: [10.1145/3576914.3587524](https://doi.org/10.1145/3576914.3587524).

vehicles would not need to be manually handled. An additional server integration named `piStatus` was built so that the system could regularly post its status to easily assess the system's health. [Figure 9](#) shows headquarters personnel monitoring `piStatus`, ensuring that vehicles pass status checks before deployment. `piStatus` would be continuously monitored throughout each experiment to note any hardware issues so that vehicles could undergo maintenance before the next deployment. A shutdown script also worked in tandem with an off-the-shelf battery-backup Pi HAT to perform automatic data uploads at the end of an experimental drive when the vehicle was shut off. [Figure 10](#) shows a Wi-Fi antenna installed in the center of the vehicle parking lot for granting each vehicle's embedded computer Internet access for data upload and OTA updates. Without this set of services, managing and maintaining a project at this scale would have been impossible.

I-24 MOTION

The CIRCLES team deployed the MegaController on I-24 southeast of Nashville, TN, USA, due to the recent creation of a new testbed, known as I-24 MOTION [53], [54]. I-24 MOTION is a 4-mi section of I-24 designed to produce ultra-high-resolution trajectory data of all vehicles on the roadway for the purposes of traffic science and experimentation on AVs and traffic management. The system produces trajectory data (Figure 11) using 276 cameras (Figure 12) on fixed roadside poles between 110 and 135 ft tall to minimize visual occlusion. The debut of the I-24 MOTION testbed coincided with the live CIRCLES experiment, for which the testbed is uniquely suited to gather data on the traffic stream impacts of a fleet of test vehicles.

Processing of raw video into vehicle trajectories by I-24 MOTION happens in two stages as follows:

- 1) A computer vision pipeline [54], [97], [99], [100] makes the initial vehicle detection and type classification from the raw video, including vehicle dimensions by using 3D bounding boxes. Vehicle classes used for object detection are sedan, midsize, pickup, van, semi, truck, and motorcycle. It tracks detected vehicles across adjacent camera views in the vehicle's direction of travel. The computer vision processing is distributed across 10 servers with contiguous groups of cameras allocated to each. Vehicles are not tracked between servers, so a vehicle trajectory covering the length of the testbed consists of at least 10 fragments; additional fragmentation may occur due to unavoidable occlusion (for example, by overpasses). The computer vision pipeline also converts image space coordinates (where vehicle detections occur) into a roadway coordinate system using a homography transformation calibrated every hour to each camera.
- 2) Postprocessing algorithms first stitch fragmented trajectories together using an online minimum-cost network flow graph problem [101]. Each trajectory is then subject to a reconciliation procedure [98] to ensure

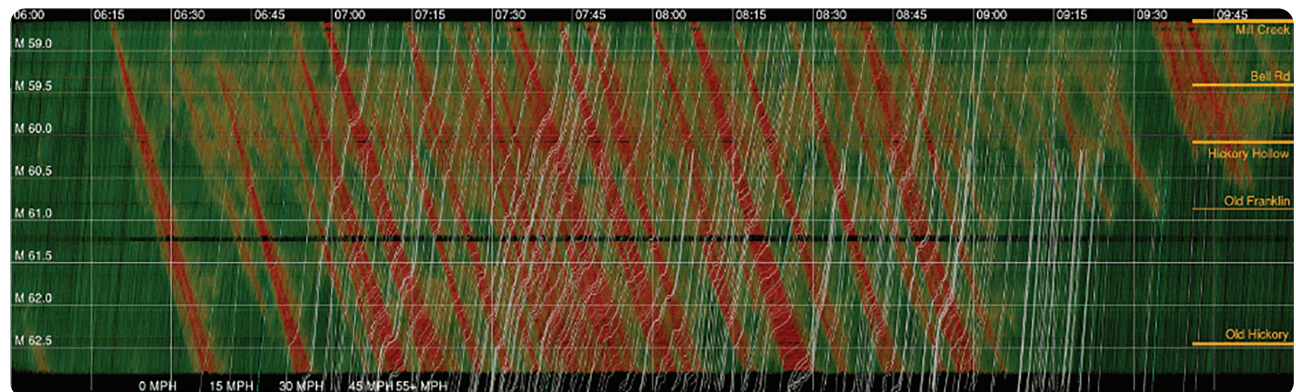


FIGURE 11 A time (horizontal axis) and space (vertical axis) diagram generated by I-24 MOTION [53] and the associated visualization library [96] during the MVT. Vehicle trajectories driving westbound (up) are colored based on the speed of vehicles (green: free flow to red: congested). The experiment vehicle trajectories are overlaid in white.

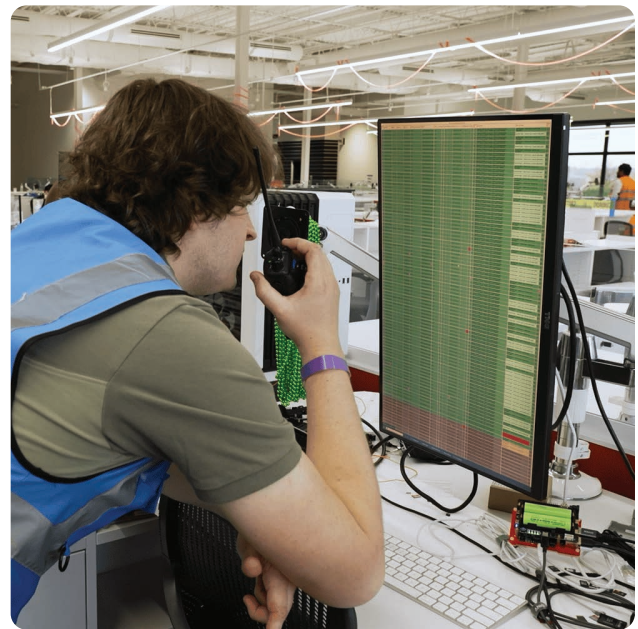


FIGURE 9 The piStatus web interface. Coauthor Matthew Bunting monitors the piStatus page to clear vehicles for experiment deployment.

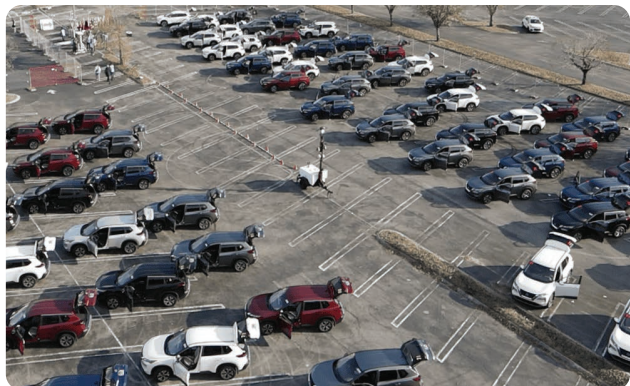


FIGURE 10 A parking lot Wi-Fi antenna. A Wi-Fi antenna is placed in the center of the vehicle parking lot, enabling OTA data uploads and software updates for each Raspberry Pi in each vehicle.

feasible and smooth higher-order dynamics (acceleration and jerk), formulated as a quadratic program. A data visualization library [96] assists with interpreting the datasets generated by the system.

Due to the critical nature of data from the MVT, the I-24 MOTION system retained a secure backup of the experiment data and baseline traffic conditions. Raw I-24 MOTION imagery is not accessible outside of the I-24 MOTION administrators, per the testbed's privacy policy. However, this backup allows reprocessing of the video and/or the raw vehicle detections from the computer vision

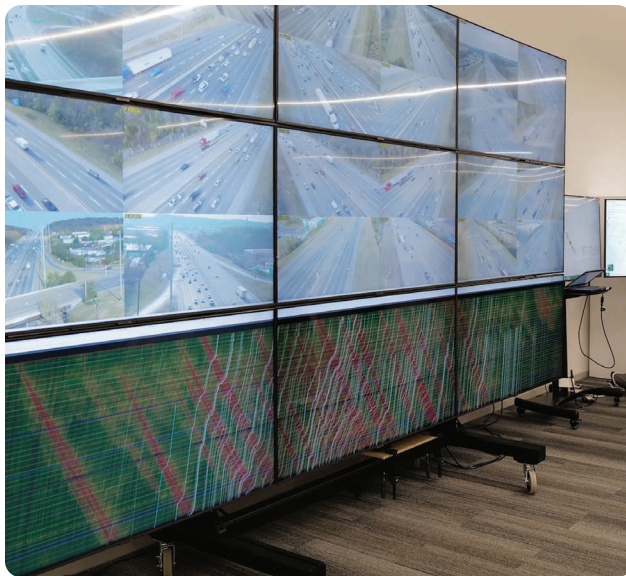


FIGURE 12 A visualization wall in the operation center. The display shows live video feeds from the I-24 MOTION cameras installed along the highway as well as a time–space diagram generated from the I-24 MOTION and AV data (see Figure 11 for more details).

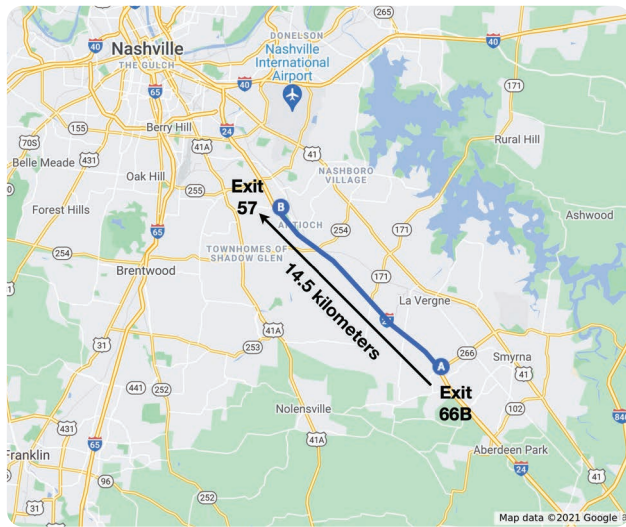


FIGURE 13 A portion of the I-24 highway where the experiment happened, near Nashville, TN, USA. The 14.5-km (9 mi) portion approximately spans between Exit 57 and Exit 66B.

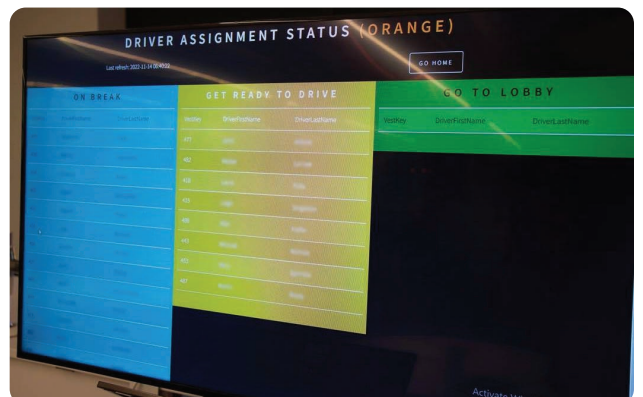
pipeline as the data generation pipeline advances. The current released version of the data has gone through reprocessing rounds to address known errors and limitations, including using hourly recalibrated homography transformations for camera perspective [100].

Experimental Design

The live traffic experiment took place on I-24 in November 2022. With 100 vehicles to deploy, more than 150 drivers were hired from among local college students, security guards, delivery drivers, team members' relatives, and elsewhere. The drivers were trained to adhere to specific assigned routes and lanes and to activate our custom ACC system whenever driving in their assigned lanes. Safety features were implemented such that the controller would default to stock ACC behavior if engaged off of the highway.

The specific routes driven by the AVs were chosen to maximize the penetration rate where the I-24 MOTION system [53] would capture the effect on the surrounding commuters (bulk traffic). Initially, a single-loop route that would have the AVs circulating from 7:30 a.m. to 9:30 a.m. was considered. It was determined that this would likely cause increased congestion on the Exit 57 off-ramp, leading to extended queuing and potential spillback onto I-24. For this reason, we divided our AVs into two groups with the two different routes partially overlapped on I-24. The portion of the highway where the experiment happened is displayed in Figure 13.

The AVs are released at 6:00 a.m. for all 100 to be deployed by the target time of 7:30 a.m. The drivers are instructed to repeat their driving routes for 2 h—or sooner if they want a break. On a return trip, they exit the highway at Exit 60 (Hickory Hollow) to return to the field headquarters parking lot and return their car keys at a desk before leaving the lot. As the AVs return to the lot for a break, other drivers (already on break) head down to a queue to come out to the lot when needed, following instructions from our “airline reservation board” (Figure 14). With this smoothly running rotation system, we



were able to keep the 100 AVs on the routes during peak hours while keeping track of their locations in real time (Figure 15). For more details about the routes and logistical choices made for the experiment, the driver training, the daily schedule, or the penetration rate estimates, see [35].

Data Release

As a part of this publication, we are releasing to the public a dataset from the MVT. This data release will include data collected by the AVs as well as the I-24 MOTION [54] system. See also [97], [99], and [100] for other datasets generated by I-24 MOTION.

The data contain GPS and CAN data collected by the 100 AVs from all testing days. The longitudinal position along the highway is modified post hoc with an offset to account for systematic positioning error (for example, caused by the placement of the GPS unit within the vehicle). The offset is determined by finding all likely matches in the I-24 MOTION dataset and computing the median delta. All other data are provided unaltered except for interpolating onto a resampled fixed 10-Hz time grid. Lane identification is not provided; rather, the driver's assigned lane can reasonably be assumed to be the true lane when the controller is engaged.

The raw I-24 MOTION trajectory information is processed [98], [101] and then is appended with additional information. Speed and acceleration are inferred from the longitudinal position (which, as described previously, is processed to be sufficiently smooth for second-order derivatives). Road grade information is added via a parametric road grade map model. Fuel information, including various fuel rates and those for reference trajectories, are appended through the application of fuel rate models (see "Vehicle Energy Models" and [86]). Fuel rate models are selected with a one-to-one mapping of vehicle classes to fuel model classes. For each I-24 MOTION trajectory segment, a reference trajectory is constructed that matches the initial and terminal positions and speeds and minimizes the functional $\max_t a(t) - \min_t a(t)$ subject to the additional constraint $v(t) \geq 0$. This functional is a simple vehicle-independent proxy for the more complicated energy models constructed in [86], motivated by the following arguments: 1) due to the superlinear growth of fuel rate with increasing acceleration, peak accelerations should be minimized, and 2) unnecessarily heavy braking results in wasted fuel, and hence, peak braking (which is $-\min_t a(t)$ for typical trajectories) should also be minimized. By Pontryagin's maximum principle, this generally results in piecewise-constant acceleration profiles with a jump at the trajectory's midpoint in time. Lastly, using the implicit lane and longitudinal matching with the AV dataset, we also supply relative distances and vehicle IDs for nearest upstream/downstream engaged-or-not AVs to assist in subsequent analyses.

Further information on the structure of the data will be provided in the data documentation released with the data.

RESULTS

The experimental, observational, data collection, and data processing framework described previously generated a large amount of data, capturing every single vehicle on a highway during the deployment of 100 controlled vehicles. Analogous to previous seminal traffic datasets, such as NGSIM [55], the new data are expected to inspire and enable many subsequent findings. To highlight this potential, we here present some key first findings and insights, based on an analysis of the data with a macroscopic perspective.

We construct macroscopically meaningful fields in time–space, most prominently a field that shows the energy (in)efficiency of traffic at large on the I-24 highway segment. This is achieved by applying Edie's method [56] on boxes of size $h_t \times h_x$, where $h_t = 10$ s and $h_x = 200$ m, to the I-24 MOTION trajectories to construct the following fields:

- » vehicle density $\rho(t, x)$, as the total vehicle time spent in each box, divided by the size of the box, $h_t \cdot h_x$
- » flow rate $q(t, x)$, as the total distance traveled in each box, divided by $h_t \cdot h_x$
- » fuel rate density $f(t, x)$, as the total fuel consumed in each box, divided by $h_t \cdot h_x$.

From these fields, other meaningful fields are obtained, such as the bulk velocity field $u(t, x) = q(t, x) / \rho(t, x)$, the bulk fuel rate $\phi(t, x) = f(t, x) / \rho(t, x)$, and the bulk fuel consumption $\psi(t, x) = f(t, x) / q(t, x)$. The latter quantity $\psi(t, x)$, measurable for instance in grams per meter, represents the fuel demand per distance traveled of all vehicles in the $h_t \times h_x$ vicinity of the position (t, x) . Figure 16 shows $\psi(t, x)$ for two experimental days: Wednesday, 16 November and Thursday, 17 November 2022. Each plot is overlaid with the trajectories of all control vehicles. This represents the first time that a complete time–space diagram of the energy inefficiency of traffic, based on accurate trajectories of *all* vehicles on the roadway, has been provided.

In the same spirit as the purely microscopic Figure 11, one can, for both days shown in Figure 16, clearly see the



FIGURE 15 The Vehicle Tracker System (middle screen). Coauthor Jonathan Lee introduces the display to U.S. DOE stakeholder Heather Croteau. Located in the operation center, the realtime location, speed, direction, and control status of all deployed vehicles are on the map.

traffic waves traveling backwards along the highway as well as the increased fuel consumption incurred in these waves. The figure also shows the increased fuel demand in the uphill segment between $x = 5$ km and $x = 6$ km and the reduced fuel demand in the downhill segment thereafter. The AV trajectories are colored red when the automated controller is activated and white when the vehicle is under human control. The two shown test days were quite different in terms of the engagement rates of the controllers; on 16 November, the controllers were engaged 38% of all times, while on 17 November, the engagement rate went up to 78%. This difference was caused by a combination of increased driver comfort with automation and the more reliable communication of traffic information to the vehicles on 17 November.

Given the low penetration rate of the control vehicles on the highway, it was not expected that they would completely smooth out all traffic waves—and the plots in Figure 16 confirm that expectation. However, the AVs may still have had some positive contribution to the energy efficiency of the flow at large. Whether that was in fact the case, we first note that the macroscopic plots, like in Figure 16, allow for a

targeted inspection of different regions of interest in time–space. For instance, on 16 November, there is a distinct region of high fuel inefficiency, around time 8:25 a.m. and location 5.0–6.5 km, and notably, this high-fuel region coincides with all the AV controllers being inactive. In contrast, on 17 November, such clusters of inactive AVs did not occur—and the fuel consumption map does not exhibit similarly large high-fuel regions. Another notable incident occurs on 16 November in the wave that goes through $x = 2.3$ km at time 7:00 a.m. First, two active AVs notably dampen the wave; then, the wave keeps on growing while four inactive AVs run through it (at $x = 3$ km), followed by several active AVs (around $x = 4$ km) notably dampening the wave again.

Many more quantitative results and plots are available in the publications of the different teams that contributed and deployed a controller during the MVT [39], [41], [82]. Since each team deployed their controllers in different manners, on different vehicles, or at different scales, the results are not easily comparable—which leads to interesting analyses from different points of view. Each team has detailed the process they went through to clean, parse, and extract relevant information from the data to estimate their controller’s impact in

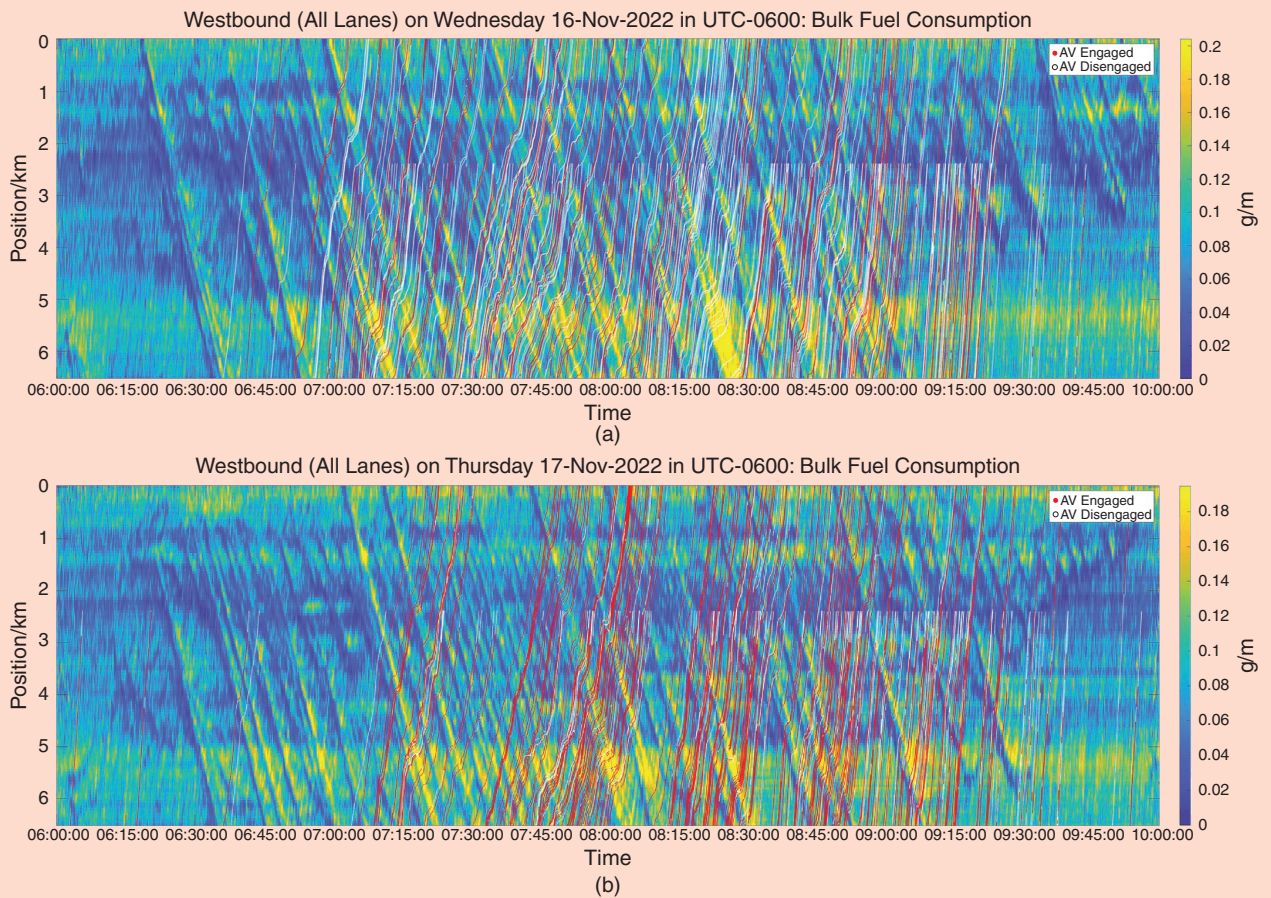


FIGURE 16 A bulk fuel consumption heatmap in time (horizontal axis) and space (vertical axis), based on I-24 MOTION [53] of all vehicles (aggregated over all lanes) driving in the westbound direction with AV trajectories overlaid (white: controller not engaged; red: controller engaged). Shown are (a) 16 November 2022 and (b) 17 November 2022.

terms of energy savings and traffic smoothing. Continued efforts to quantify our vehicles' overall impact are underway and planned for future publication(s).

CONCLUSION

This work describes the control architectures and implementations of a 100-AV deployment to improve traffic efficiency on a freeway using a small fraction of AVs. It is the largest field experiment to use connected and automated vehicles (CAVs) to regulate the overall traffic flow, and the deployment strategy enabled algorithms from diverse fields spanning model-based control to RL. The control strategy presented in this work was a hierarchical control approach in which the upper-level Speed Planner provided target velocities to a lower-level control law responsible for performance and safety. These algorithms were deployed in the largest field experiment of its kind, on a heterogeneous vehicle fleet using low-cost vehicular instrumentation. The data from the vehicles were combined with datasets generated from I-24 MOTION [53], [54], providing a large data resource for further study on the interaction of control vehicles on bulk traffic flow.

ACKNOWLEDGMENT

This material is based upon work supported by the National Science Foundation under Grants CNS-1837244 (A. Bayen), CNS-1837652 (D. Work), CNS-1837481 (B. Piccoli), CNS-1446715 (B. Piccoli), CNS-1446690 (B. Seibold), CNS-1446435 (J. Sprinkle), and CNS-1446702 (D. Work), CNS-2135579 (D. Work, A. Bayen, J. Sprinkle, and J. Lee) and by the French CNRS under Grants IEA SHYSTRA and PEPS JCJC (A. Hayat). This material is based upon work supported by the U.S. Department of Energy's Office of Energy Efficiency and Renewable Energy (EERE) under the Vehicle Technologies Office Award CID DE-EE0008872. The authors are grateful for the additional support provided by C3AI, Amazon AWS, Siemens, Toyota, GM, Nissan, Caltrans, Contra Costa Transportation Authority (CCTA), King Abdulaziz City for Science and Technology (KACST), and the Tennessee Department of Transportation. Jonathan W. Lee, Han Wang, Kathy Jang, Nathan Lichtlé, Amaury Hayat, and Matthew Bunting contributed equally to this work. Arwa Alanqary, William Barbour, Zhe Fu, Xiaoqian Gong, George Gunter, Sharon Hornstein, Abdul Rahman Kreidieh, Matthew W. Nice, William A. Richardson, Adit Shah, Eugene Vinitsky, Fangyu Wu, and Shengquan Xiang contributed equally to this work. Sulaiman Almatrudi, Fahd Althukair, Rahul Bhadani, Joy Carpio, Raphael Chekroun, Eric Cheng, Maria Teresa Chiri, Fang-Chieh Chou, Ryan DeLorenzo, Marsalis Gibson, Derek Gloudemans, Anish Gollakota, Junyi Ji Alexander Keimer, Nour Khoudari, Malaika Mahmood, Mikail Mahmood, Hossein Nick Zinat Matin, Sean McQuade, Rabie Ramadan, Daniel Urieli, Xia Wang, Yanbing Wang, Rita Xu, Mengsha Yao, Yiling You, Gergely Zachár, and Yibo Zhao contributed equally to this work. Mostafa Ameli, Mirza Najamuddin Baig, Sarah Bhaskaran, Kenneth Butts, Manasi Gowda, Caroline Janssen, John Lee, Liam Pedersen,

Riley Wagner, Zimo Zhang, and Chang Zhou contributed equally to this work.

The views expressed herein do not necessarily represent the views of the U.S. Department of Energy or the United States Government.

AUTHOR INFORMATION

Jonathan W. Lee (jonny5@berkeley.edu) received the B.S. degree in engineering physics from the University of California, Berkeley and the M.S. and Ph.D. degrees in mechanical engineering from Rice University. At Sandia National Laboratories (2011–2013), he completed his postdoctoral appointment, studying electrical and material properties via molecular dynamics simulations. He subsequently served as a senior data scientist and product manager on various teams at Uber Technologies, Inc. (from 2014 to 2019). Since 2019, he has served as an engineering manager at the University of California, Berkeley, Berkeley, CA 94720 USA, and the program manager and chief engineer of CIRCLES.

Han Wang is currently working on his Ph.D. degree in transportation engineering as well as an M.S. degree in the Department of Electrical Engineering and Computer Sciences, University of California, Berkeley, Berkeley, CA 94720 USA. His research focuses on the decentralized control of massive automated vehicle platforms and driving assistance utilizing computer vision techniques.

Kathy Jang received the Ph.D. degree in the Department of Electrical Engineering and Computer Sciences, University of California, Berkeley in 2024 and is currently a research scientist at Waymo, San Francisco, CA 94105 USA. Her research groups include Berkeley Artificial Intelligence Research (BAIR) and Berkeley Deep Drive (BDD). Her research focuses on robust reinforcement learning with applications to mixed-autonomy traffic.

Nathan Lichtlé is currently working on his Ph.D. in the Department of Electrical Engineering and Computer Sciences, University of California, Berkeley, Berkeley, CA 94720 USA, and in the Research Center in Applied Mathematics, Ecole nationale des Ponts et Chaussées, Institut Polytechnique de Paris, 77420 Champs sur Marne, France. His research groups include Berkeley Artificial Intelligence Research (BAIR) and Berkeley Deep Drive (BDD). His research focuses on reinforcement learning and mixed-autonomy traffic.

Amaury Hayat has been a professor of mathematics at the Ecole des Ponts ParisTech, 77420 Champs sur Marne, France, since 2023. He has been a faculty member at the Research Center in Applied Mathematics, Ecole des Ponts ParisTech since 2019. His research focuses on control theory, partial differential equations, traffic control, and artificial intelligence for mathematics.

Matthew Bunting received the Ph.D. degree in electrical and computer engineering at the University of Arizona and is a research scientist in the Institute for Software

Integrated Systems, Vanderbilt University, TN 37212 USA. His focus is on hardware development of autonomous vehicles, democratizing vehicle data collection and control through open source projects.

Arwa Alanqary received the B.S. degree in mechanical engineering from Alfaisal University in 2017 and the M.S. degree in computational science and engineering from the Massachusetts Institute of Technology in 2021. She is currently a Ph.D. student in electrical engineering and computer sciences at the University of California, Berkeley, Berkeley, CA 94720 USA. Her research focuses on optimal control and optimization and learning in multiagent systems.

William Barbour is a research scientist at the Institute for Software Integrated Systems, Vanderbilt University, TN 37212 USA. He is a co-principal investigator on the I-24 MOTION testbed and works on other large transportation systems projects across the state of Tennessee. His technical focus is on intelligent transportation systems, artificial intelligence, and data science.

Zhe Fu is a Ph.D. degree candidate in transportation engineering and an M.S. degree candidate at the Department of Electrical Engineering and Computer Sciences, University of California, Berkeley, Berkeley, CA 94720 USA. Her research focuses on traffic control and machine learning in mixed-autonomy traffic.

Xiaoqian Gong is an assistant professor of mathematics at Amherst College, Amherst, MA 01002 USA. She was previously an instructor at Arizona State University and a postdoctoral researcher at Rutgers University-Camden.

George Gunter is a Ph.D. student in civil and environmental engineering at the Institute for Software Integrated Systems, Vanderbilt University, TN 37212 USA. His research focuses on safety and security in applications of cyberphysical systems to civil infrastructure.

Sharon Hornstein is a researcher at General Motors R&D, Herzliya 4672513, Israel. She received the B.Sc., M.Sc. and Ph.D. degrees in mechanical engineering from the Technion, Israel. Her research focuses on the dynamic modeling of nonlinear systems.

Abdul Rahman Kreidieh received the Ph.D. in civil and environmental engineering from the University of California, Berkeley. He is an engineer at Google, Mountain View, CA 94043 USA.

Matthew W. Nice received the M.Eng. degree in cyberphysical systems and the Ph.D. degree in civil and environmental engineering from Vanderbilt University. He is a research faculty at the Virginia Tech Transportation Institute in Blacksburg, VA 24061 USA. He was a member at Vanderbilt of the Institute for Software Integrated Systems, where he led experimental research on the impact of technology in connected and automated vehicles on transportation systems. His research has been supported by multiple Dwight D. Eisenhower Transportation Fellowship Awards from the Federal Highway Administration (FHWA), as well as the National Science Foundation.

William A. Richardson is a Ph.D. student in computer science at the Institute for Software Integrated Systems, Vanderbilt University, TN 37212 USA. In 2024, he received the National Science Foundation Graduate Research Fellowship. His research has also been supported by multiple Dwight D. Eisenhower Transportation Fellowship Awards from the Federal Highway Administration (FHWA).

Adit Shah is an undergraduate student in the Department of Electrical Engineering and Computer Sciences, University of California, Berkeley, Berkeley, CA 94720 USA. His research focuses on machine learning and its societally beneficial applications.

Eugene Vinitsky is currently an assistant professor in civil engineering at New York University, New York City, NY 11201 USA. He received the Ph.D. degree in the Department of Mechanical Engineering at the University of California, Berkeley. His research focuses on reinforcement learning and mixed-autonomy traffic.

Fangyu Wu is a postdoctoral researcher at Cornell University, Ithaca, NY 14850 USA. He received the Ph.D. degree in electrical engineering and computer science at the University of California, Berkeley.

Shengquan Xiang is an assistant professor at Peking University, Beijing 100871, China.

Sulaiman Almatrudi is a Ph.D. candidate in transportation engineering at the University of California, Berkeley, Berkeley, CA 94720 USA. He received the B.S. degree in electrical engineering from King Fahd University of Petroleum and Minerals in 2017. He received the M.S. degree in transportation engineering from the University of California, Berkeley in 2020. His research focuses on traffic and energy estimation.

Fahd Althukair received the bachelor of engineering degree in electrical engineering and computer science from the University of California, Berkeley, Berkeley, CA, 94720 USA.

Rahul Bhadani is an assistant professor of electrical and computer engineering at the University of Alabama, in Huntsville, Huntsville, AL 35899 USA. He received the M.S. (2017) and Ph.D. (2022) degrees in electrical and computer engineering from the University of Arizona. He completed his postdoctoral appointment at Vanderbilt University, studying the modeling of microgrid components using SystemC-AMS. His research focuses on model-based system design for cyberphysical systems and intelligent transportation. He has led the development of software tools to design, test, and execute vehicle controllers for seminal experiments in transportation, including the Arizona Ring-road experiment and 100-car experiments on I-24 Nashville that demonstrated the impact of connected and automated vehicles in reducing urban traffic congestion and increasing fuel efficiency.

Joy Carpio is a researcher at the Nissan Advanced Technology Center in Santa Clara, CA 95051 USA. She received the Ph.D. degree in systems engineering at the University of California, Berkeley.

Raphaël Chekroun is a senior research engineer at Fovision, 75002 Paris, France. He received the Ph.D. degree

in artificial intelligence from Mines Paris and the University of California, Berkeley.

Eric Cheng is a software engineer at Unity Technologies, San Francisco, CA 94103 USA. He received his B.S. degree in electrical engineering and computer science at the University of California, Berkeley.

Maria Teresa Chiri is an assistant professor in the Department of Mathematics and Statistics at Queen's College, Kingston, ON K7L 3N6, Canada.

Fang-Chieh Chou is an assistant professor in the Department of Mathematics and Statistics at Queen's College, Kingston, ON K7L 3N6, Canada.

Ryan DeLorenzo is a research assistant at Rutgers University – Camden, Camden, NJ 08102 USA.

Marsalis Gibson is a Ph.D. student in the Department of Electrical Engineering and Computer Science at the University of California, Berkeley, Berkeley, CA 94720 USA.

Derek Gloudemans received the M.S. degree in computer science and is a doctoral candidate in the Department of Computer Science, Institute for Software Integrated Systems, Vanderbilt University, TN 37212 USA. He has led computer vision research and software implementation on the I-24 MOTION project.

Anish Gollakota is an M.S. student in the Department of Electrical and Computer Engineering at the University of California, Berkeley, Berkeley, CA 94720 USA.

Junyi Ji is a Ph.D. student in civil and environmental engineering at the Institute for Software Integrated Systems, Vanderbilt University, TN 37212 USA. His research focuses on the area of data-driven traffic flow theory and control.

Alexander Keimer is a senior researcher in the Department of Mathematics at FAU Erlangen-Nürnberg, 91058 Erlangen, Germany. He was previously a postdoctoral researcher at the University of California, Berkeley and Rutgers University-Camden.

Nour Khoudari is a Golomb visiting assistant professor in the Department of Mathematics at Purdue University, West Lafayette, IN 47907 USA. She received the Ph.D. degree in mathematics from Temple University.

Malaika Mahmood is a research assistant at Rutgers University - Camden, Camden, NJ 08102 USA.

Mikail Mahmood is a research assistant at Rutgers University - Camden, Camden, NJ 08102 USA.

Hossein Nick Zinat Matin is a postdoctoral researcher at the University of California, Berkeley, Berkeley, CA 94720 USA. His research focuses on partial differential equations and their applications in the theory of traffic flow.

Sean McQuade received the B.S. degree in mathematics from Virginia Polytechnic Institute and State University and received the Ph.D. degree in computational and integrative biology from Rutgers–Camden. He is a senior researcher at Temple University, Philadelphia, PA 19122 USA.

Rabie Ramadan is the Director of Data Science at Legal & General America, Frederick, MD 21704 USA. He received the Ph.D. degree in mathematics from Temple University.

Daniel Urieli received the Ph.D. degree in artificial intelligence (AI) from the University of Texas at Austin, where he developed AI agents that won the Power Trading Agent Competition as well as the simulated robot soccer league in the international RoboCup competition. He is a staff researcher at General Motors, R&D, Herzliya 4672513, Israel, where he has cofounded the autonomous driving research group and led research on applying AI for congestion reduction and for electric vehicle energy management.

Xia Wang is a Ph.D. student in computer science at the Institute for Software Integrated Systems, Vanderbilt University, TN 37212 USA.

Yanbing Wang is a Ph.D. student in computer science at the Institute for Software Integrated Systems, Vanderbilt University, TN 37212 USA.

Rita Xu is an undergraduate student in economics and data science at the University of California, Berkeley, Berkeley, CA 94720 USA.

Mengsha Yao is an undergraduate student in economics and data science at the University of California, Berkeley, Berkeley, CA 94720 USA.

Yiling You is a research scientist at Meta, Menlo Park, CA 94025 USA. She received her Ph.D. in applied mathematics from the University of California, Berkeley.

Gergely Zachár is a postdoctoral researcher at the Institute for Software Integrated Systems, Vanderbilt University, TN 37212 USA. He was part of the team for the hardware and software implementation on the I-24 MOTION project.

Yibo Zhao is a Ph.D. student at Northeastern University, Boston, MA 02115 USA. He received the B.A. degree in computer science and physics from the University of California, Berkeley.

Mostafa Ameli received his Ph.D. degree from the University of Paris-est, IFSTTAR (The French Institute of Science and Technology Development to Transport, Planning, and Networks), and the University of Lyon in 2019. He is an associate professor in applied mathematics, computer science, and transportation science at the Transportation Engineering and Computer Science Lab (GRET-TIA), University Gustave Eiffel Paris, 77420 Champs-sur-Marne, France. Since 2022, he has also been a research affiliate with the Department of Electrical Engineering and Computer Sciences, University of California, Berkeley, CA 94720 USA.

Mirza Najamuddin Baig is a product leader at the Nissan Advanced Technology Center in Santa Clara, CA 95051 USA.

Sarah Bhaskaran received her B.A. degree in computer science from the University of California, Berkeley. She is a software engineer at Duolingo, Pittsburgh, PA 15206 USA.

Kenneth Butts was an Executive Engineer at Toyota Motor Engineering and Manufacturing North America. He is currently retired.

Manasi Gowda received her B.A. degree in computer science from the University of California, Berkeley. She is a software engineer at Meta, Seattle, WA 98109 USA.

Caroline Janssen received the bachelor of engineering degree in Civil Engineering, and the Master of Science in Civil Engineering, from Vanderbilt University in Nashville, TN 37212 USA.

John Lee received the B.A. degree in computer science from the University of California, Berkeley. He a software engineer at Wing, Palo Alto, CA 94304 USA.

Liam Pedersen is the chief scientist at the Nissan Advanced Technology Center in Santa Clara, CA 95051 USA.

Riley Wagner received the B.S. degree in systems engineering from the University of Arizona, Tucson. She is a research program coordinator at the Institute for Software Integrated Systems, Vanderbilt University, TN 37212 USA.

Zimo Zhang received his M.S. degree in information science from the University of Pittsburgh and previously interned at the University of California, Berkeley. He is a software development engineer at Amazon, Seattle, WA 98109 USA.

Chang Zhou received her M.Eng. degree in computer science from the University of California, Berkeley. She is a software engineer at Amazon Web Services, East Palo Alto, CA 94303 USA.

Daniel B. Work is a professor of civil and environmental engineering at the Institute for Software Integrated Systems, Vanderbilt University, TN 37212 USA. His research focuses on transportation cyberphysical systems.

Benjamin Seibold is a university professor and the Joseph and Loretta Lopez Chair Professor of Mathematics at Rutgers University–Camden, Camden, NJ 08102 USA. He also served as vice chancellor for research. His research focuses span various areas of applied mathematics, including control theory, traffic flow on networks, crowd dynamics, math finance and application to autonomous driving, population health, and biomedical systems. He is author of more than 300 research papers and articles and seven books and is the founding editor of Networks and Heterogeneous Media. He is the recipient of the 2009 Fubini Prize, the plenary speaker at ICIAM 2011, and the 2012 inaugural fellow of the American Mathematical Society. He is a Senior Member of IEEE.

Jonathan Sprinkle is a professor of computer science at Vanderbilt University, TN 37212 USA since 2021. Prior to joining Vanderbilt, he was the Litton Industries John M. Leonis Distinguished Associate Professor of Electrical and Computer Engineering at the University of Arizona and the interim director of the Transportation Research Institute. From 2017 to 2019, he served as a program director in Cyber-Physical Systems and Smart & Connected Communities at the National Science Foundation in the CISE Directorate.

Benedetto Piccoli is a university professor and the Joseph and Loretta Lopez Chair Professor of Mathematics at Rutgers University–Camden, Camden, NJ 08102 USA. He also served as vice chancellor for research. His research focuses span various areas of applied mathematics, including control theory, traffic flow on networks, crowd dynamics, math finance and application to autonomous driving, population health, and biomedical systems. He is author of more than

300 research papers and articles and seven books and is the founding editor of Networks and Heterogeneous Media. He is the recipient of the 2009 Fubini Prize, the plenary speaker at ICIAM 2011, and the 2012 inaugural fellow of the American Mathematical Society. He is a Senior Member of IEEE.

Maria Laura Delle Monache is an assistant professor in the Department of Civil and Environmental Engineering, University of California, Berkeley, Berkeley, CA 94720 USA. She is the recipient of the 2023 IEEE Technical Committee on Cyber Physical Systems (TCCPS) Mid-career award, the 2023 IEEE Intelligent Transportation Systems Society (ITSS) Young researcher/Engineer award and the 2024 UC ITS Faculty of the year award. Her research research lies at the intersection of transportation engineering, mathematics, and control.

Alexandre M. Bayen is the associate provost for Moffett Field Program Development at the University of California, Berkeley, Berkeley, CA 94720 USA, and the Liao-Cho Professor of Engineering at the University of California, Berkeley, CA 94720 USA. He is a professor in the Departments of Electrical Engineering and Computer Science and of Civil and Environmental Engineering (courtesy). He is also a faculty scientist in mechanical engineering at the Lawrence Berkeley National Laboratory. From 2014 to 2021, he served as the director of the Institute of Transportation Studies at the University of California, Berkeley.

REFERENCES

- [1] W. B. Stevens, "The automated highway system program: A progress report," *IFAC Proc. Volumes*, vol. 29, no. 1, pp. 8180–8188, 1996, doi: [10.1016/S1474-6670\(17\)59010-2](https://doi.org/10.1016/S1474-6670(17)59010-2).
- [2] H.-S. Tan, R. Rajamani, and W.-B. Zhang, "Demonstration of an automated highway platoon system," in *Proc. Am. control Conf. ACC (IEEE Cat. No. 98CH36207)*, vol. 3, Piscataway, NJ, USA: IEEE, 1998, pp. 1823–1827, doi: [10.1109/ACC.1998.707332](https://doi.org/10.1109/ACC.1998.707332).
- [3] S. E. Shladover, C. Nowakowski, X.-Y. Lu, and R. Ferlis, "Cooperative adaptive cruise control: Definitions and operating concepts," *Transp. Res. Rec.*, vol. 2489, no. 1, pp. 145–152, 2015, doi: [10.3141/2489-17](https://doi.org/10.3141/2489-17).
- [4] D. Swaroop, J. K. Hedrick, C. Chien, and P. Ioannou, "A comparison of spacing and headway control laws for automatically controlled vehicles," *Veh. Syst. Dyn.*, vol. 23, no. 1, pp. 597–625, 1994, doi: [10.1080/00423119408969077](https://doi.org/10.1080/00423119408969077).
- [5] P. A. Ioannou and C.-C. Chien, "Autonomous intelligent cruise control," *IEEE Trans. Veh. Technol.*, vol. 42, no. 4, pp. 657–672, Nov. 1993, doi: [10.1109/25.260745](https://doi.org/10.1109/25.260745).
- [6] A. Girault, "A hybrid controller for autonomous vehicles driving on automated highways," *Transp. Res. C: Emerg. Technol.*, vol. 12, no. 6, pp. 421–452, 2004, doi: [10.1016/j.trc.2004.07.008](https://doi.org/10.1016/j.trc.2004.07.008).
- [7] M. Buehler, K. Iagnemma, and S. Singh, *The 2005 DARPA Grand Challenge: The Great Robot Race*, vol. 36. Berlin, Germany: Springer-Verlag, 2007.
- [8] S. Thrun et al., "Stanley: The robot that won the DARPA grand challenge," *J. Rob. Syst.*, vol. 23, no. 9, pp. 661–692, 2006, doi: [10.1002/rob.20147](https://doi.org/10.1002/rob.20147).
- [9] L. Xiao and F. Gao, "A comprehensive review of the development of adaptive cruise control systems," *Veh. Syst. Dyn.*, vol. 48, no. 10, pp. 1167–1192, 2010, doi: [10.1080/00423110903365910](https://doi.org/10.1080/00423110903365910).
- [10] G. Gunter et al., "Are commercially implemented adaptive cruise control systems string stable?" *IEEE Trans. Intell. Transp. Syst.*, vol. 22, no. 11, pp. 6992–7003, Nov. 2021, doi: [10.1109/TITS.2020.3000682](https://doi.org/10.1109/TITS.2020.3000682).
- [11] S. E. Shladover, C. Nowakowski, X.-Y. Lu, and R. Hoogendoorn, "Using cooperative adaptive cruise control (CACC) to form high-performance vehicle streams," Federal Highway Administration, McLean, VA, USA, Tech. Rep. CA18-2911, 2014.
- [12] A. Dávila and M. Nombela, *Sartre-Safe Road Trains for the Environment Reducing Fuel Consumption Through Lower Aerodynamic Drag Coefficient*. Warrendale, PA, USA: SAE International, 2011.

- [13] P. Jootel, "Safe road trains for the environment (SARTRE) final report," Tech. Rep., Technical Report for European Commission under the Framework 7 Programme Project 233683), 2012.
- [14] S. Tsugawa, S. Kato, and K. Aoki, "An automated truck platoon for energy saving," in Proc. IEEE/RSJ Int. Conf. Intell. Rob. Syst., 2011, pp. 4109–4114, doi: [10.1109/IROS.2011.6094549](#).
- [15] J. Ploeg, S. Shladover, H. Nijmeijer, and N. van de Wouw, "Introduction to the special issue on the 2011 grand cooperative driving challenge," *IEEE Trans. Intell. Transp. Syst.*, vol. 13, no. 3, pp. 989–993, Sep. 2012, doi: [10.1109/TITS.2012.2210636](#).
- [16] R. Kianfar et al., "Design and experimental validation of a cooperative driving system in the grand cooperative driving challenge," *IEEE Trans. Intell. Transp. Syst.*, vol. 13, no. 3, pp. 994–1007, Sep. 2012, doi: [10.1109/TITS.2012.2186513](#).
- [17] C. Englund et al., "The grand cooperative driving challenge 2016: Boosting the introduction of cooperative automated vehicles," *IEEE Wireless Commun.*, vol. 23, no. 4, pp. 146–152, Aug. 2016, doi: [10.1109/MWC.2016.7553038](#).
- [18] S. Shladover et al., "Cooperative adaptive cruise control (CACC) for partially automated truck platooning," California Department of Transportation, Sacramento, CA, USA, Tech. Rep. CA18-2623, 2018.
- [19] D. M. Willemse, A. J. Schmeitz, and E. Mascalchi, "EU ENSEMBLE project: Specification of an interoperable solution for a support function for platooning," *IEEE Trans. Intell. Transp. Syst.*, vol. 24, no. 6, Jun. 2023, doi: [10.1109/TITS.2023.3262397](#).
- [20] V. Milanés, S. E. Shladover, J. Spring, C. Nowakowski, H. Kawazoe, and M. Nakamura, "Cooperative adaptive cruise control in real traffic situations," *IEEE Trans. Intell. Transp. Syst.*, vol. 15, no. 1, pp. 296–305, Feb. 2014, doi: [10.1109/TITS.2013.2278494](#).
- [21] V. Milanés and S. E. Shladover, "Modeling cooperative and autonomous adaptive cruise control dynamic responses using experimental data," *Transp. Res. C: Emerg. Technol.*, vol. 48, pp. 285–300, Nov. 2014, doi: [10.1016/j.trc.2014.09.001](#).
- [22] S. E. Shladover, D. Su, and X.-Y. Lu, "Impacts of cooperative adaptive cruise control on freeway traffic flow," *Transp. Res. Rec.*, vol. 2324, no. 1, pp. 63–70, Jan. 2012, doi: [10.3141/2324-08](#).
- [23] C. Nowakowski, J. O'Connell, S. E. Shladover, and D. Cody, "Cooperative adaptive cruise control: Driver acceptance of following gap settings less than one second," *Proc. Hum. Factors Ergon. Soc. Annu. Meeting*, vol. 54, no. 24, pp. 2033–2037, 2010, doi: [10.1177/154193121005402403](#).
- [24] A. Al Alam, A. Gattami, and K. H. Johansson, "An experimental study on the fuel reduction potential of heavy duty vehicle platooning," in Proc. 13th Int. IEEE Conf. Intell. Transp. Syst., Piscataway, NJ, USA: IEEE, 2010, pp. 306–311, doi: [10.1109/ITSC.2010.5625054](#).
- [25] S. W. Smith et al., "Improving urban traffic throughput with vehicle platooning: Theory and experiments," *IEEE Access*, vol. 8, pp. 141,208–141,223, 2020, doi: [10.1109/ACCESS.2020.3012618](#).
- [26] Y. Sugiyama et al., "Traffic jams without bottlenecks—experimental evidence for the physical mechanism of the formation of a jam," *New J. Phys.*, vol. 10, no. 3, Mar. 2008, Art. no. 033001, doi: [10.1088/1367-2630/10/3/033001](#).
- [27] R. E. Stern et al., "Dissipation of stop-and-go waves via control of autonomous vehicles: Field experiments," *Transp. Res. C: Emerg. Technol.*, vol. 89, pp. 205–221, Apr. 2018.
- [28] C. Wu, A. Kreidieh, K. Parvate, E. Vinitsky, and A. M. Bayen, "Flow: Architecture and benchmarking for reinforcement learning in traffic control," 2017, *arXiv:1710.05465*.
- [29] C. Wu, A. Kreidieh, E. Vinitsky, and A. M. Bayen, "Emergent behaviors in mixed-autonomy traffic," in Proc. 1st Conf. Rob. Learn., 2017, pp. 398–407.
- [30] E. Vinitsky et al., "Benchmarks for reinforcement learning in mixed-autonomy traffic," in Proc. 2nd Conf. Rob. Learn., 2018, pp. 399–409.
- [31] K. Jang et al., "Simulation to scaled city: Zero-shot policy transfer for traffic control via autonomous vehicles," in Proc. 10th ACM/IEEE Int. Conf. Cyber-Phys. Syst., 2019, pp. 291–300, doi: [10.1145/3302509.3313784](#).
- [32] J. Cui, W. Macke, H. Yedidsion, A. Goyal, D. Urieli, and P. Stone, "Scalable multiagent driving policies for reducing traffic congestion," in Proc. 20th Int. Conf. Auton. Agents Multiagent Syst. (AAMAS), 2021, pp. 386–394.
- [33] Y. Zhang, W. Macke, J. Cui, D. Urieli, and P. Stone, "Learning a robust multiagent driving policy for traffic congestion reduction," *Proc. Adaptive and Learn. Agents Workshop*, pp. 1–14, Nov. 2023.
- [34] C. Wu, A. M. Bayen, and A. Mehta, "Stabilizing traffic with autonomous vehicles," in Proc. IEEE Int. Conf. Rob. Autom. (ICRA), 2018, pp. 6012–6018, doi: [10.1109/ICRA.2018.8460567](#).
- [35] M. Ameli et al., "Design, preparation, and execution of the 100-AV field test for the CIRCLES consortium: Methodology and implementation of the largest mobile traffic control experiment to date," *IEEE Control Syst.*, vol. 45, no. 1, pp. 139–155, Feb. 2025, doi: [10.1109/MCS.2024.3500332](#).
- [36] A. M. Bayen, J. W. Lee, B. Piccoli, B. Seibold, J. M. Sprinkle, and D. B. Work, "CIRCLES: Congestion impacts reduction via CAV-in-the-loop Lagrangian energy smoothing," presented at the 2020 Vehicle Technologies Office Annual Merit Review, Washington, DC (virtual), 2020.
- [37] A. M. Bayen, J. W. Lee, B. Piccoli, B. Seibold, J. M. Sprinkle, and D. B. Work, "CIRCLES: Congestion impacts reduction via CAV-in-the-loop Lagrangian energy smoothing," presented at the 2021 Vehicle Technologies Office Annual Merit Review, Washington, DC (virtual), 2021.
- [38] J. M. Sprinkle, A. M. Bayen, J. W. Lee, B. Piccoli, B. Seibold, and D. B. Work, "CIRCLES: Congestion impacts reduction via CAV-in-the-loop Lagrangian energy smoothing," presented at the 2022 Vehicle Technologies Office Annual Merit Review, Washington, DC, 2022.
- [39] H. Wang et al., "Hierarchical speed planner for automated vehicles: A framework for Lagrangian variable speed limit in mixed-autonomy traffic," *IEEE Control Syst.*, vol. 45, no. 1, pp. 111–138, Feb. 2024, doi: [10.1109/MCS.2024.3499212](#).
- [40] N. Kardous et al., "A rigorous multi-population multi-lane hybrid traffic model for dissipation of waves via autonomous vehicles," *Eur. Phys. J. Spec. Top.*, vol. 231, no. 9, pp. 1689–1700, 2022, doi: [10.1140/epjs/s11734-022-00580-z](#).
- [41] K. Jang et al., "Reinforcement learning-based oscillation dampening: Scaling up single-agent reinforcement learning algorithms to a 100-autonomous-vehicle highway field operational test," *IEEE Control Syst.*, vol. 45, no. 1, pp. 61–94, Feb. 2024, doi: [10.1109/MCS.2024.3503372](#).
- [42] A. Bacciotti and L. Rosier, *Liapunov Functions and Stability in Control Theory*. Berlin, Germany: Springer Science & Business Media, 2005.
- [43] K. Yosida, *Functional Analysis*. Berlin, Germany: Springer Science & Business Media, 2012.
- [44] A. Bressan and B. Piccoli, *Introduction to the Mathematical Theory of Control*. Springfield, IL, USA: American Institute of Mathematical Sciences, 2007.
- [45] E. Casas and M. Mateos, "Optimal control of partial differential equations," in *Computational Mathematics, Numerical Analysis and Applications: Lecture Notes of the XVII'Jacques-Louis Lions' Spanish-French School*, Cham, Switzerland: Springer, 2017, pp. 3–59.
- [46] L. N. Trefethen, *Approximation Theory and Approximation Practice*, Extended Edition. Philadelphia, PA, USA: SIAM, 2019.
- [47] F. Golse, "On the dynamics of large particle systems in the mean field limit," in *Macroscopic and Large Scale Phenomena: Coarse Graining, Mean Field Limits and Ergodicity*, Cham, Switzerland: Springer, 2016, pp. 1–144.
- [48] P. Baiti, P. G. LeFloch, and B. Piccoli, "Uniqueness of classical and non-classical solutions for nonlinear hyperbolic systems," *J. Differ. Equ.*, vol. 172, no. 1, pp. 59–82, 2001, doi: [10.1006/jdeq.2000.3869](#).
- [49] F. Wu and A. M. Bayen, "A hierarchical MPC approach to car-following via linearly constrained quadratic programming," *IEEE Control Syst. Lett.*, vol. 7, pp. 532–537, 2023, doi: [10.1109/LCSYS.2022.3201162](#).
- [50] Z. Fu, A. R. Kreidieh, H. Wang, J. W. Lee, M. L. Delle Monache, and A. M. Bayen, "Cooperative driving for speed harmonization in mixed-traffic environments," in Proc. IEEE Intell. Veh. Symp. (IV), Piscataway, NJ, USA: IEEE, 2023, pp. 1–8, doi: [10.1109/IV55152.2023.10186598](#).
- [51] M. Garavello, K. Han, B. Piccoli, *Models for Vehicular Traffic on Networks*, vol. 9. Springfield, MO, USA: American Institute of Mathematical Sciences (AIMS), 2016.
- [52] X.-Y. Lu and S. E. Shladover, "Review of variable speed limits and advisories: Theory, algorithms, and practice," *Transp. Res. Rec.*, vol. 2423, no. 1, pp. 15–23, 2014, doi: [10.3141/2423-03](#).
- [53] D. Gloudemans et al., "I-24 MOTION: An instrument for freeway traffic science," *Transp. Res. C: Emerg. Technol.*, vol. 155, 2023, Art. no. 104311, doi: [10.1016/j.trc.2023.104311](#).
- [54] D. Gloudemans et al., "Interstate-24 motion: Closing the loop on smart mobility," in Proc. IEEE Workshop Des. Autom. CPS IoT (DES-TION), Piscataway, NJ, USA: IEEE, 2020, pp. 49–55, doi: [10.1109/DES-TION50928.2020.00014](#).
- [55] "Next Generation Simulation (NGSIM)," US Department of Transportation Federal Highway Administration. [Online]. Available: <http://ops.fhwa.dot.gov/trafficanalystools/ngsim.htm>.
- [56] L. C. Edie, "Car-following and steady-state theory for noncongested traffic," *Oper. Res.*, vol. 9, no. 1, pp. 66–76, 1961, doi: [10.1287/opre.9.1.66](#).
- [57] A. Bayen, M. L. Delle Monache, M. Garavello, P. Goatin, and B. Piccoli, *Control Problems for Conservation Laws With Traffic Applications*:

- Modeling, Analysis, and Numerical Methods*. Berlin, Germany: Springer Nature, 2022.
- [58] A. Alanqary, X. Gong, A. Keimer, B. Seibold, B. Piccoli, and A. Bayen, "Optimal control of autonomous vehicles for flow smoothing in mixed autonomy traffic," in *Proc. IEEE 62nd Conf. Decis. Control (CDC)*, Piscataway, NJ, USA: IEEE, 2023, pp. 105–111, doi: [10.1109/CDC49753.2023.10383810](https://doi.org/10.1109/CDC49753.2023.10383810).
- [59] R. Stern et al., "Stabilizing traffic with a single autonomous vehicle," in *Proc. 7th Int. Conf. Cyber-Phys. Syst. (ICCPs)*, Piscataway, NJ, USA: IEEE, 2016, pp. 1–1, doi: [10.1109/ICCPs.2016.7479130](https://doi.org/10.1109/ICCPs.2016.7479130).
- [60] R. K. Bhadani, B. Piccoli, B. Seibold, J. Sprinkle, and D. Work, "Dissipation of emergent traffic waves in stop-and-go traffic using a supervisory controller," in *Proc. IEEE Conf. Decis. Control (CDC)*, Piscataway, NJ, USA: IEEE, 2018, pp. 3628–3633, doi: [10.1109/CDC.2018.8619700](https://doi.org/10.1109/CDC.2018.8619700).
- [61] A. Hayat et al., *A Holistic Approach to the Energy-Efficient Smoothing of Traffic via Autonomous Vehicles*. Cham, Switzerland: Springer International Publishing, 2022, pp. 285–316.
- [62] J. Baillieul and P. J. Antsaklis, "Control and communication challenges in networked real-time systems," *Proc. IEEE*, vol. 95, no. 1, pp. 9–28, Jan. 2007, doi: [10.1109/JPROC.2006.887290](https://doi.org/10.1109/JPROC.2006.887290).
- [63] S. K. V. Ahsani, M. Amin-Naseri, and A. Sharma, "Quantitative analysis of probe data characteristics: Coverage, speed bias and congestion detection precision," *J. Intell. Transp. Syst.*, vol. 23, no. 2, pp. 103–119, 2019, doi: [10.1080/15472450.2018.1502667](https://doi.org/10.1080/15472450.2018.1502667).
- [64] S. Kim and B. Coifman, "Comparing INRIX speed data against concurrent loop detector stations over several months," *Transp. Res. C: Emerg. Technol.*, vol. 49, pp. 59–72, Dec. 2014, doi: [10.1016/j.trc.2014.10.002](https://doi.org/10.1016/j.trc.2014.10.002).
- [65] M. Bunting, R. Bhadani, and J. Sprinkle, "Libpanda: A high performance library for vehicle data collection," in *Proc. Workshop Data-Driven Intell. Cyber-Phys. Syst.*, 2021, pp. 32–40, doi: [10.1145/3459609.3460529](https://doi.org/10.1145/3459609.3460529).
- [66] S. Elmudani, M. Nice, M. Bunting, J. Sprinkle, and R. Bhadani, "From CAN to ROS: A monitoring and data recording bridge," in *Proc. Workshop Data-Driven Intell. Cyber-Phys. Syst.*, 2021, pp. 17–21, doi: [10.1145/3459609.3460531](https://doi.org/10.1145/3459609.3460531).
- [67] N. Lichtenlé, E. Vinitsky, M. Nice, B. Seibold, D. Work, and A. M. Bayen, "Deploying traffic smoothing cruise controllers learned from trajectory data," in *Proc. Int. Conf. Rob. Autom. (ICRA)*, Piscataway, NJ, USA: IEEE, 2022, pp. 2884–2890, doi: [10.1109/ICRA46639.2022.9811912](https://doi.org/10.1109/ICRA46639.2022.9811912).
- [68] R. Bhadani et al., "Approaches for synthesis and deployment of controller models on automated vehicles for car-following in mixed autonomy," in *Proc. Cyber-Phys. Syst. Internet Things Week*, 2023, pp. 158–163, doi: [10.1145/3576914.3587711](https://doi.org/10.1145/3576914.3587711).
- [69] M. Nice, M. Bunting, D. Work, and J. Sprinkle, "Middleware for a heterogeneous CAV fleet," in *Proc. Cyber-Phys. Syst. Internet Things Week*, 2023, pp. 86–91, doi: [10.1145/3576914.358752](https://doi.org/10.1145/3576914.358752).
- [70] M. Nice et al., "Parameter estimation for decoding sensor signals," in *Proc. ACM/IEEE 14th Int. Conf. Cyber-Phys. Syst. (With CPS-IoT Week)*, 2023, pp. 253–255, doi: [10.1145/3576841.3589622](https://doi.org/10.1145/3576841.3589622).
- [71] M. Bunting, R. Bhadani, M. Nice, S. Elmudani, and J. Sprinkle, "Data from the development evolution of a vehicle for custom control," in *Proc. 2nd Workshop Data-Driven Intell. Cyber-Phys. Syst. Smart Cities Workshop (DI-CPS)*, Piscataway, NJ, USA: IEEE, 2022, pp. 40–46, doi: [10.1109/DI-CPS56137.2022.000013](https://doi.org/10.1109/DI-CPS56137.2022.000013).
- [72] F.-C. Chou, M. Gibson, R. Bhadani, A. M. Bayen, and J. Sprinkle, "Reachability analysis for FollowerStopper: Safety analysis and experimental results," in *Proc. IEEE Int. Conf. Rob. Autom. (ICRA)*, Piscataway, NJ, USA: IEEE, 2021, pp. 8607–8613, doi: [10.1109/ICRA48506.2021.9561360](https://doi.org/10.1109/ICRA48506.2021.9561360).
- [73] N. Lichtenlé, K. Jang, A. Shah, E. Vinitsky, J. W. Lee, and A. M. Bayen, "Traffic smoothing controllers for autonomous vehicles using deep reinforcement learning and real-world trajectory data," in *Proc. IEEE 26th Int. Conf. Intell. Transp. Syst. (ITSC)*, Piscataway, NJ, USA: IEEE, 2023, pp. 4346–4345, doi: [10.1109/ITSC57777.2023.10421828](https://doi.org/10.1109/ITSC57777.2023.10421828).
- [74] G. Gunter, M. Nice, M. Bunting, J. Sprinkle, and D. B. Work, "Experimental testing of a control barrier function on an automated vehicle in live multi-lane traffic," in *Proc. 2nd Workshop Data-Driven Intell. Cyber-Phys. Syst. Smart Cities Workshop (DI-CPS)*, Piscataway, NJ, USA: IEEE, 2022, pp. 31–35, doi: [10.1109/DI-CPS56137.2022.00011](https://doi.org/10.1109/DI-CPS56137.2022.00011).
- [75] M. Bando, K. Hasebe, A. Nakayama, A. Shibata, and Y. Sugiyama, "Dynamical model of traffic congestion and numerical simulation," *Phys. Rev. E*, vol. 51, no. 2, 1995, Art. no. 1035, doi: [10.1103/PhysRevE.51.1035](https://doi.org/10.1103/PhysRevE.51.1035).
- [76] D. C. Gazis, R. Herman, and R. W. Rothery, "Nonlinear follow-the-leader models of traffic flow," *Oper. Res.*, vol. 9, no. 4, pp. 545–567, 1961, doi: [10.1287/opre.9.4.545](https://doi.org/10.1287/opre.9.4.545).
- [77] A. Hayat, B. Piccoli, and S. Truong, "Dissipation of traffic jams using a single autonomous vehicle on a ring road," *SIAM J. Appl. Math.*, vol. 83, no. 3, pp. 909–937, 2023, doi: [10.1137/21M1414346](https://doi.org/10.1137/21M1414346).
- [78] F. Borrelli, A. Bemporad, and M. Morari, *Predictive Control for Linear and Hybrid Systems*. Cambridge, U.K.: Cambridge Univ. Press, 2017.
- [79] A. Richardson et al., "Analysis of a runtime data sharing architecture over LTE for a heterogeneous CAV fleet," in *Proc. Cyber-Phys. Syst. Internet Things Week*, 2023, pp. 164–169, doi: [10.1145/3576914.3587712](https://doi.org/10.1145/3576914.3587712).
- [80] S. Albeik et al., "Limitations and improvements of the intelligent driver model (IDM)," *SIAM J. Appl. Dyn. Syst.*, vol. 21, no. 3, pp. 1862–1892, 2022, doi: [10.1137/21M1406477](https://doi.org/10.1137/21M1406477).
- [81] X. Gong and A. Keimer, "On the well-posedness of the" Bando-follow the leader" car following model and a time-delayed version," *Netw. Heterogen. Media*, vol. 18, no. 2, pp. 775–798, 2023, doi: [10.3934/nhm.2023033](https://doi.org/10.3934/nhm.2023033).
- [82] A. Hayat et al., "Traffic smoothing using explicit local controllers: Experimental evidence for dissipating stop-and-go waves with a single automated vehicle in dense traffic," *IEEE Control Syst.*, vol. 45, no. 1, pp. 95–110, Feb. 2024, doi: [10.1109/MCS.2024.3503402](https://doi.org/10.1109/MCS.2024.3503402).
- [83] J. Schulman, F. Wolski, P. Dhariwal, A. Radford, and O. Klimov, "Proximal policy optimization algorithms," 2017, *arXiv:1707.06347*.
- [84] M. L. Puterman, *Markov Decision Processes: Discrete Stochastic Dynamic Programming*. Hoboken, NJ, USA: John Wiley & Sons, 2014.
- [85] "Autonomie vehicle system simulation tool." Argonne National Laboratory. Accessed: Sep. 25, 2023. [Online]. Available: <https://www.anl.gov/taps/autonomie-vehicle-system-simulation-tool>
- [86] N. Khoudari et al., "Reducing detailed vehicle energy dynamics to physics-like models," 2023, *arXiv:2310.06297*.
- [87] J. W. Lee et al., "Integrated framework of vehicle dynamics, instabilities, energy models, and sparse flow smoothing controllers," in *Proc. Workshop Data-Driven Intell. Cyber-Phys. Syst.*, New York, NY, USA: Association for Computing Machinery, 2021, pp. 41–47, doi: [10.1145/3459609.3460530](https://doi.org/10.1145/3459609.3460530).
- [88] M. Brackstone and M. McDonald, "Car-following: A historical review," *Transp. Res. F: Traffic Psychol. Behav.*, vol. 2, no. 4, pp. 181–196, 1999, doi: [10.1016/S1369-8478\(00\)00005-X](https://doi.org/10.1016/S1369-8478(00)00005-X).
- [89] M. Treiber, A. Hennecke, and D. Helbing, "Congested traffic states in empirical observations and microscopic simulations," *Phys. Rev. E*, vol. 62, no. 2, 2000, Art. no. 1805, doi: [10.1103/PhysRevE.62.1805](https://doi.org/10.1103/PhysRevE.62.1805).
- [90] "comma 3X." Comma. [Online]. Available: <https://comma.ai/>
- [91] "Network development tools for software defined vehicles and zonal architectures." Intrepid control systems. [Online]. Available: <https://intrepidcs.com>
- [92] R. Bhadani et al., "Strym: A python package for real-time CAN data logging, analysis and visualization to work with USB-CAN interface," in *Proc. 2nd Workshop Data-Driven Intell. Cyber-Phys. Syst. Smart Cities Workshop (DI-CPS)*, Piscataway, NJ, USA: IEEE, 2022, pp. 14–23, doi: [10.1109/DI-CPS56137.2022.00009](https://doi.org/10.1109/DI-CPS56137.2022.00009).
- [93] P. Ngo and J. Sprinkle, "Lightweight LSTM for can signal decoding," in *Proc. Workshop Data-Driven Intell. Cyber-Phys. Syst.*, 2021, pp. 27–31, doi: [10.1145/3459609.3460528](https://doi.org/10.1145/3459609.3460528).
- [94] P. Ngo, J. Sprinkle, and R. Bhadani, "CANClassify: Automated decoding and labeling of CAN bus signals," Electrical Engineering and Computer Sciences Univ. California, Berkeley, Tech. Rep. UCB/EECS-2022-151, May 2022, vol. 1.
- [95] R. Bhadani and J. Sprinkle, "Prototyping vehicle control applications using the cat vehicle simulator," 2023, *arXiv:2301.04574*.
- [96] G. Zachár, *Visualization of Large-Scale Trajectory Datasets*. New York, NY, USA: Association for Computing Machinery, 2023, pp. 152–157.
- [97] D. Gloudemans and D. B. Work, "Vehicle tracking with crop-based detection," in *Proc. 20th IEEE Int. Conf. Mach. Learn. Appl. (ICMLA)*, Piscataway, NJ, USA: IEEE, 2021, pp. 312–319, doi: [10.1109/ICMLA52953.2021.00005](https://doi.org/10.1109/ICMLA52953.2021.00005).
- [98] Y. Wang et al., "Automatic vehicle trajectory data reconstruction at scale," 2022, *arXiv:2212.07907*.
- [99] D. Gloudemans, Y. Wang, G. Gumm, W. Barbour, and D. B. Work, "The interstate-24 3D dataset: A new benchmark for 3D multi-camera vehicle tracking," 2023, *arXiv:2308.14833*.
- [100] D. Gloudemans et al., "So you think you can track?" 2023, *arXiv:2309.07268*.
- [101] Y. Wang, J. Ji, W. Barbour, and D. B. Work, "Online min cost circulation for multi-object-tracking on fragments," in *Proc. IEEE Int. Intell. Transp. Syst. Conf. (ITSC)*, Piscataway, NJ, USA: IEEE, 2023, pp. 2803–2810, doi: [10.1109/ITSC57777.2023.10422670](https://doi.org/10.1109/ITSC57777.2023.10422670).

Urban Network Resilience Analysis and Equity Emphasized Recovery based on Reinforcement Learning

Han Wang¹ and Maria Laura Delle Monache¹

Abstract— This paper introduces an equity emphasized recovery planning method for urban traffic networks based on a data driven approach. An integrated evaluation index is proposed to assess equity in territorial accessibility during hazards recovery, which brings the variance in accessibility between communities as a penalty term into the overall accessibility. Taking the improvement of the integrated index as the reward function, the equity emphasized recovery control strategy is designed with a reinforcement learning algorithm to determine the recovery priority of the affected links. To test the performance of the proposed approach, a simulation environment with reference to the San Francisco Bay Area was constructed. Experiment results indicate that, compared with the explicit strategies, the proposed recovery strategy is able to maintain a more equitable approach during the reconstruction process.

I. INTRODUCTION

With the climate change in recent decades, the increasing frequency of extreme weather and natural hazards can bring massive impairment to the urban transportation network, resulting in substantial reduction in network service capacity. *Resilience* is an important metric that captures the robustness and recoverability of a transportation network in natural hazards. The work in [1] defines the term *resilience of transportation network* as "the ability of a transportation system to absorb disturbances, maintain its basic structure and function, and recover to a required level of service within an acceptable time and costs after being affected by disruptions". Subsequently, [2] proposed a taxonomy of resilience based on the time span: including *mitigation strategies, emergency response and long term recovery*. Node-and-link-removal simulation experiments are widely applied in studies that quantitatively analyze transportation networks resilience [3]: remove some elements from a network model represented by nodes and links, in order to determine the numerical metric of interest [4]–[6]. This numerical metric is commonly computed as the difference between the network service capability before and after a natural disaster [7]–[9]. However, in most studies, social equity is a factor which tends to be ignored in the calculation of the resilience metrics. Equity in terms of network resilience indicates whether there are communities suffering significant decrease in service level during natural hazards with respect to other communities, and monitors whether the recovery strategy provides the equal restoration of service levels to all communities.

¹H. Wang and M. L. Delle Monache are with the Department of Civil and Environmental Engineering, University of California, Berkeley, USA hanw@berkeley.edu, mldellemonache@berkeley.edu

In this paper, we focus on equitable resilience during emergency response in the short term post-disaster to evaluate the network performance after natural hazards and the effectiveness of emergency recovery strategies. In order to evaluate if equity is maintained during natural hazards and recovery process, we propose a social-physical integrated evaluation index to comprehensively assess the performance of network in terms of both efficiency and equity. Taking the integrated index as the optimized goal, we propose an equity emphasized recovery control strategy based on a reinforcement learning algorithm. A simulation environment with reference to the San Francisco Bay Area was reconstructed based on open source data to examine the performance of the proposed method. The paper is organized as follows: Section II describes the different methods used to analyze the transportation network, its recovery and describes the integrated index. In Section III, the different datasets used for the analysis and the reinforcement learning environment are described and finally, in Section IV the results of the different experimental scenarios are shown.

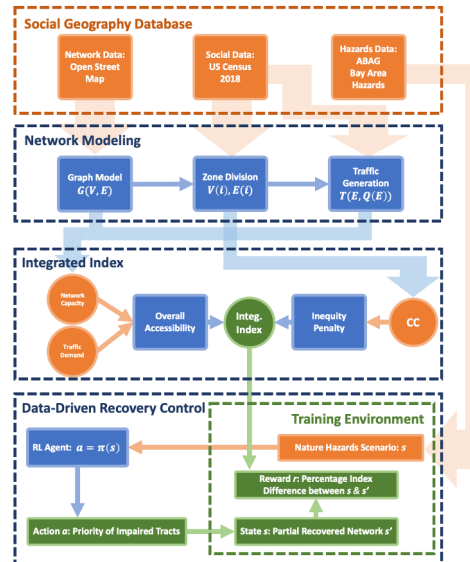


Fig. 1: Pipeline of proposed methodology

II. METHODOLOGY

The workflow pipeline of the proposed methodology is shown in **Figure 1**. This section introduces the three main modules of the methodology: network modeling, integrated index and data-driven recovery control strategy.

A. Network Modeling

In the proposed method, the transportation network will be represented by a *graph model*:

$$G(V, E), V^O(E), V^D(E), \quad (1)$$

where V is the set of *vertices*, E is the set of *edges*, $V^O(E)$ and $V^D(E)$ are the mappings of the edges to their origin and destination vertices. The first step to network modeling is to map *nodes* and *links* in the real world transportation network to the vertices and edges in the graph model, based on the network topology structure. For clarity purpose, the objects, in both the graph model and the transportation network, will be referred as node and link in the following. We assume that the network is directed and that the capacity of each link $C(E)$ is provided.

The study area is divided into *analysis zones*. In each zone, the social features such as land use, economy and demography should be consistent. The natural characteristics of the zones should be similar and the risk of natural hazards such as floods and fires should be consistent. Once the study area is divided into N_I zones, each zone is denoted by an ID index $i \in I = \{1, 2, \dots, N_I\}$. Links and nodes are connected to the affiliated zones with the mappings $V(i)$ and $E(i)$, each indicating the subset of nodes and links that belongs to zone i . The nodes are assigned to the zone where they are located. While, the links are assigned to the zone where the geometric center of each link lands.

For the evaluation of the network accessibility, we use a metric that relies on travel time. In this work, the travel time of each link, $T(E)$, is calculated using the *Bureau of Public Roads (BPR) power function* [10]:

$$T(E, Q(E)) = T_0(E)(1 + \beta_1 \frac{Q(E)}{C(E)})^{\beta_2}, \quad (2)$$

wherein $T_0(E)$ is the *free flow travel time*, $Q(E)$ is the *traffic flow* and $C(E)$ is the *practical capacity* of links. Coefficients β_1 and β_2 are determined by the property of specific roads and traffic, and calibrated using field collected data.

To obtain the traffic flow $Q(E)$ as the input of formula (2), traffic demand data $D = \{d_{ij}\}_{i,j \in I}$ is required. Ideally, traffic demand data should be a *origin-destination (OD) matrix*, in which rows and columns indexes are the zone IDs and each element d_{ij} corresponds to the traffic demand with the row zone i as origin and the column zone j as destination, usually in unit of trips per day. If the OD matrix of each analysis zone is not directly available, it can be obtained with trip generation methods. The core idea of trip generation is to evaluate the instigation of zones to produce or attract a trip (e.g. home-work and work-home commuting trip) based on the social features (e.g. land use, job density, demography statistics) of the zones. Depending on the data availability, various techniques based on regression analysis, category analysis, or even logit models could be used to derive the trip demand [11]. Once the OD matrix is available and the travel time of links can be computed using the BPR function, the link traffic flow $Q(E)$ can be obtained through iteration based *dynamic traffic assignment (DTA)* methods, of

which classical implementations include *column generation* [12], *Frank-Wolfe algorithm* [13] and *method of successive average (MSA)* [14] etc.

B. Integrated Accessibility Assessment

To comprehensively evaluate the performance of the network, we need an integrated index to indicate not only the efficiency performance of the network but also its equity. Similar to the idea in [9], the network resilience in terms of both efficiency and equity can be measured by the change of an integrated index during natural hazards and recovery process. The integrated index R proposed in this paper consists of two terms:

$$R = A - J, \quad (3)$$

the overall efficiency performance of whole network A and the inequity penalty term J .

As shown in formula (4), inspired by [3], [9],

$$A(G, D) = \sum_{i \in I} \frac{W_i}{\sum_k W_k} \cdot A_i \quad (4)$$

$$A_i = \sum_{j \in I, j \neq i} \frac{W_j}{T_{ij}} \quad (5)$$

the efficiency performance is evaluated as the aggregated territorial accessibility $A(G, D)$ of whole network G and specific traffic demand D . For each zone $i \in I$, the accessibility A_i is calculated by the gravity formed indicator, which is commonly considered as a balance between explainability and complexity [3], [15]–[18]. W_j is the mass weight of zone j , T_{ij} is the distance between zone i and zone j . In this paper, we select the resident population as mass weight and the shortest travel time as distance.

The inequity penalty is computed as follows:

$$J = |r_{pb}(A_i, X_i^{cc})| \cdot A, i \in I \quad (6)$$

wherein $r_{pb}(A, X_i^{cc})$ is the point-biserial coefficient between the accessibility A_i of zone i , and the binary variable X_i^{cc} that indicates if the zone i includes a *community of concern* or not. Community of concern refers to the areas in which there is a significant proportion of vulnerable and underserved communities. To determine a community of concern different criteria can be used. Once the community of concern is determined and noted by the variable $X_i^{cc} \in \{0, 1\}$, the point-biserial coefficient is obtained by:

$$r_{pb}(A_i, X_i^{cc}) = \frac{\bar{A}_{cc} - \bar{A}_{ncc}}{s_n} \sqrt{\frac{n_{cc} n_{ncc}}{n^2}}, \quad i \in I \quad (7)$$

In (7), the zones are divided into two groups to distinguish a community of concern with subscript cc with one that is not with subscript ncc . \bar{A}_{cc} and \bar{A}_{ncc} are the mean values of the accessibility within the two groups. n_{cc} and n_{ncc} are the number of the zones in each group and n is the total number of zones. s_n is the standard deviation of the accessibility on the whole sample. The point-biserial coefficient is the measure of the linear relationship between the value of the accessibility and the community of concern. It indicates

whether those communities are offered a significantly different network accessibility from others, i.e. inequity. The total integrated index will be obtained by subtracting the inequity penalty from the overall accessibility:

$$R = (1 - |r_{pb}(A_i, X_i^{cc})|) \cdot \frac{1}{\sum_k W_k} \sum_{i \in I} \sum_{j \in I, j \neq i} \frac{W_i W_j}{T_{ij}} \quad (8)$$

Thereby, the network resilience in accessibility and equity is measured by the percentage loss of the integrated index through the hazards:

$$L(S, S') = \frac{R(S') - R(S)}{R(S)} \cdot 100\% \quad (9)$$

wherein $S = \{G, D\}$ and $S' = \{G', D'\}$ are the states of the network before and after the hazards. It is worth to note that, in formula (8) the point-biserial coefficient r_{pb} is taken as absolute value, which indicates that both the positive and negative linear relation between the community of concern and the accessibility will lead to a decrease of the integrated index.

C. Recovery Strategy

In order to ensure that equity is well maintained and that the accessibility of each community is equally considered in the recovery process, we design the recovery control strategy based on reinforcement learning with the integrated index as the goal to maximize. To apply the reinforcement learning algorithm, we model the network recovery control problem into a *Markov decision process (MDP)* problem [19]: a finite MDP problem can be represented by a tuple $\mathcal{P}(S, A, P, R)$. For agents in MDP, select an action $a \in A$ when the state $s \in S$ is observed at time step t , which results in a new state s' with probability $P(s'|s, a)$ and obtain a reward $r(t) = R(s, a, s')$. The current state will be updated to s' and the process will be repeated until the end criteria of the episode is met. In this case: the state space S is the whole network state space represented by the joint tensor of capacity and travel time of links $\{C(E), T(E), Q(E)\}$; the action space A is the set of zones ID, from where the policy selects one zone $a \in I$ to be reconstructed according to the network state observed for each step; the reward function is the percentage of reconstructed integrated index loss, which is essentially calculated by a similar formula than the one in (9):

$$r(s, s') = \frac{(R(s') - R(s))}{(R(s_1) - R(s_0))} \cdot 100\%$$

A policy $\pi(s)$ is a mapping $S \mapsto A$ from states to actions, guiding agents to choose actions corresponding to states. The objective of the MDP problem is to find the optimized policy π^* to maximize the total reward (expectation).

We make the following assumptions for each episode. We define the scale of impairment of natural hazards as the total number of affected zones λ . Between iterations under different natural hazards scenario in the same experiment λ can be different. Then, we define, the rescue capability

of the agent as the number of zones that the agent could reconstruct in short term post-disaster μ . Accordingly, μ should be consistent within each experiment. The procedure reads as follows:

- 0) Initialize the parameters: policy parameter θ , value function parameters ω , learning rate α^θ , discount factor γ , impairment scale λ and recovery capability μ . Set steps in each episode $T \leftarrow \mu$. Set network to unimpaired state s_0 .
- 1) Generate a random hazards scenario by setting the capacity of links in total λ zones to 0, wherein λ is the integer parameter dependent on scenario setting, $t \leftarrow 0$;
- 2) Obtain the capacity and travel time of all links, i.e. the state s_1 ;
- 3) Collect the action by input state into current policy, $a \leftarrow \pi(s)$;
- 4) Recover the capacity of links in zone a ;
- 5) Obtain the capacity and travel time of all links after recovery, i.e. the state s' ;
- 6) Calculate the reward r by formula (8);
- 7) $t \leftarrow t + 1$. If $t \neq T$, $s \leftarrow s'$ and back to 3); if $t = T$, reset all the links and back to 1).

The collected trajectories will be utilized to update the policy. Theoretically, this procedure support most of the policy based reinforcement learning algorithms. The main difference between different algorithms happens in the implementation of the initialization and the policy update. The actor-critic algorithm with replay buffer is applied in this paper, the pseudo code is given in **Table I**.

TABLE I: Pseudo Code of Actor-Critic

Batched Actor–Critic (episodic)	Stage
Input: differentiable parameterized policy π^θ	
Input: differentiable parameterized value function $v^\omega(s)$	Initialization
Parameters: learning rate α^θ , discount factor γ	
Initialize θ and ω	
Iterate:	Iteration:
Sample trajectory with π^θ and save $\{s_i, a_i\}$	
pairs into replay buffer:	
Initialize s	1), 2)
Obtain $a = \pi^\theta(s)$	3)
Obtain s'	4), 5)
Obtain r	6)
If episode not end, $s \leftarrow s'$, back to stage 3)	7)
If episode end, back to stage 1)	
Update Policy Parameters:	
Update ω to fit $V^\omega(s)$ to samples	
$\delta_i \leftarrow r(s_i, a_i) + \hat{v}^\omega(s'_i) - \hat{v}^\omega(s_i)$	
$\theta \leftarrow \theta + \alpha^\theta \sum_i \delta_i \nabla_\theta \log \pi^\theta(a_i s_i)$	Policy Update

III. DATA DESCRIPTION

As shown in **Figure 1**, the operation of both resilience evaluation and recovery control relies on the social geography database. This section introduces the data needed for the proposed system and sources used to simulate the San Francisco bay area experiment.

A. Network Data

The graph model of the traffic network is abstracted from various *geography information system (GIS)* based data

sources. In the simulation of this paper, the graph model is represented in the format of *general modeling network specification (GMNS)* [20], which is a network data format designed for multi-modal static and dynamic transportation planning and operations models. The GMNS data of San Francisco Bay area network is generated based on the OpenStreetMap [21] data. The visualized GMNS data of SF Bay area is shown in **Figure 2**. Including all arterials, collectors and local roads the study area network consists of 416677 links and 228160 nodes.

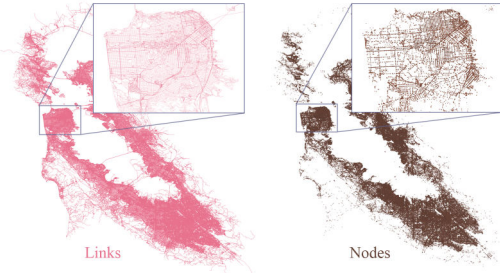


Fig. 2: Visualization of San Francisco Bay Area GMNS Data

B. Social Data

As discussed in the methodology section, social data defined in a desired geographical division is required to generate traffic demand and identify a community of concern. In the simulations of this paper, *U.S. Census 2018* [22] data is used. Correspondingly, the U.S. Census tracts division [23] is applied as the analysis zone division, as shown in **Figure 3b** with black line boundaries. The *equity priority community (EPC)* [24] determined based on U.S. Census data by the *Metropolitan Transportation Commission (MTC)* is utilized to detect the communities of concern.

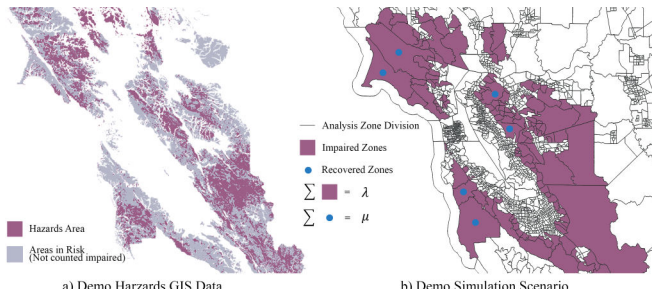


Fig. 3: Demonstration of Scenario Generation

C. Natural Hazards Data

Natural hazards data is required to design realistic simulation scenarios for training purpose. The *curated data for Bay area hazards* [25] from the *Association of Bay Area Governments (ABAG)* is used to generate training scenarios. A detailed scenario generation method is explained in the next section. It is worth noticing that, besides the training scenarios generation, the real-time natural hazards data is not required for the practice of well trained recovery control

policy, which only takes network state as input data to operate.

IV. SIMULATION

A. Scenario Generation

The effect of natural hazards on the transportation network is captured in the training scenarios as failures of the impaired links. In this paper, we assume that the links are disabled and recovered in unit of zones. In addition, for implementation purposes, this assumption has relevance: the damage suffered by adjacent roads is not independent, since natural hazards tend to impair most of the roads in the area; and it is also more feasible for the management agency to conduct rescue construction to all the roads within the same area, compared with same amount of roads but scattered throughout the city. With this assumption, there are two critical steps in the scenario generation: 1) obtain the number of affected zones λ , which indicates the scale of impairment; 2) select the set of zones $I^{imp} = I\{i|X_i^{imp} = 1\}$ impaired, which indicates the spatial distribution of impairment and are denoted by the variable $X_i^{imp} \in \{0, 1\}, \sum_{i \in I} X_i^{imp} = \lambda$. To enhance the generalization ability of the policies and prevent overfitting, randomness is introduced into the scenario generation process. According to the different ways in which step 1 and 2 are applied, three types of scenarios are generated with equal probability in the experiment, as shown in **Table II**. A demo of a scenario generation is shown in **Figure 3**. The specific curated data for the Bay area hazards used in the experiment is described in **Table III**.

B. Training Setting

The parameters of the simulation experiments and the training setting are shown in **Table IV**.

The OD demand is generated by *trip generation* and *trip distribution* from the *4 steps model* [30] based on U.S. Census data. Dynamic traffic assignment is conducted with modified column generation algorithm [31]. The shortest travel time is calculated by modified label correcting [32].

C. Benchmarks

As the benchmark for the proposed learning-based control strategy, two random control strategies and two explicit control strategy are implemented to select the zones to be recovered in the same simulation environment. The random strategy $\tilde{\pi}_1$ randomly select μ zones from all zones I and random strategy $\tilde{\pi}_2$ randomly select μ zones from impaired zones $I\{i|X_i^{imp} = 1\}$. The explicit control strategy $\bar{\pi}_1$ takes the capacity of each zone $C(i) = \sum C(E(i)), i \in I$, which is the aggregation of the capacity of affiliated links before hazards, as the recovery priority. The explicit control strategy $\bar{\pi}_2$ takes the residential population as the recovery priority.

D. Results

The resilience evaluation and strategy performance is shown in **Table V**. The PB correlation coefficient of unimpaired network is $|r_{pb}(t=0)| = 0.187, p = 0.61$. According to the PB correlation coefficient at initial state in **Table V**,

TABLE II: Three Types of Scenario Generation

Scenario Type	Impairment Scale λ	Impaired zones Selection
Event Reproduction	Exzoneing natural hazards layers from ABAG hazard data. Matching to analysis zones layer in GIS based on geographic coordinates. Identify zones with affiliated affected links above a certain percentage threshold as impaired. The value of λ in scenario is equal to the number of GIS-determined impaired zones.	Same impaired zones determined from GIS matched up layers.
Spatial Redistribution	The value of λ in scenario is equal to the number of GIS-determined impaired zones.	Randomly select λ zones.
Random	Randomly generate λ using Poisson distribution: $\lambda \sim \pi(\bar{\lambda})$, wherein $\bar{\lambda}$ is the mean value of the number of affected zones in the sample of GIS records of target hazards.	Randomly select λ zones.

TABLE III: Curated Data for Bay Area Hazards [25]

GIS Data Layer	Impairment Mapping
Wildfire [26]	Determine the wildfires footprint in past 10 years (2011-2020) larger 10 acres as link impaired area. Areas suffered multiple historic wildfires won't be double counted in λ .
Landslide [27]	Areas identified as "Mostly landslides" with the largest and most concentrated landslides are all determined as link impaired; "few landslides" and "flat land" area are determined as unimpaired.
Flood [28]	The 100 and 500 year floodplains designated by <i>Federal Emergency Management Agency (FEMA)</i> , as well as potential floodplains currently protected by levees, are all determined as link impaired area.
Earthquake [29]	Different faults and different magnitude hazards are projected into different shaking scenarios by <i>United States Geological Survey (USGS)</i> . "Violent Shaking", "Severe Shaking" and "Very Strong Shaking" zones in each shaking scenarios are determined as link impaired area.

TABLE IV: Parameter Setting for Simulation Experiment

Parameters	Value
Episode Length $T = \mu$	600
Batch Size	1800
Learning Rate α^θ	0.001
Discount Coefficient γ	0.95
Number of target updates	10
Number of gradient updates	10

the disasters implemented in the simulation did not bring significant changes to the PB correlation coefficient. The performance of strategies are not evaluated in the wildfire scenario because the recovery capability $\mu = 600$ is larger than the number of impaired zones in all wildfire scenarios. The learning curve of the policies is shown in **Figure 4**, wherein the performance of the benchmark is marked as horizontal lines. Over all, the proposed control strategy reaches a 13.8% improvement based on capacity emphasized strategy and 26.3% on population emphasized strategy. As the best performed benchmark strategy, the capacity emphasized strategy recovered 33.7% impaired integrated index averagely, while the PB correlation coefficient at the end of the recover $|r_{pb}(t = \mu)| = 1.91, p = 0.89$ doesn't have significant change with the initial state $|r_{pb}(t = 0)| = 0.187, p = 0.61$. Compared to the capacity emphasized

and population emphasized strategy, the proposed equity emphasized strategy significantly reduces the PB correlation coefficient to $|r_{pb}(t = \mu)| = 0.118, p = 0.54$ with the same amount of zones recovered, thus improving the average increment of the integrated index.

The comparison between strategies shows that the proposed recovery strategy is more capable than the explicit one to maintain the equity of communities in terms of accessibility during the reconstruction process with the same reconstruction capability.

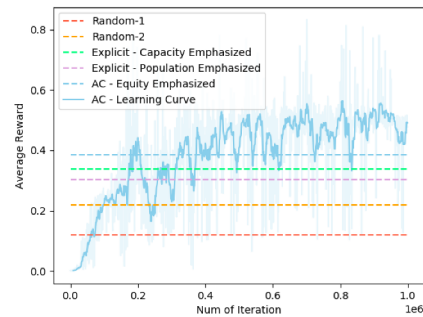


Fig. 4: Learning Curve of Batched Actor Critic

V. CONCLUSIONS

In this work, we show that a social physical integrated index is effective for a comprehensive evaluation of traffic network resilience when considering the equity factor as well, and for guiding the equity emphasized emergency recovery strategy. To test the proposed reinforcement learning method, the simulation experiment based on San Francisco Bay area is built and a corresponding social geography database is constructed. The experiment result is shown to outperform the capacity emphasized recovery strategy in maintaining equity during the post-disaster recovery process.

For the feasibility in practice, given that the proposed method is intended for application in post-disaster emergency response, the timeliness of the required input date is critical to the timely implementation of recovery operations. The proposed recovery policy takes traffic network condition as input, which requires a completed post-disaster capacity assessment for every edge of the network. The speed of access to assessment result depends to a large extent on the development of local digital transportation infrastructure.

TABLE V: Summarize of Experiment Outcome

Average Value of	Wildfire	Landslide	Flood	Earthquake	All Hazards
Impaired zones λ	179	1066	892	1943	1475
Accessibility loss $E(A(s) - A(s'))$	0.87%	15.2%	8.5%	41.3%	28.0%
Integrated index loss $E(L(s, s'))$	1.03%	12.0%	13.7%	44.9%	36.6%
PB coefficient at initial state $ r_{pb}(t = 1) $	0.184	0.175	0.179	0.183	0.191
Performance:			Increment of Integrated Index		$ r_{pb}(t = \mu) $
Random Strategy $\bar{\pi}_1$	/	23.7%	19.2%	9.0%	12.1%
Random Strategy $\bar{\pi}_2$	/	40.2%	48.1%	12.7%	21.9%
Explicit Strategy $\bar{\pi}_2$: Population Emphasized	/	71.0%	74.9%	12.3%	30.4%
Explicit Strategy $\bar{\pi}_1$: Capacity Emphasized	/	69.7%	75.1%	16.0%	33.7%
Equity Emphasized Strategy π^*	/	70.8%	76.2%	21.3%	38.4%

In the future work, multiple social factors could be involved into the integrated index to provide more comprehensive evaluation. For the recovery control strategy, techniques for dealing with large scale state and action space, or architectures for multi-agent system might be helpful to improve the performance.

REFERENCES

- [1] C. Wan, Z. Yang, D. Zhang, X. Yan, and S. Fan, “Resilience in transportation systems: a systematic review and future directions,” *Transport reviews*, vol. 38, no. 4, pp. 479–498, 2018.
- [2] N. Zhang, A. Alipour, and L. Coronel, “Application of novel recovery techniques to enhance the resilience of transportation networks,” *Transportation research record*, vol. 2672, no. 1, pp. 138–147, 2018.
- [3] B. Martín, E. Ortega, R. Cuevas-Wizner, A. Ledda, and A. De Montis, “Assessing road network resilience: An accessibility comparative analysis,” *Transportation Research Part D: Transport and Environment*, vol. 95, p. 102851, 2021.
- [4] E. Jenelius and L.-G. Mattsson, “Road network vulnerability analysis of area-covering disruptions: A grid-based approach with case study,” *Transportation research part A: policy and practice*, vol. 46, no. 5, pp. 746–760, 2012.
- [5] D. Xu, C. Wei, P. Peng, Q. Xuan, and H. Guo, “Ge-gan: A novel deep learning framework for road traffic state estimation,” *Transportation Research Part C: Emerging Technologies*, vol. 117, p. 102635, 2020.
- [6] Y. Yang, S. T. Ng, S. Zhou, F. J. Xu, and H. Li, “Physics-based resilience assessment of interdependent civil infrastructure systems with condition-varying components: A case with stormwater drainage system and road transport system,” *Sustainable Cities and Society*, vol. 54, p. 101886, 2020.
- [7] V. Knoop, H. van Zuylen, and S. Hoogendoorn, “The influence of spillback modelling when assessing consequences of blockings in a road network,” *European Journal of Transport and Infrastructure Research*, vol. 8, no. 4, 2008.
- [8] U. Bhatia, D. Kumar, E. Kodra, and A. R. Ganguly, “Network science based quantification of resilience demonstrated on the indian railways network,” *PLoS one*, vol. 10, no. 11, p. e0141890, 2015.
- [9] E. Ortega, B. Martín, and Á. Aparicio, “Identification of critical sections of the spanish transport system due to climate scenarios,” *Journal of Transport Geography*, vol. 84, p. 102691, 2020.
- [10] U. B. of Public Roads. Office of Planning. Urban Planning Division, *Traffic Assignment Manual for Application with a Large, High Speed Computer*. US Department of Commerce, 1964.
- [11] S. Maerivoet and B. De Moor, “Transportation planning and traffic flow models,” *arXiv preprint physics/0507127*, 2005.
- [12] T. Leventhal, G. Nemhauser, and L. Trotter Jr, “A column generation algorithm for optimal traffic assignment,” *Transportation Science*, vol. 7, no. 2, pp. 168–176, 1973.
- [13] M. Frank, P. Wolfe *et al.*, “An algorithm for quadratic programming,” *Naval research logistics quarterly*, vol. 3, no. 1-2, pp. 95–110, 1956.
- [14] Y. Sheffi, *Urban transportation networks*. Prentice-Hall, Englewood Cliffs, NJ, 1985, vol. 6.
- [15] E. López, J. Gutiérrez, and G. Gómez, “Measuring regional cohesion effects of large-scale transport infrastructure investments: an accessibility approach,” *European Planning Studies*, vol. 16, no. 2, pp. 277–301, 2008.
- [16] J. Gutiérrez, A. Condeço-Melhorado, E. López, and A. Monzón, “Evaluating the european added value of ten-t projects: a methodological proposal based on spatial spillovers, accessibility and gis,” *Journal of Transport Geography*, vol. 19, no. 4, pp. 840–850, 2011.
- [17] A. Monzón, E. Ortega, and E. López, “Efficiency and spatial equity impacts of high-speed rail extensions in urban areas,” *Cities*, vol. 30, pp. 18–30, 2013.
- [18] E. Ortega, I. Otero, and S. Mancebo, “Titim gis-tool: A gis-based decision support system for measuring the territorial impact of transport infrastructures,” *Expert Systems with Applications*, vol. 41, no. 16, pp. 7641–7652, 2014.
- [19] M. L. Puterman, *Markov decision processes: discrete stochastic dynamic programming*. John Wiley & Sons, 2014.
- [20] S. Smith, I. Berg, C. Yang *et al.*, “General modeling network specification: documentation, software, and data,” 2020.
- [21] M. Haklay and P. Weber, “Openstreetmap: User-generated street maps,” *IEEE Pervasive computing*, vol. 7, no. 4, pp. 12–18, 2008.
- [22] U. C. Bureau, American Community Survey 5-Year Data (2009–2019). (2021, Oct 10). [Online]. Available: <https://www.census.gov/data/developers/data-sets/acs-5year.html>
- [23] TIGERweb. REST API: Census Tracts 2018. (2021, Oct 10). [Online]. Available: https://tigerweb.geo.census.gov/tigerwebmain/TIGERweb_restmapservice.html
- [24] M. T. Commission. MTC Plan Bay Area 2050 Equity Priority Communities. (2021, Oct 10). [Online]. Available: <https://github.com/BayAreaMetro/Spatial-Analysis-Mapping-Projects/tree/master/Project-Documentation/Equity-Priority-Communities>
- [25] A. of Bay Area Governments. Curated Data for Bay Area Hazards. (2021, Oct 10). [Online]. Available: <https://abag.ca.gov/our-work/resilience/data-research>
- [26] C. FIRE. The Fire and Resource Assessment Program (FRAP) - Fire Perimeters. (2021, Oct 10). [Online]. Available: <https://frap.fire.ca.gov/frap-projects/fire-perimeters/>
- [27] C. M. Wentworth, S. E. Graham, R. J. Pike, G. S. Beukelman, D. W. Ramsey, and A. D. Barron, “Summary distribution of slides and earth flows in the san francisco bay region, california,” US Dept. of the Interior, US Geological Survey, Tech. Rep., 1997.
- [28] F. E. M. Agency. FEMA Flood Maps. (2021, Oct 10). [Online]. Available: <https://www.fema.gov/flood-maps>
- [29] C. G. Survey. Hazards Program, 2018. (2021, Oct 10). [Online]. Available: <https://www.conservation.ca.gov/cgs/shp>
- [30] M. G. McNally, *The four-step model*. Emerald Group Publishing Limited, 2007.
- [31] X. Zhou. STALite/DTALite/NeXTA Software. (2021, Oct 10). [Online]. Available: https://github.com/xzhou99/stalite-dtalite_software_release
- [32] X. Z. JDLP. Boost Shortest Path Algorithm Implementations using Proper Data Structures. (2021, Oct 10). [Online]. Available: <https://github.com/jdlph/shortest-path-algorithms>